



AMERICAN UNIVERSITY OF BEIRUT

CURCUMIN MEDIATED GREEN SYNTHESIZED GOLD  
NANOPARTICLES FOR SENSING APPLICATIONS

by  
SHEHAB YOUSSEF AL SHEHAB

A thesis  
submitted in partial fulfillment of the requirements  
for the degree of Master of Science  
to the Department of Chemistry  
of the Faculty of Arts and Sciences  
at the American University of Beirut

Beirut, Lebanon  
May 2020

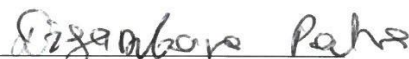
AMERICAN UNIVERSITY OF BEIRUT

CURCUMIN MEDIATED GREEN SYNTHESIZED GOLD  
NANOPARTICLES FOR SENSING APPLICATIONS


by  
SHEHAB YOUSSEF AL SHEHAB

Approved by:

\_\_\_\_\_  
Prof. Digambara Patra, Professor  
Chemistry

  
Advisor

\_\_\_\_\_  
Prof. Rabih Sultan, Professor  
Chemistry

  
Member of Committee

\_\_\_\_\_  
Prof. Faraj Hasanayn, Professor  
Chemistry

  
Member of Committee

Date of thesis: May 28, 2020

# AMERICAN UNIVERSITY OF BEIRUT

## THESIS, DISSERTATION, PROJECT RELEASE FORM

Student Name: Al Shehab Shehab Youssef  
Last First Middle

Master's Thesis       Master's Project       Doctoral Dissertation

I authorize the American University of Beirut to: (a) reproduce hard or electronic copies of my thesis, dissertation, or project; (b) include such copies in the archives and digital repositories of the University; and (c) make freely available such copies to third parties for research or educational purposes.

I authorize the American University of Beirut, to: (a) reproduce hard or electronic copies of it; (b) include such copies in the archives and digital repositories of the University; and (c) make freely available such copies to third parties for research or educational purposes after : **One** ---- year from the date of submission of my thesis, dissertation, or project.  
**Two** ~~---~~ years from the date of submission of my thesis, dissertation, or project.  
**Three** ---- years from the date of submission of my thesis, dissertation, or project.



Signature

25/06/2020

Date

## ACKNOWLEDGMENTS

There are no proper words to express my deep gratitude and respect for my thesis and research advisor Prof. Digambara Patra. It has been a real privilege for me to share of his exceptional scientific knowledge and also of his extraordinary human qualities. It is whole-heartedly appreciated that your great advice for my study proved monumental towards the success of this study.

My sincere thanks go to Ms. Riham El Kurdi. I recognize the invaluable assistance that Ms. El Kurdi provided during my study.

I am most grateful to the members of my thesis committee: Prof. Rabih Sultan and Prof. Faraj Hasanayn for the knowledge and experience that you shared with us, whether in class or in the laboratory. It was a pleasure being your student.

Finally, my deep and sincere gratitude to my family for their continuous and unparalleled love, help and support.

## AN ABSTRACT OF THE THESIS OF

Shehab Youssef Al Shehab for Master of Science  
Major: Chemistry

Title: Curcumin Mediated Green Synthesized Gold Nanoparticles for sensing applications.

Nanotechnology is growing immensely due to its wide applications in various areas of science and technology. In this work, gold nanoparticles (AuNPs) were successfully prepared by using a simple, clean, non-toxic, cost effective and eco-friendly method. In this method AuNPs were reduced from  $\text{Au}^{3+}$  to  $\text{Au}^0$  using curcumin, a natural and non-toxic food spice. The effect of the surfactant, pH and temperature were studied during synthesis to understand the size and shape of the formed nanoparticles and their influence on linear surface plasmon resonance (LSPR), fluorescence and resonance Rayleigh scattering (RRS) spectra. Three different poly (ethylene glycol) based polymers, such as, PEG Thiol Acid, mPEG Thiol and mPEG Amine were used to stabilize the formed gold nanoparticles. The coated AuNPs were small in size, in the range of 18 - 40 nm. The prepared materials were also characterized in detail by SEM, XRD, TGA and FT-IR spectroscopy. The functional group of the stabilizing agent that was pointing toward the solution was found to interact with the analyte for the determination of various analytes. AuNPs prepared using PEG-Thiol Acid were employed as an optical method for the determination of melamine, a white powder that is often found in adulterated milk. The combination of melamine with the AuNPs decreased both LSPR signal and the fluorescence emission intensity of the AuNPs in the presence of 0 to 10 mM of melamine. The method is simple, cheap, and fast with 33 nM detection limit. The concentration of the gold nanoparticles during estimation of melamine was optimized, and selectivity study showed that the method is selective to melamine against analogue components. In the second part AuNPs functionalized with mPEG Thiol were used in such a manner that the methoxy group is pointed toward the aqueous solution to serve as anchor point to many metal ions. Exposure of the mPEG Thiol functionalized AuNPs to different concentrations of metal cations in the range between 0 and 100  $\mu\text{M}$  resulted in the decrease in the fluorescence intensity of the AuNPs unlike free curcumin in aqueous solution. Excited state lifetime measurements further validated quenching mechanism to be static in nature. The binding constant and number of binding sites for such interaction were evaluated. The order of association of the metal ions studied based on observed bimolecular quenching rate constant

values is Pb (II) > Hg (II) >Hg (I) > Cd (II)>Al (III) >Ni (II) >Cu (II) >Na<sub>2</sub>HAsO<sub>4</sub>. These interactions between the mPEG Thiol conjugated AuNPs and the metal ions in solution contribute a proof-of-concept that mPEG Thiol functionalized curcumin mediated AuNPs can be used as a simple, cheap and straightforward, on-site detection system for toxic and even essential metal ions in solution.

## CONTENTS

ACKNOWLEDGEMENTS .....	v
ABSTRACT.....	vi
LIST OF ILLUSTRATIONS.....	X
LIST OF TABLES.....	xiii
LIST OF ABBREVIATIONS.....	Xiv
Chapter	
I. INTRODUCTION.....	1
A. Colloid Definition and Structure .....	1
B. Gold Colloid: A Brief Historical Background .....	2
C. Traditional Syntheses Methods of AuNp.....	3
1. Turkevish Method.....	3
2. Brust Method.....	4
3. Seeded Growth Method .....	4
4. Syntheses of Gold Nanoparticles Using Plant extracts.....	5
D. Shape and Size of AuNps .....	5
E. Green Syntheses.....	5

1. Stabilizing Agents for Nanoparticles Preparation.....	6
2. Curcumin Applicability in Nanoparticles Syntheses.....	7
F. Surface Plasmon Resonance (SPR) .....	8
G. Fluorescence of Nanoparticles.....	11
1. The Frank -Condon principle.....	13
2. Stokes' Shift	14
3. Kasha's Rule	15
4. Quantum Yield and Lifetime of Fluorescence	15
5. Steady State and Time Fluorescence Resolved	16
H. Applications of Gold Nanoparticles.....	17
I. AuNps As a Chemical Sensor.....	17
J. Objectives of this work.....	17
<b>II. GREEN SYNTHESIS OF CURCUMIN MEDIATED PEG</b>	<b>19</b>
<b>THIOL ACID CONJUGATED GOLD NANOPARTICLES FOR</b>	
<b>THE DETERMINATION OF MELAMINE</b>	
A. Introduction .....	19
B. Methods .....	20
1. Syntheses of Curcumin Conjugated Gold Nanoparticles.....	20
2. Sample preparation for Melamine Sensing.....	21
C. Results and Discussion .....	21
D. Conclusion .....	51
<b>III. BINDING OF METAL IONS TO THE CURCUMIN</b>	<b>53</b>
<b>MEDIATED METHOXY POLYETHYLENE GLYCOL</b>	
<b>THIOL CONJUGATED GREENLY SYNTHESIZED</b>	
<b>GOLD NANOPARTICLES: A FLUORESCENCE</b>	
<b>QUENCHING STUDY</b>	
A. Introduction .....	56



B. Materials and Methods.....	56
1. Materials .....	56
2. Syntheses of mPEG AuNps using Curcumin .....	56
3. Sample Preparation for Metal Ion Binding.....	57
C. Results and Discussion.....	57
1. Characterization of mPEG mediated AuNPs.....	57
a. Visual identification of Au Nps.....	57
b. UV-Vis absorption and SEM Studies .....	59
c. XRD, TGA and FT-IR .....	60
2. Binding of AuNps with metal Ions Fluorescence Quenching Study	62
3. Binding Constant and Binding Site.....	71
E. Conclusion.....	73
IV. CONCLUSIONS AND FUTURE PROSPECTS.....	75
REFERENCES.....	76

## ILLUSTRATIONS

Figure		Page
1.	Tyndall effect: Scattering of laser light when passed through mixture ii (Gold Nps).....	2
2.	Various methods used in the syntheses of AuNPs.....	3
3.	Chemical Structure of Curcumin in its keto form.....	8
4.	Schematic representation of a localized surface plasmons in gold nanoparticles; b. electric field E and magnetic field H.....	9
5.	Jablonsci Diagram.....	13
6.	Franck–Condon principle energy diagram.....	14
7.	The Stoke’s Shift.....	15
8.	Applications of AuNPs.....	17
9.	Solution color after 24 hours A: without curcumin, B: with Curcumin.....	22
10.	(A) Fluorescence emission spectrum excited at $\lambda = 425$ nm, (B) Fluorescence emission spectrum excited at $\lambda = 500$ nm, (C) Synchronous fluorescence spectra at $\Delta\lambda = 0$ nm and (D) UV-Vis spectra of curcumin functionalized Au NPs prepared using different surfactant.....	24

11.	SEM images of curcumin functionalized gold nanoparticles prepared using different surfactant: (A) PEG thiol acid, (B) mPEG amine and (C) mPEG thiol.....	26
12.	EDX of curcumin functionalized gold nanoparticles prepared using different surfactant: (A) PEG thiol acid, (B) mPEG amine and (C) mPEG thiol.....	27
13.	(A) Fluorescence emission spectrum excited at $\lambda = 425$ nm, (B) Fluorescence emission spectrum excited at $\lambda = 500$ nm, (C) Synchronous fluorescence spectra at $\Delta\lambda = 0$ nm and (D) UV-Vis spectra of curcumin functionalized Au NPs prepared at different pH.....	28
14.	SEM images of curcumin functionalized gold nanoparticles prepared using different pH: (A) pH 4, (B) pH 7, (C) pH 10 and (D) pH 13.....	29
15.	Zeta potential value of curcumin functionalized gold nanoparticles prepared at (A) pH 4 and (B) pH 13.....	31
16.	Particle size distribution value of curcumin functionalized gold nanoparticles prepared at (A) pH 4 and (B) pH 13.....	33
17.	(A) Fluorescence emission spectrum excited at $\lambda = 425$ nm, (B) Fluorescence emission spectrum excited at $\lambda = 500$ nm, (C) Synchronous fluorescence spectra at $\Delta\lambda = 0$ nm and (D) UV-Vis spectra of curcumin functionalized Au NPs prepared at different temperatures.....	35
18.	SEM images of curcumin functionalized gold nanoparticles prepared using different temperatures: (A) T= 30 °C, (B) T= 45 °C, (C) T=60 °C and (D) T=75 °C	37
19.	X-ray diffraction pattern of curcumin functionalized gold nanoparticles prepared at pH 4, pH 13 and curcumin	38
20.	TGA of curcumin functionalized gold nanoparticles prepared at pH 4, pH 13 and curcumin.....	40
21.	FT-IR spectra of curcumin functionalized gold nanoparticles prepared at pH 4, pH 13 and curcumin	41
22.	Change in absorbance of curcumin (A), change in absorbance of Au NPs (B) during its synthesis in extreme alkaline condition and (C) UV-Visible spectra during preparation of curcumin functionalized gold nanoparticles at pH 13 at different time.	42
23.	(A) UV-Visible spectra, (B) Fluorescence emission spectrum excited at $\lambda = 425$ nm, (C) LSPR measurement and (D) Plot of $I/I_0$ of curcumin functionalized gold nanoparticles in presence of melamine	47

24.	Ratio of emission intensity ( $I/I_0$ ) of Au NPs in the presence of melamine	49
25.	Plot of $I/I_0$ of curcumin functionalized nanoparticles with time in the absence and presence of melamine.	50
26.	UV-Visible spectra of curcumin functionalized gold nanoparticles with increase concentration in the absence and presence of melamine.	51
27.	Tautomerization reaction between curcumin enol and keto form.....	59
28.	(a) UV-Vis absorption spectrum of PEG thiol AuNPs measured after 24 h ;(b) Illustration of ligands containing methoxy PEG-SH used to functionalize the surface of gold nanoparticle.....	59
29.	(a) SEM images reveal that the mPEG Thiol functionalized AuNPs retain their roughly spherical shape, and (b) corresponding EDX image.....	60
30.	XRD patterns observed for Au nanoparticle's colloid.....	60
31.	FTIR spectrum of curcumin and AuNPs obtained by curcumin extract and mPEG thiol stabilizing agent.....	61
32.	TGA of mPEG thiol functionalized gold nanoparticles.....	62
33.	Fluorescence emission spectra excited at $\lambda = 425$ nm for mPEGT conjugated AuNPs titrated with varying concentrations of (A) $Cd^{2+}$ and $Al^{3+}$ ions.....	64
34.	Fluorescence emission spectra excited at $\lambda = 425$ nm for free curcumin titrated with varying concentrations of (A) $Hg^{2+}$ and $Ni^{2+}$ ions....	66
35.	Stern–Volmer plot for fluorescence quenching of mPEGT conjugated AuNPs by (A) $Cd^{2+}$ ion and (B) $Al^{3+}$ ion.....	68
36.	Time-resolved fluorescence decays of mPEGT conjugated AuNPs in the presence concentrations of (A) $Pb^{2+}$ and $Ni^{2+}$ ions.....	71
37.	Plot of $\log\{I_0-I\}/I$ vs. $\log [Hg^+]$ for the estimation of binding constant (K) and number of binding sites (n).....	73

## TABLES

Table		Page
1.	Table 1 compares this method to other recent similar methods. Our method shows better or similar detection limit, within the same dynamic range, to recently reported procedure.....	49
2.	Table 2: Stern-Volmer constant ( $K_{sv}$ ) and bimolecular quenching rate constant ( $k_Q$ ) for the fluorescence quenching of mPEGT conjugated AuNPs by various metal ions.....	68
3.	Table 3: Excited state lifetimes of mPEGT conjugated AuNPs in the presence of varying concentrations of $Pb^{+2}$ and $Ni^{2+}$ ions. The excited state lifetime was measured at $\lambda_{exc} = 405$ nm and $\lambda_{em} = 540$ nm.....	71
4.	Table 4: Binding constant (K) and number of binding sites (n) of various metal ions while associating with mPEGT conjugated AuNPs.....	73

## ABBREVIATIONS

CU	Curcumin
DLS	Dynamic light scattering
FRET	Fluorescence Resonance Energy Transfer
FT IR	Fourier transform infrared spectroscopy
HPLC	High-performance liquid chromatography
MPEG A	Methoxy Polyethylene glycol amine
MPEG T	Methoxy Polyethylene Glycol thiol
NP	Nanoparticle
PEG TA	Polyethylene glycol thiol
SPR	Surface Plasmon resonance

# CHAPTER I

## INTRODUCTION

### A. Colloid Definition and Structure

Derived from the Greek name kolla = glue, eidos= like, a colloid is a solution which has particles ranging in size between 1 and 1000 nanometers in diameter. These particles, also known as colloidal dispersions, can remain evenly distributed inside the solution, fully dispersed without settling to the bottom of the container. Colloids are classified in terms of dispersed substance in dispersing medium. To correctly specify a solution as colloid, the substance that will be classified should be larger than a molecule but can't be seen by the naked eye. Quantitatively, the substance size should be between 1 and 1000 nm. If the dimensions are less than 1 nm, the substance is called a solution and if they are greater than 1000 nm, the substance is called a suspension.

A colloid can be prepared by two approaches: The first approach is called Dispersion. In this method, larger pieces are broken down to smaller one. Addition of dispersing aids or agents such as surfactant, polymer, and small particle will adsorb at the solid-liquid interface and provide an electrostatic or steric barrier and inhibit the rapid flocculation of the newly formed particles. The second approach is termed Condensation: where colloids are formed by aggregation of a molecular dispersion to the size range of a colloid. Colloid formation occurs via emulsion polymerization. As Polymerization proceeds, the growing chain will precipitate and will continue to grow by the new monomer that is taken from the reservoir of the emulsified materials. Polymerization will continue until all available monomers are consumed [2]. One way to determine if a solution is colloidal is by Tyndall effect where scattering will occur in colloidal solution (see fig 1).

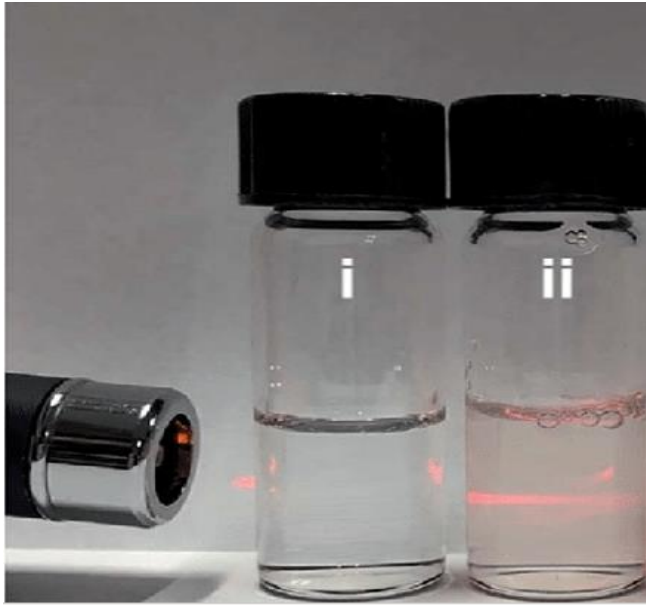


**Fig.1 Tyndall effect: Scattering of laser light when passed through mixture ii (Gold Nps)**

## **B. Gold Colloid: A Brief Historical Background**

In 1852, Michael Faraday gave a lecture at the Royal Institute in London entitled ‘Experimental Relations of Gold (and Other Metals) to light’. Faraday was the first scientist that related the optical properties of gold nanoparticles to their small size. In his studies, Faraday described the Au colloid solutions as ‘a beautiful ruby fluid’ and attributed the effect to ‘a mere variation in the size of particles’ [3]. Michael Faraday reduced Au-chloride by heat treatment, because of the side reactions with many reagents [4]. Later, Zsigmondy started to investigate different methods for reproducing Au colloids. Zsigmondy could determine exact sizes of the particles. Theodor Svedberg also became involved in the properties of colloids, so he built an ultracentrifuge, which could generate forces over 100,000 times of gravity [5] [6]. Svedberg developed his first low-speed ultracentrifuge and then the high-speed ultracentrifuge to determine the shape and size of the protein particle. Ostwald tried to focus on the importance of



size for particle dispersion. He depicted several examples to explain the process of Au sols and other colloids. Besides, he explained the mechanism for the formation of Liesegang rings during diffusion reaction, when drops of colloidal Au rod solutions evaporated.

### C. Traditional Synthesis Methods of Gold Nanoparticles

There are two techniques to synthesize gold nanoparticles: bottom up method and top down method [7]. Bottom up method involves assembly of atoms which are produced by reduction of ion into the desired nanostructures. This method includes electrochemical, photochemical, chemical, templating, thermal and sonochemical reduction methods [8]. Top down methods require the removal of matter from the bulk material to get the desired nanostructure, examples include photolithography and electron beam lithography [9] [10]. The disadvantages of the bottom up method are poor monodispersity. The disadvantages of the top down method are the huge waste of material. See fig.2 for a summary of the different methods for syntheses of AuNps.

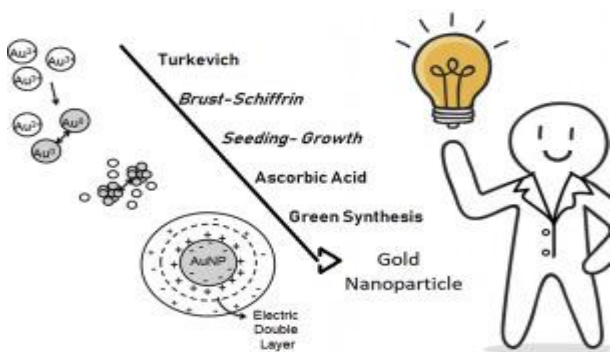


**Fig 2. Various methods used in the syntheses of AuNPs**

#### 1. *Turkevich method*

To synthesize gold nanoparticles in the size between 10-20 nm, Turkevich method is the classical traditional method that was first described in 1951 [11]. This method involves

reduction of gold ions ( $\text{Au}^{3+}$ ) to gold atoms ( $\text{Au}^0$ ) in the presence of reducing agents like citrate, amino acids, ascorbic acid or UV light. The size of gold nanoparticle was stabilized via capping or stabilizing agent. Further researchers could expand the size of gold nanoparticles, synthesized via this method. Later, the effect of temperature, stabilizing agent, and pH was studied on the effect of the size [12] [13].

## ***2. Brust-Schiffrin Method***

Generating small nanoparticles in the range between 1.5 nm -5.2. nm requires the Brust method, which is a two-phase process that requires organic solvents and the ratio of thiol to gold should be varied. This method involves transfer of gold salt from aqueous solution to an organic solvent such as toluene using a phase transfer agent, for instance Tetraoctylammonium bromide (TOAB). The gold is then reduced using sodium borohydride in presence of an alkanethiol. The alkanethiols stabilize the AuNPs, resulting in a color change of the reaction from orange to brown [14].

## ***3. Seeded Growth Method***

The most applicable technique to get gold nanoparticles with shapes such as rods, cubes, and tubes, is seed mediated growth [15]. Gold salts should be reduced with a strong reducing agent like sodium borohydride. The seed particles should be added to a solution of metal salt in presence of a weak reducing agent such as ascorbic acid and structure directing agent, which will prevent further nucleation and will accelerate the anisotropic growth of AuNPs. Geometry of gold nanostructures can be changed by varying the concentration of seeds, structure directing agents and reducing agents [16].

#### ***4. Synthesis of Gold Nanoparticles Using Plant Extract***

Various biocomponents present in plants such as curcumin are involved in synthesis of AuNPs because they possess functional groups, which catalyze the reduction and stabilization of gold NPs. The procedure involves mixing the gold salt with extracts of plant for definite amount of time under varied reaction conditions like incubation time, pH, and temperature to obtain specific sizes and shapes of gold nanoparticle [17].

#### **D. Shape and Size of Gold Nanoparticles**

Gold nanoparticles (AuNPs) can be easily made into various structures of narrow size distribution; examples include gold Nanospheres, Nanocages, Nanorods, and Nano shells [18]. The diameters could vary from 2-100 nm, by varying the ration of citrate and gold salt [19]. As the particle size increased, the absorption peak will shift to a longer wavelength. Furthermore, the width of the peak indicated the range of size distribution [20]. Au Nanocages are hollow, porous structures with dimensions less than 100 nm [21]. Au nanorods are gold nanoparticles which are elongated along one direction [22]. Gold Nano shells (AuNShs) are constituted of a silica core coated by a thin gold metallic shell [23].

#### **E. Green Synthesis**

Green synthesis of gold nanoparticles makes use of non-toxic, environmentally friendly, and safe reagents. Gold Nanoparticles synthesized using biological techniques or green technology have higher stability and appropriate dimensions because they are synthesized using a one-step procedure. Gold Nanoparticles can be synthesized using a variety of methods which are listed

above. But using Chemical and Physical methods have many limitations, such utilizing high radiation and highly concentrated reductants and stabilizing or capping agents that are toxic and harmful for the environmental and to human health. Therefore, green synthesis of nanoparticles is a single step bio-reduction method and less energy is used to synthesize eco-friendly [24]. The twelve principles of green chemistry have now become a reference guide for researchers, scientists, chemical technologists, and chemists around the globe for developing less hazardous chemical products and by products .Therefore, green nanobiotechnology is a promising alternate route for synthesis of biocompatible stable nanoparticles . The general procedure using plants to produce metallic nanoparticles uses the dried biomass of the plants and metallic salt, as bio reducing agent and precursor, respectively. Three main steps are followed for the synthesis of nanoparticles using a green nanotechnology :1) the choice of solvent medium use, 2)the choice of an eco-friendly and environmentally benign reducing agent , 3)the choice of a nontoxic material as a capping agent is to stabilize the synthesized nanoparticles [24].

### ***1. Stabilizing Agents for Nanoparticles preparation***

A milestone of nanomaterials research is to enhance the biocompatibility of materials by using biocompatible molecules for their surface coating. Polyethylene Glycol (PEG) is a feasible alternative being a hydrophilic polymer, non-toxic, commonly used in many pharmaceutical formulations. Surface coating with PEG will also prevent non-specific interactions of blood serum proteins with nanoparticles, reducing the gold NPs' interaction with the immune system and leading to longer circulation times in the blood stream (25). A shell of stabilizing molecules surrounds colloidal gold nanoparticles. One end of the stabilizing molecule is chemically linked or adsorbed on the gold surface; the other end is pointing toward the solution and providing

colloidal stability. A ligand exchange reaction involves the exchange of the stabilizing molecule with another ligand. As thiol moieties bind with high affinity to gold surfaces, mostly thiol-modified ligands are utilized which bind to the surface of the Au particles called monolayer-protected clusters by formation of Au-Sulfur bonds. Ligand exchange allows the transfer of Au NPs from an organic to an aqueous phase and vice versa. In this way, the surface properties of the particle can be tuned or adjusted by choosing certain surfactants with specific functional groups that give them unique properties. For applications in aqueous solution typically thiol-based surfactants with carboxylic groups at the other end pointing towards the solution are used. The negative charge of these particles provides colloidal stability and, they can be used as anchor points for the further attachment of biological molecules (26).

## ***2. Curcumin Applicability in Nanoparticle Syntheses***

Curcumin, extracted from the ground of curcuma, is a phenolic flavonoid of structure (1,7-bis(4-hydroxy-3-methoxyphenyl)-1,6-heptadiene-2,5-dione (27) (see fig. 3). It is well known for its multiple effective therapeutic properties as an antioxidant against cancer and microbial infection (28), anti-inflammatory drug (29), diabetic wounds (30), anti-inhibitor of angiogenesis and hepatic disorders (31), etc. Since curcumin has low molecular weight and has a hydrophobic nature, it can penetrate the blood brain barrier effectively. Besides, curcumin can inhibit the generation of free radical species, which plays an important role in the concept of the H atom from the C12 methylene group. A few researchers have recently demonstrated the anti-cancer property of curcumin (abstraction of the H atom from the C12 methylene group) by inhibiting the free radicals in cancer (32). Therefore, to elaborate the use of curcumin in new fields, it was being developed to be involved in the production of AuNPs. In general, noble metal nanoparticles have

shown a primary role in the development of new biosensors for sensing variety of biomolecules (33, 34). Au NPS have been used essentially and investigated for possible use in biosensors (35). The efficiency of gold nanoparticles as biocatalyst probe has been established in the making of new optical biosensors according to the enhanced localized Surface Plasmon Resonance (36).

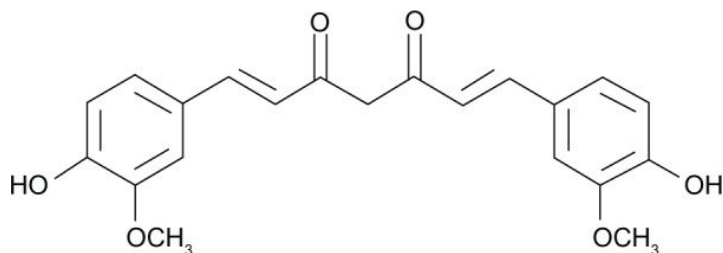


**Fig.3 Chemical Structure of Curcumin in its keto form**

#### **F. Surface Plasmon Resonance (SPR)**

Plasmon resonance is the collective oscillations of free conduction electrons in the surface of the metals that is stimulated by an incident light[37]. Plasmon's, in analogy to a real plasma, can be described as a negatively charged electron cloud coherently displaced from its equilibrium position around a lattice made of positively charged ions[38]. When an optical beam is irradiated on a metal Np, the metal Np will be excited, then electrical fields are formed in the particle and the electrons are transported collectively with respect to the positive charges. Because opposite charges are collected at opposite sides of the nanoparticle, restoring forces come into play, and electron oscillate at a frequency that is determined by the size of the nanoparticles, polarizability of the metal, and the surrounding medium. When there is a match between the collective oscillation frequency and frequency of the excited field, very small optical excitation causes large responses, which is the resonance condition of localized plasmons [147]. A schematic representation of the generation of a surface plasmon oscillation is shown in Figure 4.

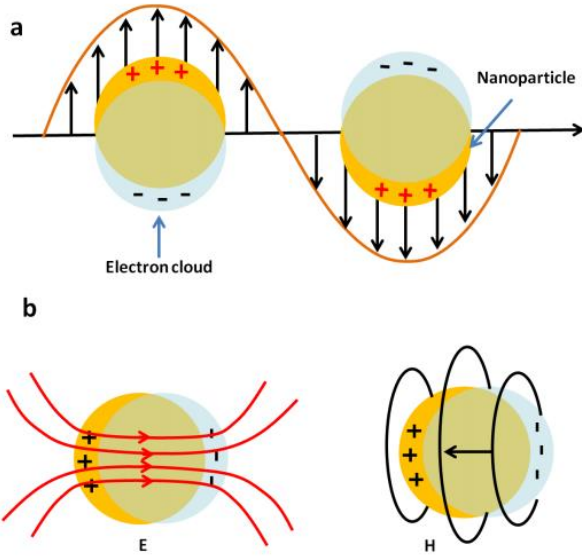


**Fig 4 Schematic representation of a localized surface plasmons in gold nanoparticles; b. electric field E and magnetic field H.**

Au Nps, which are characterized by surface plasmons which simultaneously carry electrons and photons, can afford very high electromagnetic field intensities within a small mode wavelength. For Nps much smaller than the wavelength of incident light, Maxwell's equations can be solved under a quasi-static approximation to give out the electromagnetic field outside the particle:

$$E_{out}(x, y, z) = E_0 \vec{k} - \left[ \frac{\epsilon_{in} - \epsilon_{out}}{\epsilon_{in} + 2\epsilon_{out}} \right] a^3 E_0 \left[ \frac{\vec{z}}{r^3} - \frac{3z}{r^5} (x\vec{i} + y\vec{j} + z\vec{k}) \right]$$

where  $\epsilon_{in}$ : Dielectric constant of the metal nanoparticle;  $\epsilon_{out}$ : Dielectric constant of the external environment; and a: Particle size.

Since  $\epsilon_{in}$  is strongly dependent on wavelength, the electromagnetic field is enhanced relative to the incident field and the resonance condition for the plasmon absorption is roughly fulfilled when

$\epsilon_{in} = -2 \epsilon_{out}$ . AuNps are interesting because this condition is satisfied in the visible region, which make it a valuable material for devices that allows optical signals to be controlled at sub-wavelength scale. Difference in particle size, shape and medium can lead to a change of electron density of gold nanoparticles, therefore leading to a change of plasmon resonance [148].

In other words, In the case of metallic NPs such as gold nanoparticles, i.e. with size comparable to the metal skin depth, the electric field of incident light can penetrate the metal and polarize the conduction electrons [39]. When the plasmons in nanoparticle have size much smaller than photon wavelength, these plasmons are non-propagating excitations and they are called localized surface plasmons (LSPs), because the resulting plasmon oscillation is distributed over the whole particle volume [38]. The coherent displacement of electrons from the positively charged lattice will generate a restoring force, which pulls the polarized electrons back to the lattice. Therefore, the plasmon in a nanoparticle can be considered as a mass-spring harmonic oscillator driven by the energy resonant light wave, where the electron cloud oscillates just like a simple dipole in parallel direction to the electric field of the electromagnetic radiation [40-42].

LSPR of gold nanoparticles results in a strong absorbance peak in the visible region between 500 nm and 600 nm, which can be measured by UV-Vis spectroscopy. The LSPR spectrum depends on the size and shape of gold nanoparticles. As the particle diameter increases, the peak absorbance wavelength increases with particle diameter. Also, for an uneven shaped particle, the absorbance spectrum shifts into the far-red region of the spectrum when compared to a spherical particle of the same diameter [43].

The equation represented below can explain the absorption change when gold nanoparticles are subjected to a different environment:

$$\lambda_{max} = m\Delta n \left[ 1 - \exp\left(-\frac{2d}{l_d}\right) \right]$$



where  $\lambda_{\max}$ : Shift of absorption peak;  $m$ : Bulk refractive-index response of the nanoparticle;  $\Delta n$ : Change in refractive index;  $d$ : Effective adsorbent layer thickness;  $l_d$ : Electromagnetic field decay length. When local medium changes, refractive index ( $n$ ) surrounding the particles will change and make a direct effect on the maximum absorption peak ( $\lambda_{\max}$ ) [148].

### **G. Fluorescence of Gold Nanoparticles**

Fluorescence is a luminescence technique based on exciting a molecule by electromagnetic radiation and collecting emitted light in return. Fluorescence is a simple highly sensitive technique that is used in wide range of applications in biotechnology, sensing and DNA sequencing [43]. The singlet ground, first, and second electronic states are represented by  $S_0$ ,  $S_1$ , and  $S_2$ , respectively. At each of these electronic energy levels, the fluorophores can exist in a number of vibrational energy levels, denoted by 0, 1, 2, etc. The transitions between states are shown as vertical lines to explain the instantaneous nature of light absorption. Transitions occur in about 10–15 s, a time very short for significant displacement of nuclei. This is the Franck-Condon principle [44] (see fig. 5).

After the absorption of light, a fluorophore is excited to higher vibrational singlet states of  $S_1$  and  $S_2$ . Internal conversion is when molecules in condensed phases quickly relax through a radiationless process to the lowest vibrational level  $S_1$ , in approximately 10-12s.

After the completion of this process, fluorescence emission takes place from a thermally equilibrated singlet state, where the electrons in the ground and the excited state orbitals have opposite spin orientations to the ground state. This phenomenon is extremely short and occurs approximately in 10 nanoseconds. Intersystem crossing (ISC) by definition is the intramolecular

crossing from one state to another of different multiplicity without the emission of radiation. It when molecules in the S1 state can undergo a spin conversion to the first triplet state T1. The excited electron and the ground state electron have the same spin orientation, thus the transition from the triplet excited state to the ground state is forbidden. However, it can happen and in this case the emission of light is known as phosphorescence which is a slow process which occurs in a duration that ranges from few milliseconds to seconds.

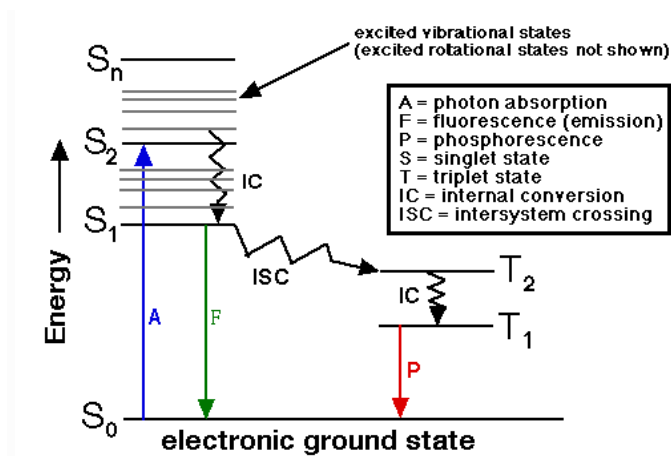


**Fig 5 Jablonski Diagram**

### 1. The Franck-Condon principle

The Franck-Condon Principle illustrates the intensities of emission of a photon, the absorption, or vibronic transitions. It states that when a molecule is undergoing an electronic transition, the nuclear configuration of the molecule will not change. This is because nuclei are much more massive than electrons and the electronic transition takes place faster than the nuclei can respond. When the nucleus realigns itself with the new electronic configuration, the theory states that it must undergo a vibration, see fig 6. Nuclear axis shows a consequence of the internuclear separation and the vibronic transition is indicated by the blue and green vertical arrows. This

figure demonstrates three things: a) An absorption leads to a higher energy state, b) fluorescence leads to a lower energy state, and c) the shift in nuclear coordinates between the ground and excited state is indicative of a new equilibrium position for nuclear interaction potential. Since fluorescence arrow is shorter than the absorption indicates that fluorescence has less energy, or that its wavelength is longer. Since electronic transitions are very fast compared with nuclear motions, vibrational levels are favored when they correspond to a minimal change in the nuclear coordinates. The potential wells are shown favoring transitions between  $v=0$  and  $v'=2$ [149].

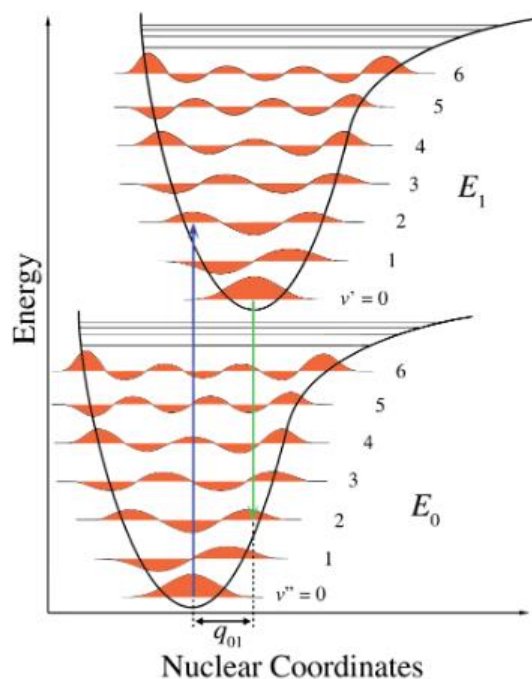


**Fig. 6 Franck–Condon principle energy diagram.**

## 2. *Stoke's Shift*

The emission energy is less than that of absorption. This phenomenon known as Stokes' shift corresponds to a red shift in the emission spectrum relative to that of absorption spectrum. The causes of the stoke's shift are internal conversion, the decay of the fluorophores to higher

vibrational levels of  $S_0$  results in further dissipation of excitation energy. And excited-state reactions, energy transfer, solvent effects, and complex formation. The Stokes' shift is represented in fig 7 [44].

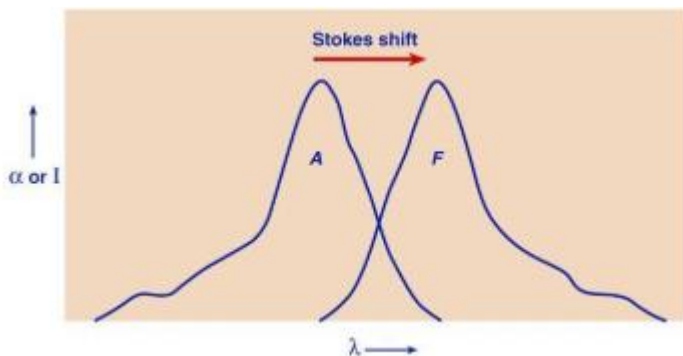


**Fig 7 The Stoke's Shift**

### 3. *Kasha's rule*

Kasha postulated that irrespective of the excitation wavelength, the same emission spectrum is generally observed. Fluorescence is the emission of light from the lowest vibrational states of  $S_1$  to the higher vibrational states of  $S_0$ . Therefore, upon excitation the excess of energy absorbed is lost by internal conversion making all fluorescent transitions similar [150].

### 4. *Quantum Yield and Lifetime of Fluorescence*

Fluorescence quantum yield is defined as the ratio of the number of molecules that fluoresce to the total number of excited molecules, or the ratio of photons emitted to photons absorbed.

$$\Phi_f = \frac{k_f}{k_f + k_{nr}}$$

Where  $k_f$  represents the first order rate constant for fluorescence relaxation and  $k_{nr}$  represents the rate constant for radiationless relaxation.

The excited state lifetime,  $\tau_0$ , represents the sum of radiative and radiationless processes that the excited fluorophore undergoes upon decaying back to the ground state. The fluorescence lifetime,  $\tau$ , is the portion responsible for emitting a photon and is related to the quantum yield of the fluorophore (see the equation below).

$$\phi = \frac{\tau}{\tau_0}$$

### 5. *Steady State and Time Resolved Fluorescence*

Two types of fluorescence exist: steady state and time resolved fluorescence. In steady state measurement, the sample is continuously illuminated, and the intensity versus wavelength is monitored. However, in time resolved fluorescence, the sample is exposed to a light pulse, shorter than its decay time and the intensity decay versus time is recorded.

For a fluorophore displaying a single decay time ( $\tau$ ), the intensity  $I$  is given by

$$I(t) = I_0 e^{-\frac{t}{\tau}}$$

where  $I_0$  is the intensity at  $t = 0$  immediately after the pulse.

The steady state intensity  $I_{SS}$  and the decay time are related by:

$$I_{SS} = \int_0^{\infty} I_0 e^{-t/\tau} dt = I_0 \tau$$

For a probe on a molecule existing in two conformations, steady-state measurements show average intensities; however, a time-resolved measurement shows two decay times.

## H. **Application of Gold nanoparticles**

Gold nanoparticles have wide range of applications. Colorimetric sensing is one of the promising tools being a rapid, cheap, and simple method for determination of analytes. Gold

nanoparticles was utilized to detect wide range of analytes such as nucleic acid , where Au Nps have the ability to interact with the nitrogenous bases of single stranded DNA/RNA, leading to immobilization of theses bases on the Au atoms surface[45] , peptides and proteins , amino acids , inorganic ions , anions , melamine , pesticides [45].Gold nanoparticles have been used in photodynamic therapy a treatment that is used to kill cancer cells, photothermal therapy where electromagnetic radiation is utilized ( In particular IR ) to treat cancer , X-ray imaging and drug delivery[46], (See figure 8).



**Fig. 8 Applications of AuNPs**

### **I. Gold nanoparticles as a chemical sensor**

Chemical sensors constitute a signaling unit or fluorophore and a guest-binding site or a receptor: the fluorophore and the receptor are usually separated by a spacer unit. Fluorescence is considered as the emission of photon after relaxation from an electronic excited state to the ground state .Chemical sensors based on changing in the fluorescent intensity or surface plasmon resonance signal are gaining great attention due to their simplicity of measurement , high efficiency and high sensitivity. The readout of a chemical sensor is usually a change in the fluorescence intensity, intensity decay lifetime or a shift in the emission wavelength [47].

Gold nanoparticles was utilized to detect wide range of analytes such as: nucleic acid , where Au Nps have the ability to interact with the nitrogenous bases of ssDNA/RNA, leading to immobilization of these bases on the Au atoms surface[48] proteins: Disease can be diagnosed by detecting the presence of certain biomarkers related to the disease. For instance , AuNP was used for the detection of Ricinis communis agglutinin (RCA120), (Lectin Con A) ,cholera toxin , inter-leukin , vascular endothelial growth factors , Annexin II and MUC5AC antigens , antigens of Schistosoma japonicum , Salmonella typhi , Escherichia coli O157:H7 and osteoprotegerin [49].Also , gold nanoparticles are used for detection of amino acids such as cysteine , and peptides . inorganic ions (  $Pb^{2+}$ ,  $Cd^{2+}$ ,  $Co^{2+}$  ,  $[Ru(bpy)_3]^{3+}$ )  $Hg^{2+}$ ,  $Cu^{2+}$ ), anions ( $AcO^-$ ,  $HPO_4^{2-}$ , dihydrogen phosphate,  $I^-$  and  $PF_6^-$  ,  $Cl^-$ ,  $Br^-$ ,  $I^-$ ,  $AcO^-$ , and  $NO_3^-$  , malonate ,F<sup>-</sup>) [50] melamine , pesticides [51].

## **J. Objective of this work**

Curcumin and Polymer of PEG were used as a reducing and stabilizing agent respectively which is considered as a green syntheses route for NP syntheses. The chemical method for syntheses of gold nanoparticle is often used. It involves reductive and capping agents such as sodium borohydride, sodium citrate and sodium dodecyl sulfate. Most of these chemicals are toxic and their use in medical research is restricted. In addition, some of these chemicals remain unreacted and free in solution and can end up as environmental pollution.

Considering the adulteration of melamine in milk and animal feeds, there is a need for establishing sensitive and reliable methods that are capable of screening samples and confirming the presence and quantities of melamine and other metabolites. Curcumin mediated

AuNps conjugated with PEG thiol acid was proved as a simple method for determination of melamine.

Presence of some metals such as cadmium, lead mercury etc., in environment cause health risks and hazards. Many spectrophotometric, electroanalytical methods are available to detect trace amount of metals in many relevant samples which can be used. However, these are time consuming, expensive set up is required. That is why an easier and less expensive technique is required. Chemosensing is a fluorescence-based method having the advantages over the aforementioned methods, where a chemo-sensor is used to detect trace amount of metal in relevant samples.



## CHAPTER II

### GREEN SYNTHESIS OF CURCUMIN MEDIATED PEG THIOL ACID CONJUGATED GOLD NANOPARTICLES FOR THE DETERMINATION OF MELAMINE

#### A. Introduction

Nanotechnology is a rapidly expanding and large domain involving nanoparticles which are considered as a discovery of the twentieth century (52, 53). The simplest definition of nanoparticles takes into consideration the size/shape as an initial parameter, which is limited conventionally to about 100 nm in any direction (52). Nanoparticles are classified base on different criteria starting with the origin (natural or anthropogenic), the size (between 1-10 nm, 10-100 nm or >100 nm) to end up with the chemical composition (inorganic or organic substances) (54). Essentially, nanomaterials have been used in different area starting with their main application as sensors for the detection of chemicals [55], pesticides [56], heavy metals [57], food borne pathogens and toxins [58,59]. In addition, they are known for their ability to remove contaminants [60,61] as antimicrobials [62,63] and as antioxidants [64]. Michael Faraday in 1857 was the first one to discover the ruby gold nanoparticles (Au NPs), which became the foundation for the modern nanotechnology [65]. Au NPs have wide range of uses in biomedical fields, such as in, sensor [66], clinical chemistry [67], labeling and visualizing [68], single molecule tracking [69], drug delivery [70], immunoassays [71] and genomics [72]. The optical properties of gold nanoparticles, in particular Surface Plasmon Resonance render them a promising tool as a biosensor (73). In the past decades, gold nanoparticles were synthesized using various chemical reduction methods (74), physical method (75), electrochemical methods (76), seeding growth methods (77) and biological methods (78). The optical properties of Au

NPs, in particular Surface Plasmon Resonance absorption, render them a promising tool as a biosensor.

Generally, the chemical reduction method is mainly used, and it is divided in two main parts. The first one consists in the reduction through reducing agent as borohydrides, citric and oxalic acids, sulfites, etc., and the second part using stabilizing agents as trisodium citrate, phosphorous ligand and sulfur ligand. Thus, the used of citrate solution or sodium borohydride considered as toxic may contaminate the finished gold nanoparticles through capping or infiltration which limits its application in biomedical and biological domain especially for clinical purposes (79, 80). For this purpose, it was necessary to find nontoxic and friendly reducing and stabilizing agent to produce Au NPs in different shape. Polymer and curcumin were found to be environmentally friendly and effective in the synthesis of AuNPs.

## **B.Methods**

### ***1.Synthesis of curcumin conjugated gold nanoparticles***

Initially, the synthesis was carried out in neutral aqueous media of pH 7. Since curcumin is insoluble in double distilled water, methanol was used to dissolve it. First of all, 30 mM of PEG thiol acid were dissolved in 15 ml double distilled water and kept at 45 °C for 15 minutes. Second of all, 1 mM of H<sub>2</sub>AuCl<sub>4</sub> dissolved in 15 ml of double distilled water was added. Curcumin at 10 mM was mixed to the solution at the end. The solution was kept in the oven at 45°C for 24 hours. To finalize and to precipitate the gold nanoparticles, the final solution was centrifuged at 20,000 rpm for 25 min at 35°C. To optimize the synthesis conditions, three initial parameters were modified: starting with the surfactant, pHs and finally temperatures. As for the surfactant, PEG thiol acid, mPEG Thiol, and mPEG amine were tested, after that 4

different temperatures were analyzed 30, 45, 60 and 75°C and finally the effect of 4 different pHs was established 4, 7, 10 and 13.

### ***1. Sample preparation for melamine sensing***

For sensing of melamine, 18.91 mg of melamine was dissolved in 15 ml DDW to prepare the stock solution of 10 mM concentration. To prepare different concentrations of melamine ranging between 0 and 10 mM, desired volume from the stock melamine solution was diluted to a volume of 2 ml in DDW. Then 0.2 ml of each melamine solution was added to 0.5 ml Au NRs and 2300 ml DDW. The solution is allowed to rest for 30 minutes for the reaction to take place. The study was established by fluorescence measurements and UV-Visible analysis.

## **B. Results and discussion**

Initially, gold nanoparticles were prepared through one simple pot green synthesis mixing HAuCl<sub>4</sub> with mPEG Thiol acid and curcumin in aqueous media. In fact, the formation of Au NPs depends strongly on the reducing and stabilizing agent, where Au<sup>3+</sup> are reduced to Au<sup>0</sup> by the effect of the reducing agent and they are stabilized according to the stabilizing agent present in the mixture. To demonstrate the role of PEG Thiol acid and curcumin as surfactant/stabilizing and reducing agent respectively, two different experiments were carried out with/without curcumin. The difference between the two experiments was obvious as is noticed in Figure 9A&B. Interestingly, after 24 h, only with curcumin, AuNPs were formed and this was confirmed from the color change of the solution when curcumin is added to the surfactant. However, without curcumin, the solution remained colorless without any gold nanoparticles formation indicating that no reaction has occurred. Hence, the difference was significant in the

presence of curcumin, where the color changed from pale yellow to dark grey. Therefore, it can be deduced that curcumin is an essential reducing component for this synthesis procedure while mPEG thiol acid help in stabilizing the AuNPs formed. In fact, after adding curcumin to the solution the hydrogen atoms are dissociated from the two OH groups of curcumin from  $\text{Cur}^{3-}$  inducing the deprotonating of curcumin. The second step involves the reduction of  $\text{Au}^{3+}$  to  $\text{Au}^0$ , where  $\text{Au}^0$  undergoes the nucleation and form Au clusters. Further growth occurs the accumulation and the cleavage of Au NPs where Au clusters are adsorbed on the surface and form aggregation to end up with the maturation and the formation of stabilized Au NPs.



**Figure 9 Solution color after 24 hours A: without curcumin, B : with Curcumin**

To evaluate the effect of the surfactant on the synthesis procedure three different PEG surfactants were used: PEG Thiol Acid, mPEG Thiol and mPEG Amine. The difference in the results was first recorded by measuring the emission intensity and the synchronous spectra. In order to determine the emission spectrum, the AuNPs were excited at two wavelengths: 425 nm

for curcumin and 500 nm for AuNPs, in the emission wavelength range between 440 and 700 nm and 510–800 nm respectively. The emission spectra at both excitation wavelengths  $\lambda_{\text{ex}} = 440$  nm and  $\lambda_{\text{ex}} = 500$  nm, of AuNPs obtained for the two experiments are shown in Figure 10A and 10B respectively. Both the excitation wavelengths gave similar emission pattern, two main peaks at ~496 nm and ~540 nm and another emission band at ~ 604 nm. The main peak is similar to that of curcumin in aqueous media confirming conjugation of curcumin at the AuNPs surface. The band at 604 nm can be due to emission from AuNPs. However, the change in the intensity for the three surfactants was not that much remarkable. The resonance Rayleigh scattering spectra were measured by applying synchronous fluorescence scan mode by keeping the wavelength interval ( $\Delta\lambda$ ) at 0nm. The resonance Rayleigh scattering spectrum of curcumin conjugated Au NPs at 45°C for three different stabilizing agents is depicted in Figure 10C. The RRS spectra showed two bands, the first band is the excitation band and the other one is around the emission band region of curcumin mediated PEG stabilized Au NPs. Hence, in the region between 500-600 nm relative to the Au NPs bands the higher intensity was obtained when preparing the Au NPs using mPEG Amine and PEG Thiol Acid. To clarify more the effect of the different surfactant the absorbance of the Au NPs was measured. As it is shown in Figure 10D Surface Plasmon Resonance (SPR) absorption for Au NPs appears at a wavelength >520 nm (81).

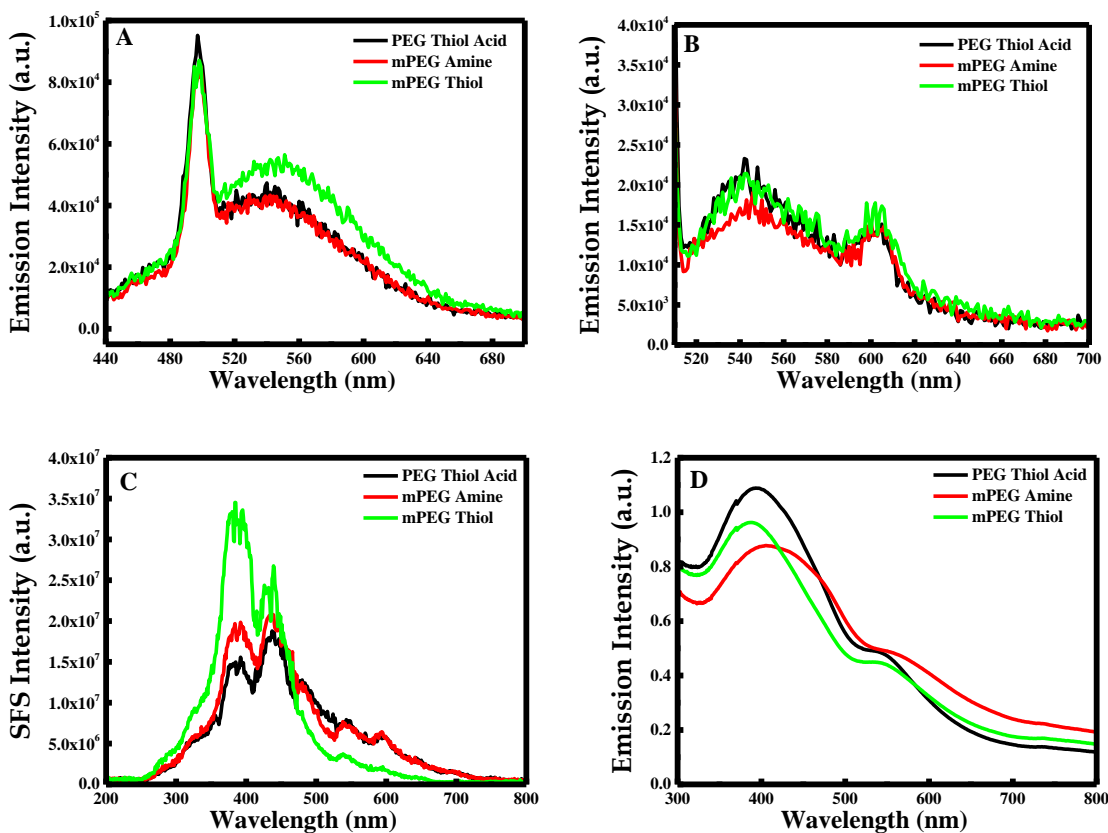
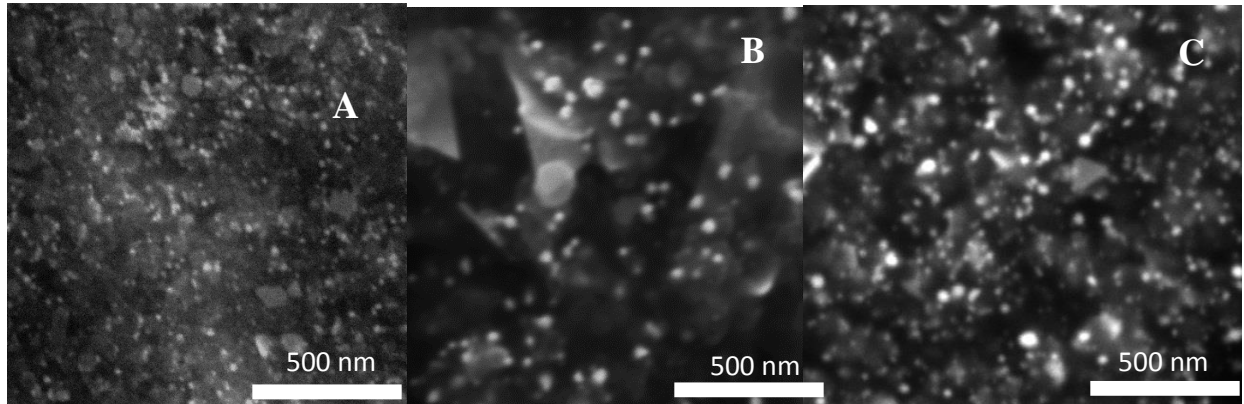


Figure 10: (A) Fluorescence emission spectrum excited at  $\lambda = 425$  nm, (B) Fluorescence emission spectrum excited at  $\lambda = 500$  nm, (C) Synchronous fluorescence spectra at  $\Delta\lambda = 0$  nm and (D) UV-Vis spectra of curcumin functionalized Au NPs prepared using different surfactant.

The maximum and the SPR absorption of the Au NPs depend strongly on the size/shape of the particles formed. In fact, the Au NPs prepared using PEG Thiol Acid have the shorter wavelength  $\lambda = 545$  nm, indicating the formation of smaller Au NPs. This wavelength is red shifted to longer  $\lambda$  equal to 550 and 560 nm for mPEG Thiol and mPEG amine respectively. This shift in the wavelength inducing different particle sizes was easily verified in the SEM. The SEM

images are depicted in Figure 11A, B and C for PEG Thiol Acid, mPEG Amine and mPEG Thiol respectively. Au NPs stabilized with mPEG Thiol Acid have shown the smallest size, ranging between 10 and 50 nm. AuNPs prepared when adding mPEG Thiol and mPEG Amine have relatively larger size which ranges between 30-80 nm. In fact, PEG Thiol Acid have a thiol group (SH group), the Au-to-thiol bond is not covalent (but it has Lewis acid-base interactions) and can thus be affected by “on” and “off” binding. Therefore, a higher order of coordination will drastically decrease the probability of dissociation ligand (via the chelate effect), ultimately producing enhanced affinity to the nano crystal. Stewart et al. found that increasing the number of thiol group per PEG chain, increases the stability of the nanoparticle (82). Consequently, there is a positive correlation between the particle size and the absorbance, RRS and emission intensity, where the AuNPs stabilized with PEG Thiol Acid showed the smallest diameter of Au NPs. The Presence of Au NPs was verified also by EDX analysis, where EDX spectrum demonstrated the presence of Au peaks and carbon peak relative to capping of PEG Thiol Acid /curcumin (See Figure 12A, 12B and 12C). To explain why different trend was obtained in figure C and D, it was noticed that the highest RRS peak in figure C is for Gold nanoparticles synthesized using PEG thiol followed by mPEG amine followed mPEG thiol acid. This trend is attributed to the difference in size of the gold nanoparticles where Au NPs synthesized by PEG Thiol have the smallest diameter as evidenced by SEM. As the size increases, it is expected to scatter more, thus, increasing the RRS intensity. This trend is correlated with the obtained nanoparticle size in SEM. However, in the UV-VIS absorption spectra, two peaks are obtained, one for gold nanoparticles at  $\lambda = 560$  nm and other for curcumin  $\sim 400$  nm. For the peak for AuNPs synthesized with different PEG polymer, the absorbance values were close suggesting amount of AuNPs produced in the three cases was similar. But, the absorbance for curcumin peak is higher

for Thiol acid conjugated gold nanoparticles followed by mPEG thiol and mPEG amine, this can give an insight that curcumin concentration attached to the gold surface is slightly higher in the order of PEG thiol acid, mPEG thiol and mPEG amine.



**Figure 11: SEM images of curcumin functionalized gold nanoparticles prepared using different surfactant: (A) PEG thiol acid, (B) mPEG amine and (C) mPEG thiol.**



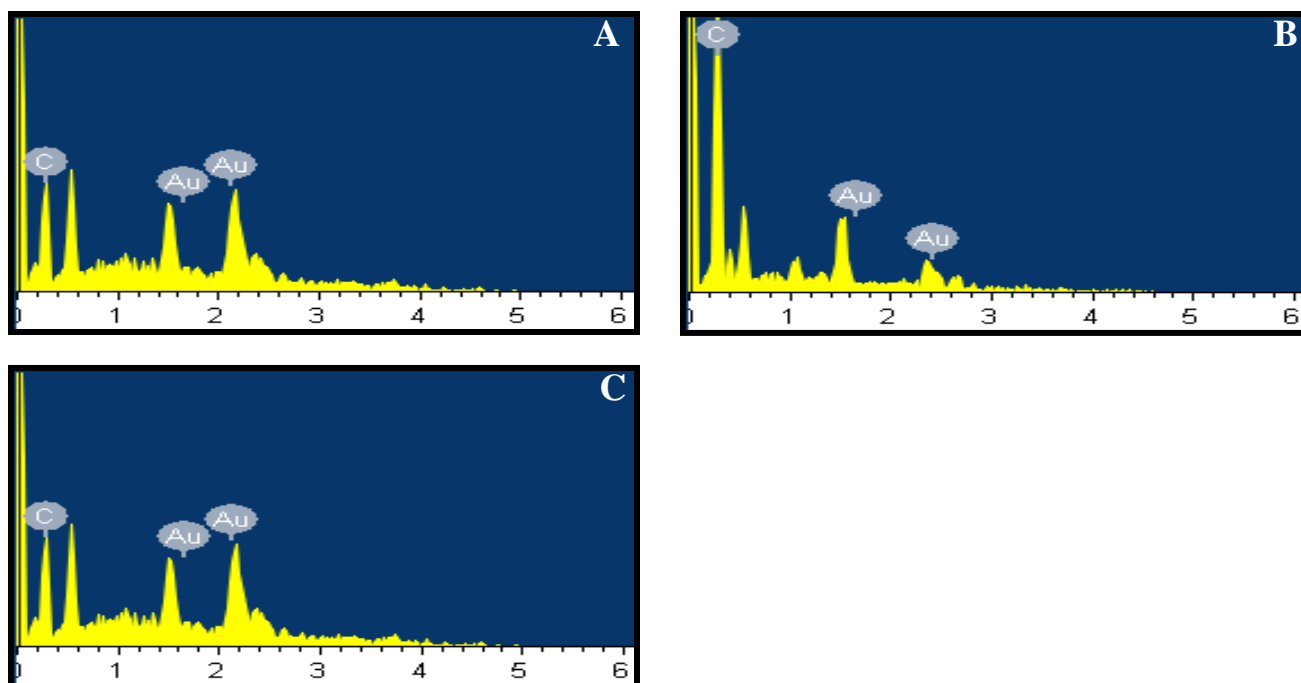


**Figure 12: EDX of curcumin functionalized gold nanoparticles prepared using different surfactant: (A) PEG thiol acid, (B) mPEG amine and (C) mPEG thiol.**

In fact, in acidic or neutral media, curcumin is present in bis-keto form and acts as a potent proton donor. In contrast, in basic media, the enolate form of curcumin in the heptadienone chains predominates; in consequence it acts as an electron donor (83). Hence, the effect of the pH was established on the Au NPs synthesis. For this purpose, 4 different pHs were study respectively; acidic, neutral, basic and extreme basic. As is it shown in Figure 13A&B, when excited at 425 nm and 500 nm, the higher emission intensity was obtained for pH 4 with a slight change in the intensity for pH 7, 10 and 13. However, when measuring the RRS spectrum, the SFS intensity decreases remarkably when increasing the pH as shown in Figure 13 C. Interestingly, the difference was clearer when measuring the absorbance (See Figure 13D) In fact, at extreme alkaline condition (pH 13), a clear peak was obtained at 550 nm for Au NPs otherwise no peak of curcumin was noticed. In contrast at pH 4, 7 and 10 where the Au NPs peak was not well shaped, curcumin peak was obtained at 425 nm. However, the absorbance of the curcumin peak decreases when increasing the pH verifying the role of curcumin as electron

donor in basic media to promote the reduction of  $\text{Au}^{3+}$  to  $\text{Au}^0$ . Hence, a blue shift of Au NPs peak was observed when increasing the pH from  $\lambda=560$  nm (pH 4 and 7) to  $\lambda=545$  nm (pH 13) resulting in the formation of smaller particles in alkaline media.

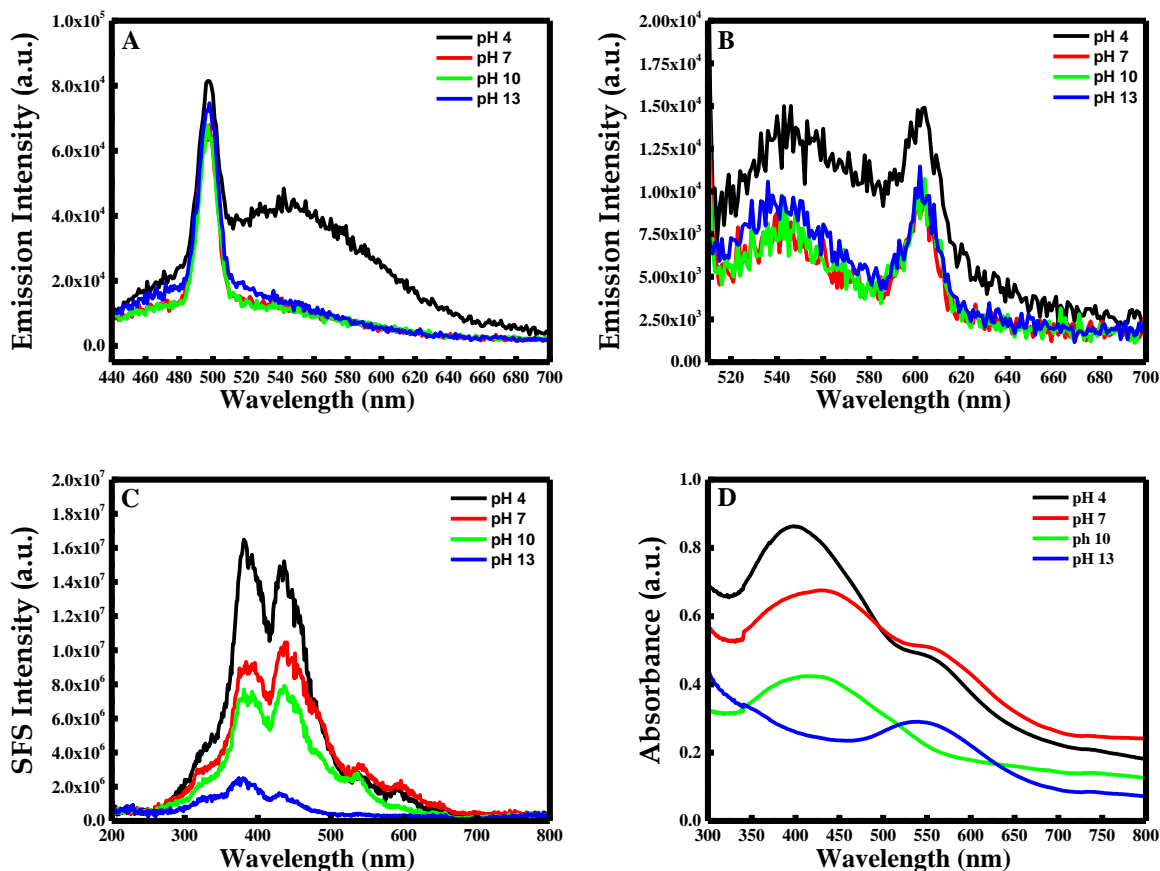


**Figure 13: (A) Fluorescence emission spectrum excited at  $\lambda = 425$  nm, (B) Fluorescence emission spectrum excited at  $\lambda = 500$  nm, (C) Synchronous fluorescence spectra at  $\Delta\lambda = 0$  nm and (D) UV-Vis spectra of curcumin functionalized Au NPs prepared at different pH.**

The different in the size was verified by SEM, where at pH 4 and 7 spherical particles were obtained with size ranging between 30-50 nm and spherical particles  $<20$  nm where formed at pH 13 (See Figure 14A,B,C&D).

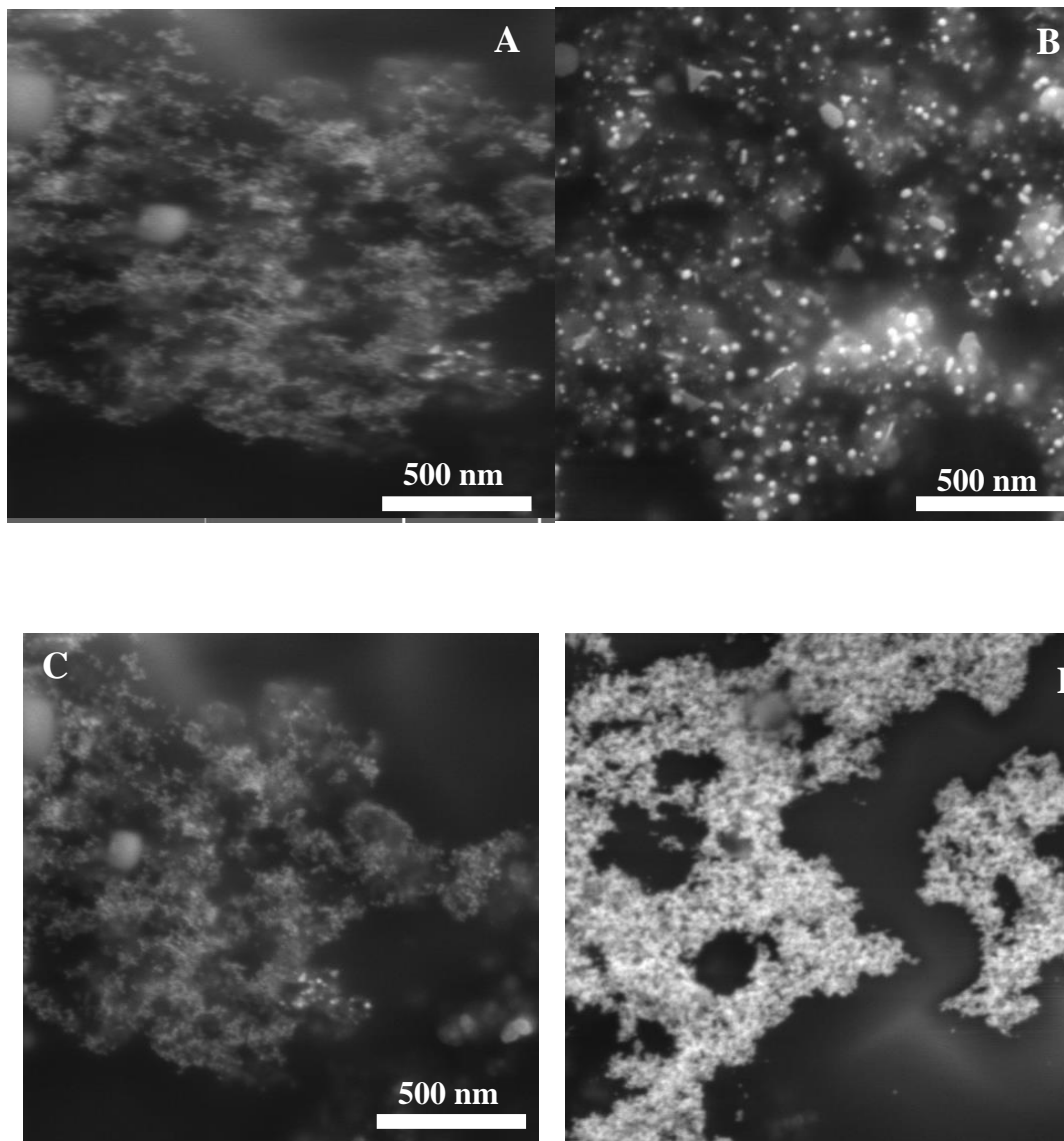


**Figure 14: SEM images of curcumin functionalized gold nanoparticles prepared using different pH: (A) pH 4, (B) pH 7, (C) pH 10 and (D) pH 13.**

The effect of pH was also investigated using zeta potential analysis. As seen in Figure 15A&B, zeta potential value of AuNPs prepared at pH 4 and 13 were equal to -18.86 mV and -0.18 mV respectively. Sun et al. studied the effect of pH on citrate coated Au NPs, they found that at low pH, the Au nanoparticles have less potential because of the increased chemical potential of H<sup>+</sup> ions in solution. Between pH 4.0 and pH 8.0, the zeta potential changes mildly. At pH 12.0, the zeta potentials of Gold NPs reach the minimum values less than -30 mV. However, at pH > 12.0, the zeta potentials dramatically increase. In this case, the colloidal particles aggregate to large agglomerates (93). This perfectly correlates with our Zeta Potential values, where for pH 4, the zeta potential is equal to -18.86 mV, and for pH 13 (pH > 12.0) the zeta potential value is -0.18 mV.

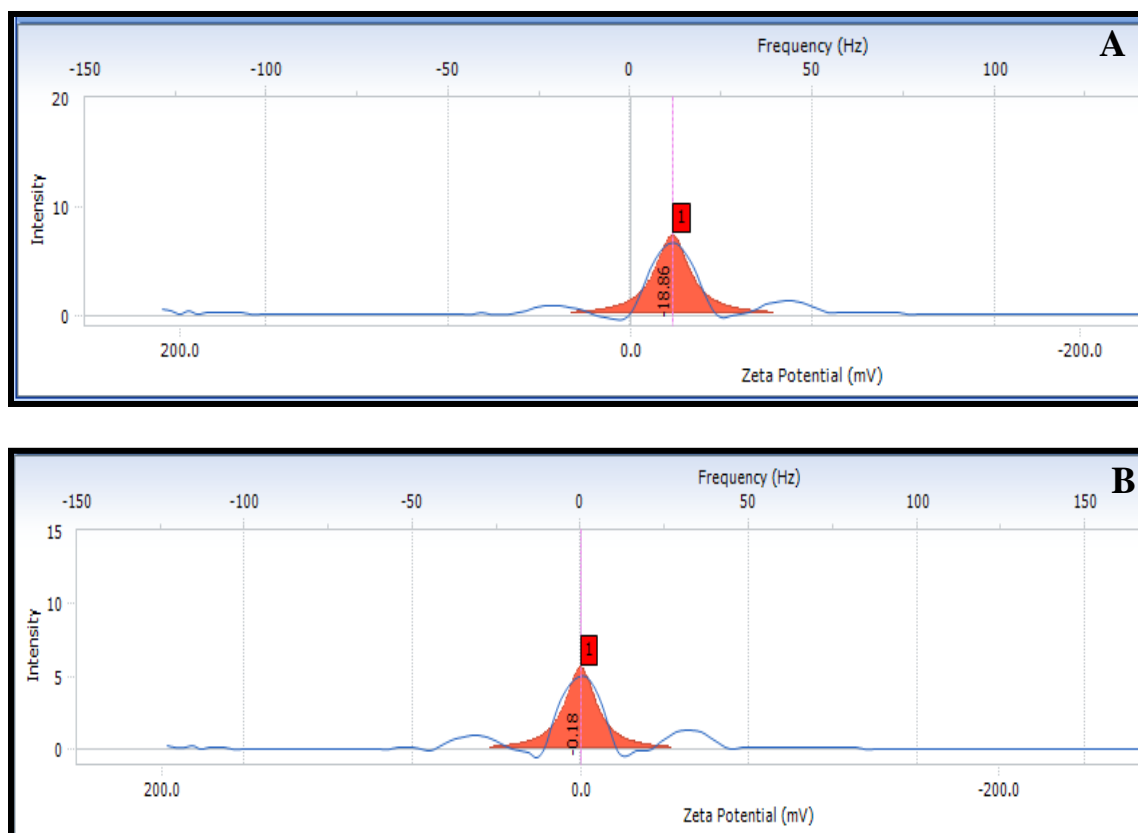


**Figure 15: Zeta potential value of curcumin functionalized gold nanoparticles prepared at (A) pH 4 and (B) pH 13.**

As for the particle size, dynamic light scattering measurement was done to evaluate the exact diameter of the nanoparticles formed at pH 4 and pH 13. Dynamic light scattering (DLS) technique is utilized as a diagnostic tool for particle size distribution (PSD) in colloidal suspensions or solution, which has been widely used in science and industry. Dynamic Light scattering (DLS) is usually used to monitor the size of gold nanoparticles. In our experiment, DLS is used at temperature of 25 °C and for 25 accumulation times to detect the size and possible aggregation of gold nanoparticles synthesized at two different pH: pH 4 and 13. The average diameter at pH 4 was found to be 257 nm, which contrast the results obtained by SEM where extremely small nanoparticles are formed .This suggests the possibility of aggregation of the concerned nanoparticles at pH 4. At pH 13, DLS successfully monitors the distribution of the gold nanoparticle size, the average of it was found to be equal to 57.5nm, slightly higher than the value obtain using SEM, verifying the stability of the particles prepared at pH 13 where no aggregation was occurred. Particle size analysis is shown in Figure 16A&B.

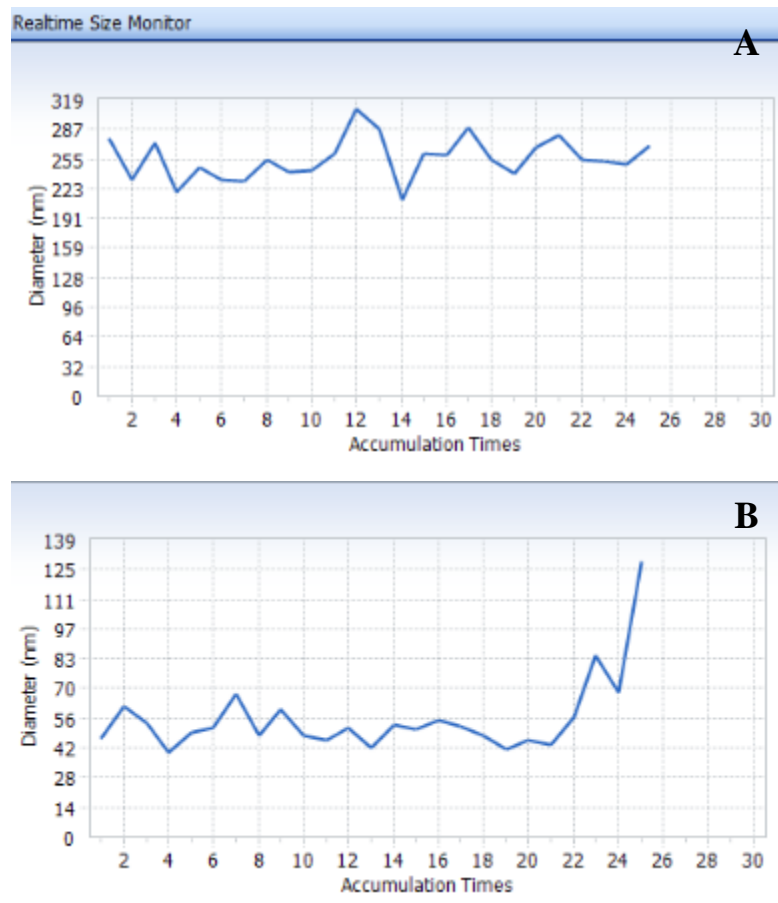


**Figure 16: Particle size distribution value of curcumin functionalized gold nanoparticles prepared at (A) pH 4 and (B) pH 13.**

During synthesis, four different temperatures were tested: 30, 45, 60 and 75°C. In fact, the temperature had a significant effect on the Au NPs synthesis. The emission spectrum at  $\lambda_{ex}=425$  nm and  $\lambda_{ex}=500$  nm was depicted in Figure 17 A&B respectively. It is remarkable that the Au NPs prepared at 45°C presented the high emission intensity. In fact, the RRS signal showed in Figure 17 C reveal high intensity for 45°C and 75°C degree at 500 and 600 nm. The main difference between these two temperatures was when measuring the UV-Visible spectra, where at 45°C a well-defined peak at 560 nm was obtained inducing small particle size of the Au NPs formed at 45°C (See Figure 17D).



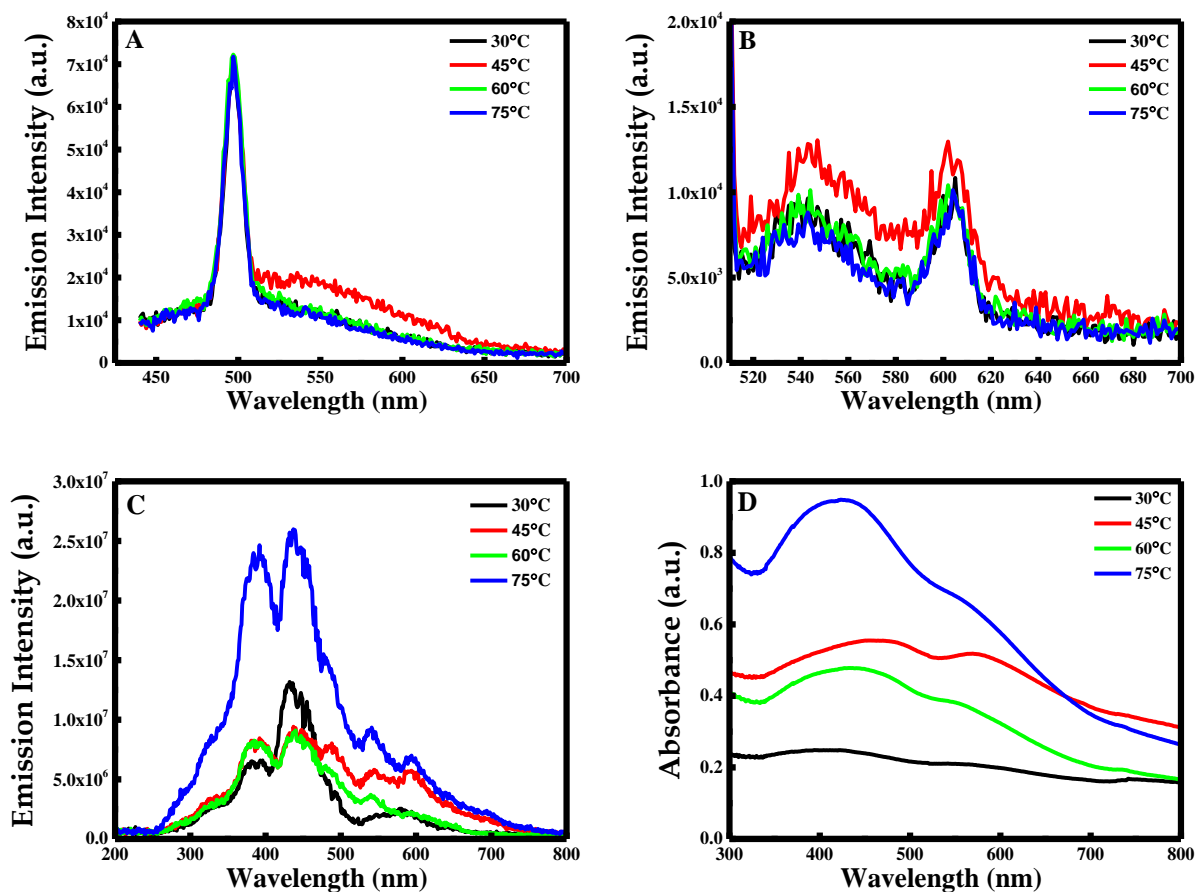


**Figure 17:** (A) Fluorescence emission spectrum excited at  $\lambda = 425$  nm, (B) Fluorescence emission spectrum excited at  $\lambda = 500$  nm, (C) Synchronous fluorescence spectra at  $\Delta\lambda = 0$  nm and (D) UV-Vis spectra of curcumin functionalized Au NPs prepared at different temperature.

Hence, SEM images depicted in Figure 18 A, B, C &D, reveals the formation of small Au NPs with 20 nm diameter when the reaction temperature is equal at 45°C. In contrast bigger Au NPs with a diameter equal to 40-50 nm were obtained when the mixture was carried out at 30, 60 and 75 °C.

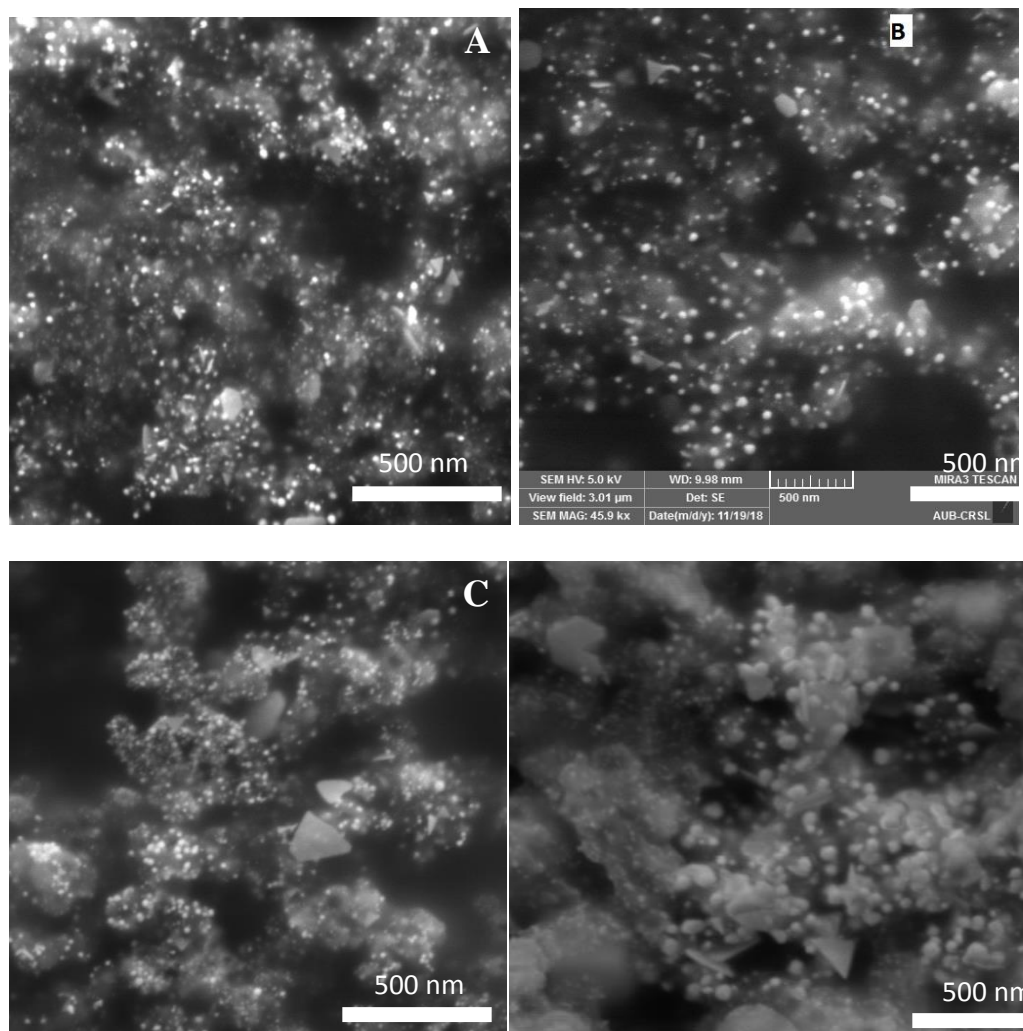


**Figure 18: SEM images of curcumin functionalized gold nanoparticles prepared using different temperature: (A) T= 30 °C, (B) T= 45 °C, (C) T=60 °C and (D) T=75 °C.**

Gold nanoparticles prepared at pH 4 and 13 were characterized through X-Ray diffraction technique (XRD). The X-ray diffractograms depicted in Figure 19 were similar for the Au NPs prepared at pH 4 and pH 13. The characteristic peaks of AuNPs are found to be at  $38.269^\circ$ ,  $44.600^\circ$ ,  $64.678^\circ$ , and  $77.549^\circ$ . These peaks are assigned to the (111), (200), (220), and (311) reflections of the face centered cubic unit cell respectively, which are typical for gold nanoparticles (84). As for the curcumin, the characteristic peaks were present at  $14.20^\circ$ ,  $17.53^\circ$ ,  $18.44^\circ$ ,  $22.55^\circ$ ,  $24.54^\circ$ ,  $25.86^\circ$  and  $27.01^\circ$ (85). However, it is clear that in both cases most of curcumin peak were absent in the X-Ray diffractograms of AuNPs except the peak at  $14.20^\circ$  was present in the AuNPs prepared at pH 4 at high intensity and it was absent at pH 13 revealing that curcumin was more reacted at pH 13.

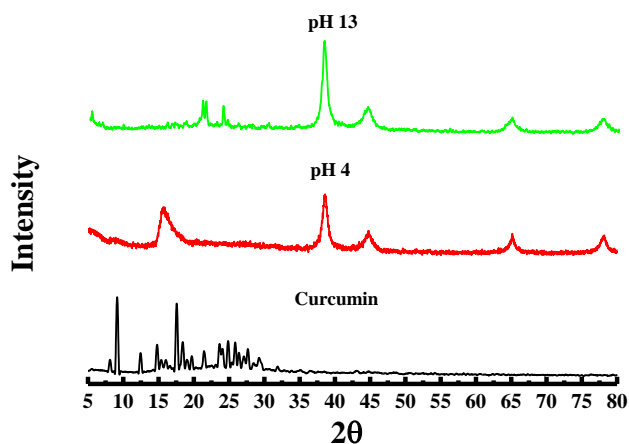


**Figure 19: X-ray diffraction pattern of curcumin functionalized gold nanoparticles prepared at pH 4, pH 13 and curcumin.**

In addition, the two different cases and curcumin were characterized using TGA analysis (See Figure 20). Results showed that weight loss of water was around 10 % in the AuNPs synthesized at pH 4 and around 17 % in AuNPs synthesized at pH 13 between 30 to 130 °C.

However, from 170–420 °C both curcumin and PEG residues are decomposed. A Poly ethylene glycol polymer standard was seen to degrade at a temperature lower than 300 °C; however, the PEG attached nanoparticles appeared to degrade at higher temperatures (300–500° C), this is due to the fact that a higher energy is required to cleave the Au thiol bond, and the local boost in PEG density at the Au NPs surface compared to the free PEG polymer in the standard sample(86). The TGA curve shows that 50% weight loss of curcumin is occurred at 400 °C. In fact, at pH 4 the loss mass in curcumin was higher than the mass loss for the particles prepared in basic media. This is due to the fact that in acidic media, curcumin is not 100% soluble which means that unreacted curcumin is being mixed with the relative AuNPs. In addition, for pH 4 at T°C higher than 500 °C no remarkable loss mass were obtained. However, a weight loss of 50 % was found at ~900°C for pH 13, indicating that PEG thiol acid was being more attached on the AuNPs surface.

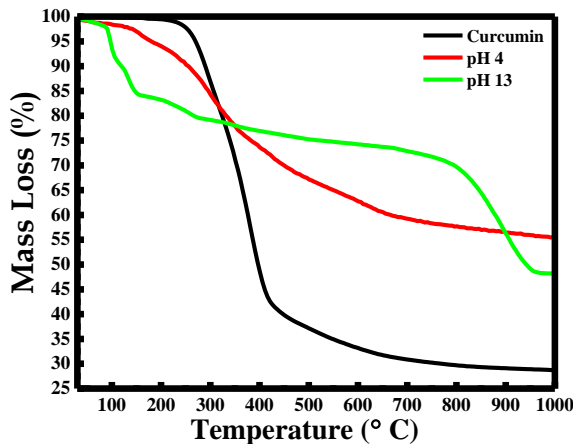


**Figure 20: TGA of curcumin functionalized gold nanoparticles prepared at pH 4, pH 13 and curcumin.**

Furthermore, FTIR spectra were done for curcumin and AuNPs prepared at pH 4 and pH 13 in the wavenumber range between 3800 and 500  $\text{cm}^{-1}$  (See Figure 21). FT-IR spectra for curcumin alone, Au stabilized nanoparticles at pH 4 and 13 were recorded. For curcumin alone, a spaced doublet at 1628 and 1600 can be attributed to the unsymmetric and symmetrical stretching of the two alkene groups conjugated to 1, 3-diketone functional group. At 1508 nm, the peak is attributed to the aromatic ring. As clearly noticed, the aforementioned peak at 1628 and 1600 are still present in the gold peaks at pH 4 and 13. The peak at 1508 is present at pH 4, however absent at pH 13. Moreover, the peak at 1700 which corresponds to the carbonyl group show a shift at pH 13; however, it did not change at pH 4. This might suggest that curcumin better stabilizes gold nanoparticles at pH 13, where a reaction has taken place by the replacement of Au Nps with the enolic H; moreover, the carbonyl group helps in the reduction process of Au NPs. No peak is present at 2971 which corresponds to the OH stretch of the carboxyl group of the PEG thiol acid.

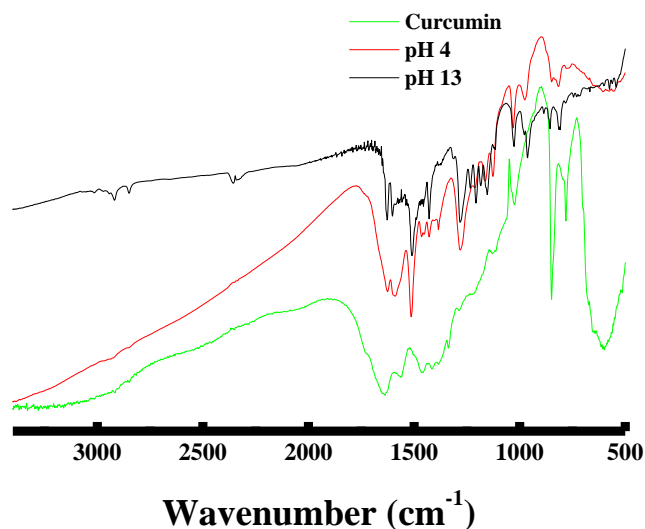


**Figure 21: FT-IR spectra of curcumin functionalized gold nanoparticles prepared at pH 4, pH 13 and curcumin.**

Indeed, during synthesis it was noticed that the color of the solution changed directly from yellow to red under pH 13 and after that to purple when  $\text{Au}^{3+}$  are being reduced to  $\text{Au}^0$ . To investigate the kinetic of the Au NPs growth, curcumin mediated Au NPs using PEG TA as stabilizing agent and under pH 13 was established by measuring the absorbance of Au NPs formed through the reaction time by stopping the synthesis in a given interval time. The growth of Au NPs started at  $t=15$  minutes (See Figure 22A) where the LSPR peak in the UV-Visible spectrum appear at  $\lambda=550$  nm and curcumin peak shifted from  $\lambda=440$  nm to  $\lambda=400$  nm. Hence, the absorbance of curcumin decreases respectively within time inducing an increasing in the Au NPs absorbance indicating the progressive formation of the nanoparticles. However, as depicted in Figure 22B, the increasing in the absorbance at  $\lambda=550$  nm stopped around  $t=90$  minutes and remain stable for 24 hours. In contrast, the absorbance of curcumin measured at 425 nm decreased remarkably when the Au NPs are being formed and saturated at  $t=90$  minutes (See Figure 22C).

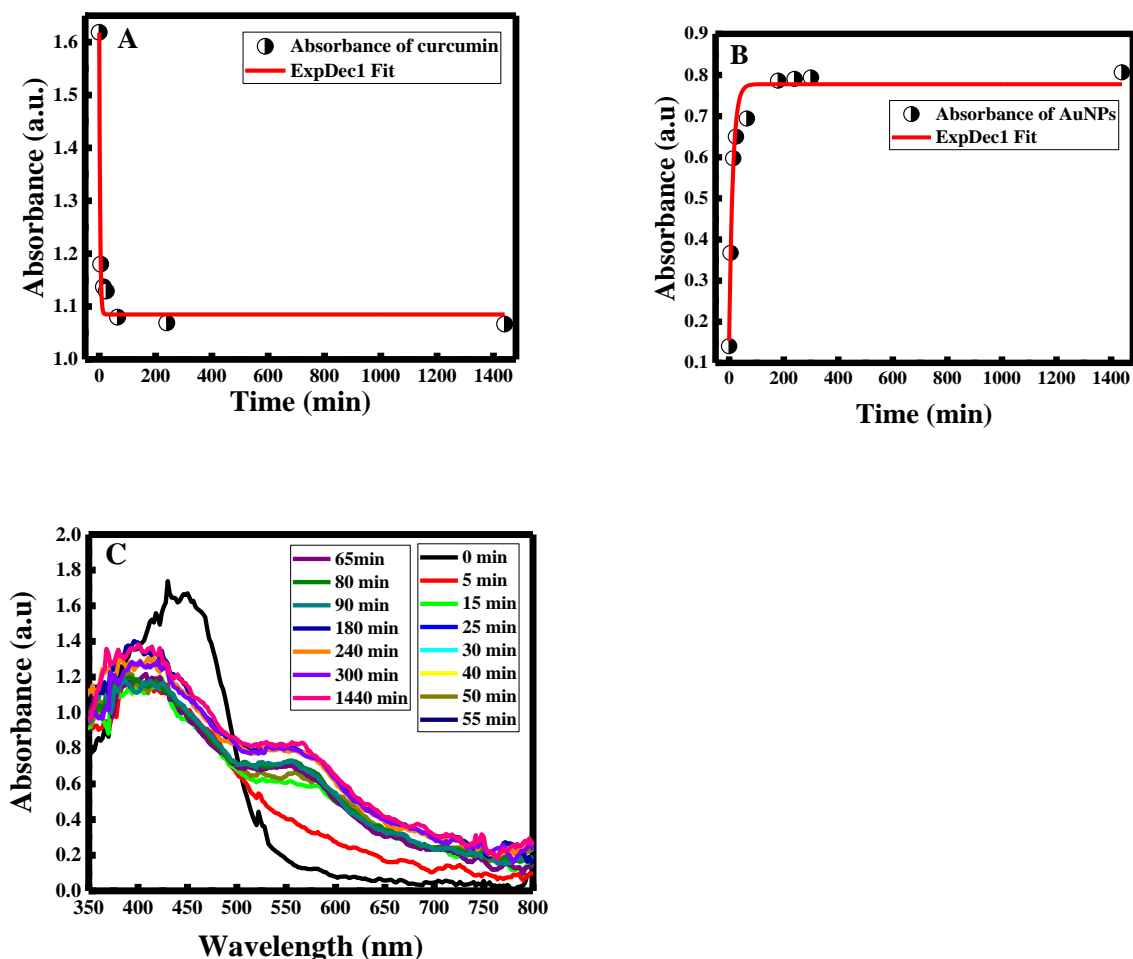


**Figure 22: Change in absorbance of curcumin (A), change in absorbance of Au NPs (B) during its synthesis in extreme alkaline condition and (C) UV-Visible spectra during preparation of curcumin functionalized gold nanoparticles at pH 13 at different time.**

Gold nanoparticles have interesting physical and chemical properties, quite different from those of bulk solids that render them excellent starting material for the synthesis of novel chemical and biological analytical methods (87). Since uniform gold nanoparticles with small size were obtained using PEG Thiol Acid at 45°C in basic media, they were used to design a new sensor to detect melamine. Melamine (2,4,6-triamino-1,3,5-triazine), contain 66% by mass of nitrogen. In March 2007, melamine became one of the most interests in North America when there are reported two cases involving the addition of melamine and its analogues in food (88).



Most of all, analytical methods were used to detect melamine such as liquid chromatography-tandem mass spectrometry (89) and gas chromatography/mass spectrometry (90), gas chromatography-mass spectrometry (91). To this end, other spectroscopic methods were used for melamine determination. For instance, near- and mid-infrared spectroscopy methods (NIR, FTIR-ATR, FTIR-DRIFT) were evaluated for the detection and quantification of melamine in infant formula powder (92). Also, the presence of melamine in milk was detected by interpreting its Raman scattering spectra where intense band at  $676\text{ cm}^{-1}$  determines melamine [93]. These methods are highly sensitive and specific; however, they are time-consuming, and require expensive instrumentation, extensive sample preparation and skilled staff.

In the past decade, gold nanoparticles were extensively utilized in the detection of melamine, because of its simple preparation procedure, and the ability to tune its surface characteristics allowing its functionalization, thus exhibiting good stability for excellent spectral properties such as fluorescence. Interesting work was done by several researchers utilizing these optical properties. Poly(adenine) (poly (A))-templated Au nanoclusters (AuNCs) was employed to determine melamine, where after adding  $\text{Hg}^{2+}$ , the luminescence of AuNCs was quenched by  $\text{Hg}^{2+}$  through the metallophilic interactions between  $\text{Au}^+$  and  $\text{Hg}^{2+}$ . When melamine was added, the fluorescence intensity of sensing system could be recovered, the detection limit is  $16.6\text{ nM}$  [94]. Similar approach was used on gold nanoparticles. Thioglycolic acid-capped CdTe QDs was introduced to citrate-stabilized AuNPs, the fluorescence of CdTe QDs was quenched via the IFE of AuNPs. With the presence of melamine, melamine could cause the aggregation and corresponding absorbance change of AuNPs, the consequence was the recovery of IFE-decreased emission of CdTe QDs [95]. Furthermore, AuNPs functionalized by 3-amino-5-mercapto-1,2,4-triazole (AMTr-AuNPs) was employed to determine melamine. Upon adding melamine to TPN-

AuNCs, a large decrease in their fluorescence intensity was observed, where an electrostatic attraction between melamine and the surface of the TPN-AuNCs which causes the aggregation of TPN-AuNCs, the detection limit was as low as 10 fM/L [96]. Moreover, Fluorescence resonance energy transfer (FRET) between upconversion nanoparticles (UCNPs) and gold nanoparticles (AuNPs) was utilized to determine melamine. An electrostatic interaction between the positively charged UCNPs, which acts as a donor, and the negatively charged AuNPs, which acts as an acceptor, caused the fluorescence quenching of UCNPs through binding. Upon addition of melamine, gold nanoparticles were released from the surface of UCNPs and aggregation due to the N-Au interaction between melamine and AuNPs, which causes recovery to fluorescence intensity of UCNPs. The detection limit of 18.0 nM [97].

Besides colorimetric detection of melamine was widely investigated using gold nanoparticles. In sum, adding melamine will induce aggregation accompanied change in color from red to blue or purple, which can be tracked in decrease or increase in the absorbance intensity of uv-vis spectrum. Using distance-dependent optical properties of gold nanoparticles, melamine could quickly induce the aggregation of gold nanoparticles synthesized in neutral media, thus resulting in red-to-blue or purple color change with detection limit of 0.4  $\mu\text{g/mL}$  [98]. Similar approach was utilized at the ppb-level, when melamine is added to gold nanoparticle, the solution shows a highly sensitive color change from red to blue and rapid aggregation kinetics within the initial 5 min, which can directly be seen with the naked eye and monitored by UV-vis absorbance spectra with a detection limit of 25 ppb [99]. In addition, Colorimetric detection of melamine, by change in color monitored by change in surface plasmon resonance peak of gold nanoparticles, was done by Kumar et al. [100] with detection limit of  $3.96 \times 10^{-7}$  M. Also, Methanobactin (Mb) conjugated gold nanoparticles (Au-NPs) were used to

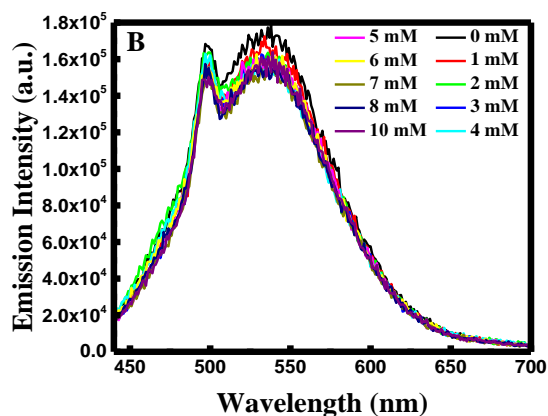
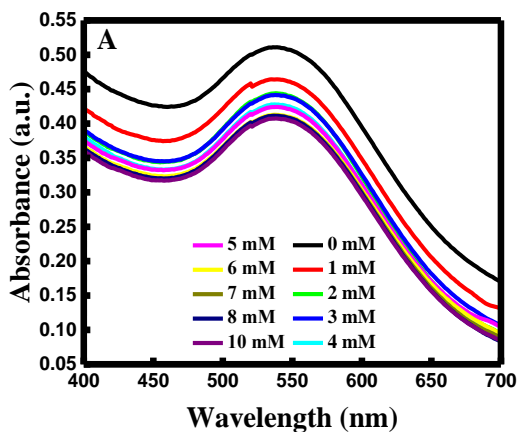
detect melamine. The later interacted with oxazolone ring of Mb, which interrupted the formation of Au-NPs. Too, Melamine could also stimulate the aggregation of formed Au-NPs with a detection limit of  $5.56 \times 10^{-6}$  M (0.7 mg/kg) [101]. Moreover, PEGylated AuNPs with large size could still induce a color change from purple to blue with a detection limit of 1.05 nM [102]. These methods are highly selective, and sensitive for melamine determination. A further insight is provided in this work by Au NPs synthesized through one simple green route using curcumin as reducing agent and PEG thiol acid as stabilizing agent to study later on their capability as sensor in melamine sensing based on LSPR technique.

Melamine sensing in the range of 1-10 mM was studied using gold nanoparticles as probe. The test was established in an essay format where the melamine was added to the prepared Au NPs solution, followed by the addition of melamine in different concentration. The interaction of Au NPs with the melamine molecule was accompanied with a slight change in the color from dark pink to purple upon the addition of melamine, which make the AuNPs came into close to each other and became aggregated. This change in the color was verified by measuring the absorbance and the emission spectrum at 425 nm (See Figure 23A&B). This color change was also associated with the decreasing of the absorbance and the emission intensity along with a red shift from 535 to 540 nm and from 530 to 535 nm respectively. The emission intensity and absorbance are sensitive to particle size/aggregate; thus, presence of melamine in the solution helps in creating aggregates and boosts LSPR intensity. In order to study quantitatively study the efficiency of Au NPs as probe in melamine sensing, the calibration curve was made by measuring the absorbance and the emission intensity in different concentration of melamine. Hence, the absorbance and the emission intensity decreased rapidly once adding melamine. The LSPR measurements for the absorbance and  $I_0/I$  intensity are plotted in Figure 23C&D. As it is

shown in the plot, in the range between 0 and 10 mM the curve showed a well fitted linear change with a linear equation  $Y= 0.0574x +0.46317$  with  $R^2= 0.99254$  for the absorbance measurement and a linear equation  $Y= 0.10796x+1.02452$  with  $R^2= 0.98935$ . Such a good correlation verifies the efficiency of the described method for the determination of melamine in the range between 1 and 10 mM with limit of detection equal to 33nM which was determined by : For a linear calibration curve, it is assumed that the instrument response  $y$  is linearly related to the standard concentration  $x$  for a limited range of concentration ,it can be expressed as  $y=a + bx$  Where limit of detection can be estimated by:

$$LOD=3S_{a/b}$$

where  $S_a$  is the standard deviation of the response and  $b$  is the slope of the calibration curve. The standard deviation of the response can be estimated by the standard deviation of either  $y$ -residuals, or  $y$ -intercepts, of regression lines.



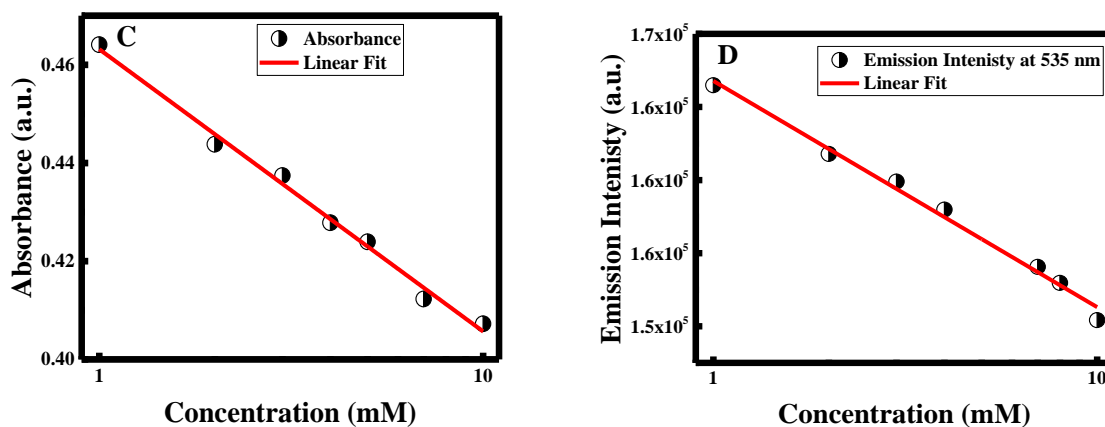


**Figure 23: (A) UV-Visible spectra, (B) Fluorescence emission spectrum excited at  $\lambda = 425$  nm, (C) LSPR measurement and (D) Plot of  $I/I_0$  of curcumin functionalized gold nanoparticles in presence of melamine.**

Method	Linear Range	Limit of Detection (LOD)	References
CdTe doped Si nanoparticles and AuNPs	$7.5 \times 10^{-9} - 3.5 \times 10^{-7}$ M	$8.9 \times 10^{-7}$ M	103
Bare gold nanoparticles (colorimetric)	$1.00 \times 10^{-3} - 6.00$ $\mu$ M	$1.00 \times 10^{-9}$ M	104
Thymine Derivative-Functionalized AuNPs (colorimetric)	0.200–0.450 $\mu$ M	$1.00 \times 10^{-7}$ M	105
Aptamer-functionalized AuNPs(colorimetric)	0 - 1 $\mu$ M	$22 \times 10^{-9}$ M	106

polyethyleneimine functionalized reduced graphene oxide and gold nanoparticles modified electrode	$1 \times 10^{-6}$ - 1.00 $\mu\text{M}$	$2.66 \times 10^{-7}$ M	107
Au@Carbon quantum dots nanocomposites	1 $\mu\text{M}$ -10 $\mu\text{M}$	$3.6 \times 10^{-9}$ M	108
Turn-on fluorescence/Au NCs	0.5–10.0 $\mu\text{M}$	$0.15 \times 10^{-7}$ M	109
Our Method	0 - 10 mM	$33 \times 10^{-9}$ M	-

**Table 1 compares this method to other recent similar methods. Our method shows better or similar detection limit, within the same dynamic range, to recently reported procedure.**

Interestingly, when potential interference like adenine and ascorbic acid was tested instead of melamine no change in the intensity or the absorbance was observed, inducing that our proposed method is selective for melamine sensing (See Figure 24).

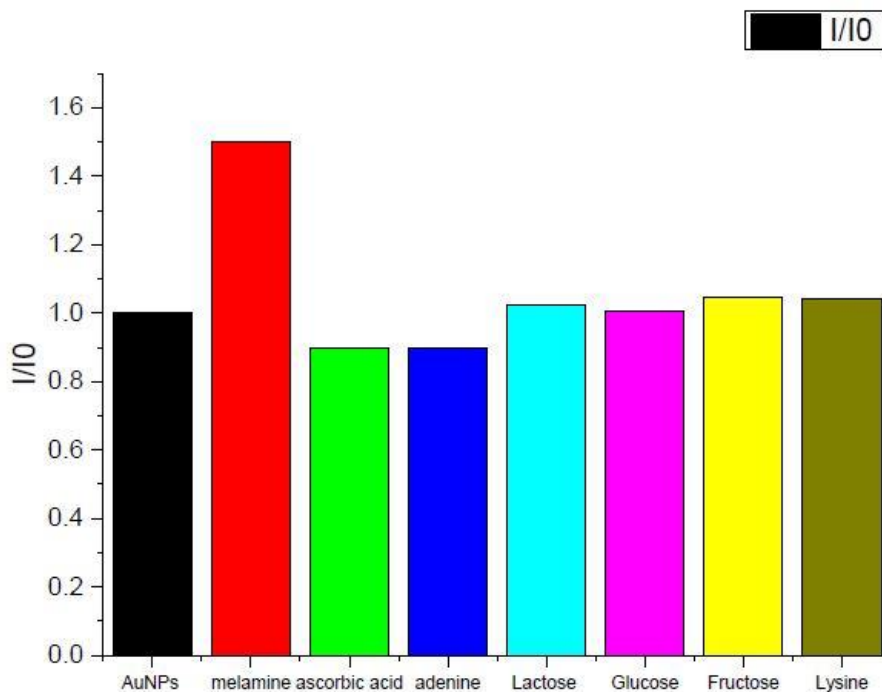


**Figure 24: Ratio of emission intensity (I/I<sub>0</sub>) of Au NPs in the presence of melamine, ascorbic acid, lactose, glucose, fructose, lysine and adenine.**

At the end, in order to investigate the photostability of the Au NPs prepared the emission intensity was measured within 1 hour every 5 minutes with/without melamine as shown in Figure 25. Hence, the I<sub>0</sub>/I signal was found to be stable indicating that our sensor is quite stable during time measurement. Figure 26 shows UV-Visible spectra of curcumin functionalized gold nanoparticles with increase concentration in the absence and presence of melamine.

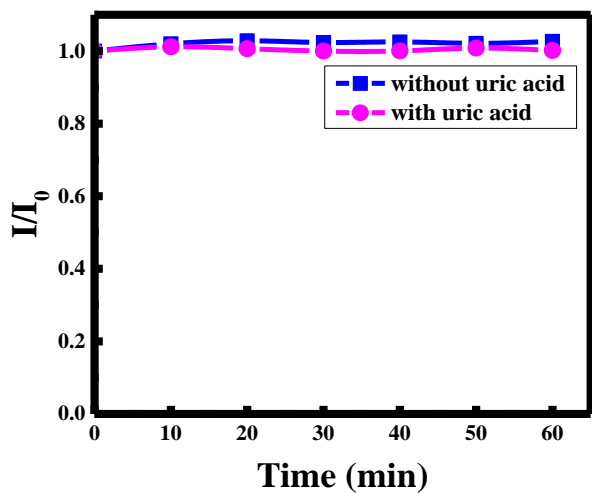
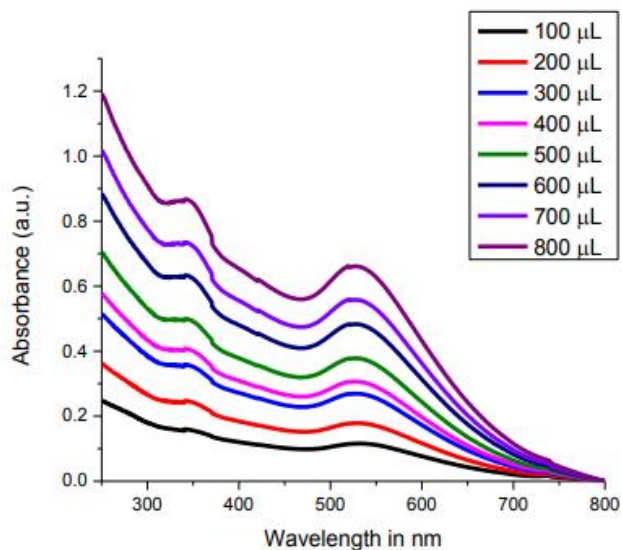


**Figure 25: Plot of  $I/I_0$  of curcumin functionalized nanoparticles with time in the absence and presence of melamine.**



Without Melamine



With Melamine

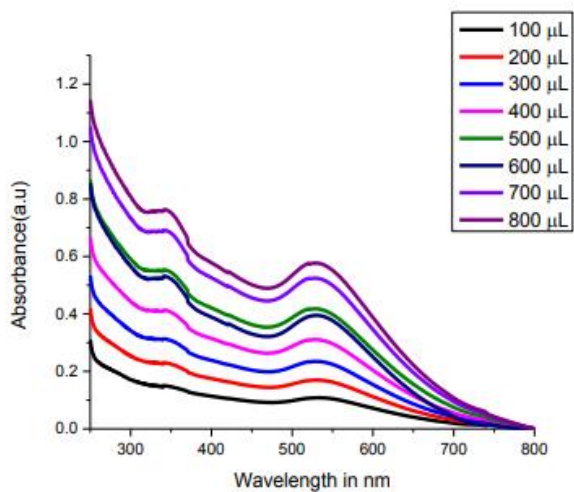


**Figure 26: UV-Visible spectra of curcumin functionalized gold nanoparticles with increase concentration in the absence and presence of melamine.**

### C. Conclusion

It was successfully verified that curcumin mediated stabilized Au NPs could be easily synthesized in a green procedure using eco-friendly reagent. Mainly the synthesis method gave different sizes

of gold nanoparticles in spheres shapes when varying the type of surfactant, the pH and the reaction temperature. It was shown that the Au NPs prepared at pH 13 and at 45 °C are small in size with a diameter equal to 20 nm, which was reflected in a high intensity in RRS peak and UV-vis absorption peak. The formed Au NPs have shown high thermal stability and crystallinity. The produced AuNPs were successfully exploited to design optical method for melamine detection in the range between 0 and 10 mM. The detection limit for melamine was equal to 33nM. The use of curcumin and thiol acid functionalized gold nanoparticles was found to be a high selective probe in measuring melamine, where no interference was occurred when adding Au NPs to dopamine and ascorbic acid. Thereby, the use of curcumin functionalized gold nanoparticles in direct analysis of melamine can be used to develop simple, fast and sensitive novel bio-sensing techniques.

## CHAPTER III

# BINDING OF METAL IONS TO THE CURCUMIN MEDIATED METHOXY POLYETHYLENE GLYCOL THIOL CONJUGATED GREENLY SYNTHESIZED GOLD NANOPARTICLES: A FLUORESCENCE QUENCHING STUDY

### A. Introduction

Designing and fabricating new fluorescent sensing systems for metal ions are of great demand because of their potential applications to chemo-sensors, a device that senses analyte with fluorescent signal transduction [110]. Fluorescent chemosensors are made up from a signaling unit or fluorophore and a guest-binding site or a receptor: the fluorophore and the receptor are usually separated by a spacer unit. Fluorescence is considered as the emission of photon after relaxation from an electronic excited state to the ground state [111]. Chemo-sensors based on changing in the fluorescent intensity are gaining great attention due to their simplicity of measurement, high efficiency, and high sensitivity. The readout of a fluorescent chemosensor is usually a change in the fluorescence intensity, decay in lifetime or a shift in the emission wavelength [112].

Recently, several fluorescence spectroscopic approaches used quenching with metal ions as an approach to design highly sensitive chemosensors. Captopril was studied for binding interaction with biologically active metal ions such as Mg(II), Ca(II), Mn(II), Co(II), Ni(II), Cu(II) and Zn(II) in an aqueous acidic medium by fluorescence spectroscopy[113]. A synthesized chemosensor was found to bind four different transition metal ions such as Hg<sup>2+</sup>, Cu<sup>2+</sup>, Ag<sup>+</sup> and Ni<sup>2+</sup> in mixed aqueous solution at pH 7.2[114].

Suwannee River fulvic acid was investigated for binding with several metal ions, only Al (III), Cu (II), Pd (II) and Tb (III) showed quenching of the fluorescence intensity [115]. Levofloxacin was studied for binding interactions with toxic metal ions such as  $\text{Cd}^{+2}$ ,  $\text{Hg}^{+2}$  and  $\text{Pb}^{+2}$  by fluorescence spectrophotometry. The metal ions quench the fluorescence intensity of LF by forming LF2-metal complex [116]. Moreover, silica nanoparticles having covalently linked luminescent chemosensors were also used, copper, cobalt and nickel ions cause a strong quenching of the fluorescence intensity [117]. Three different anthrylazacrown ethers showed a decrease in fluorescence intensity upon binding of paramagnetic metal cations, like  $\text{Mn}^{2+}(\text{d}5)$ ,  $\text{Co}^{2+}(\text{d}7)$ ,  $\text{Cu}^{2+}(\text{d}9)$  [118]. Fluorescent lifetime quenching of molecular dyes near  $d = 1.5$  nm of the AuNPs showed energy transfer to the metal surface [119]. Fluorophore-labeled DNA oligonucleotides showed extensive quenching when using divalent transition metal ions because of direct DNA-metal ion interactions, leading to combined static and dynamic quenching, with quenching increasing with the number of unpaired electrons in the metal ion and decreasing with the concentration of monovalent ions [120]. Dye-labeled histidine-containing peptides showed quenching with Cu (II) and Ni (II). A strong reduction in steady-state fluorescence was obtained and it was to be unaccompanied by any noticeable changes in lifetime kinetics. This static nature of quenching is not consistent with the dynamic Förster resonance energy transfer (FRET) phenomenon, which was assumed to dominate the quenching mechanism, and is likely caused by shorter range orbital coupling [121].

Heavy metal ions have originally become a world concern, because of their adverse health effects on human; these metal ions are detected in water and soil sources; making water and soil full of contamination [122]. For instance, lead toxicity has severe effects,

such as renal malfunction and the brain development inhibition, so the serum level of lead in young children should not exceed 100 ppb [123]. The toxicity of heavy metal ions is well known, yet even essential metals such as zinc and also copper are toxic at higher concentrations. In the past decade, several methods were used for the detection of metal ions; for example, atomic absorption spectroscopy [124], inductively coupled plasma mass spectrometry [125], electrochemical sensors [126] etc. However, these methods are expensive, time consuming, require sophisticated instruments, and trained staff. Therefore, a rapid, simple and cheap method for the determination of metal ions is of great desire for the public.

Metal nanoparticles, because of their unique optical, electronic, photonic, catalytic, and thermal properties, were widely researched in the past decade. AuNPs of size 3 to 100 nm are of high interest for detection of analytes, because their surface can be tuned by chemical modifications [127]. Due to the wide applications that AuNPs has, scientists around the globe are becoming more interested in environmentally friendly procedures for the syntheses of AuNPs by engineering processes to eliminate the use of hazardous substances through green chemistry. Using plant extract such as curcumin exhibits the ability of reducing the nanoparticle through the hydroxyl and the carboxylic groups which play an important role in the reduction process of  $\text{Au}^{3+}$  to  $\text{Au}^0$  [128]. Compared to chemical, physical and biological synthesis method, the green synthesis method is considered easy, environmentally friendly, and of lower cost [129].

AuNPs were intensively employed in a variety of colorimetric detection of heavy metal ions [130]. Detecting the shifts in surface Plasmon resonance peak, accompanied by change in color, is because of change in the dielectric constant around the nanoparticles

because of adsorption of analyte molecules, or due to analyte-induced agglomeration or aggregation of the nanoparticles [131]. The Surface Plasmon Resonance of AuNPs is also affected by metal ion binding [132]. Through mPEGT (methoxy polyethylene glycol thiol), a stable Au–S bond can be formed. This organic monolayer is obtained through a self-assembly process, which results in a high stable multivalent system. To the best of our knowledge, this is the first work that describes binding of AuNPs conjugated mPEGT with metal ions by fluorescence spectroscopy. In this work, green synthesized AuNPs are established using a simple one-pot methodology with curcumin, as a reducing and methoxy PEGT as capping/conjugating agent to trap metal ions. These AuNP colloidal solutions were used as fluorescence sensors of different metal ions in aqueous solution such as  $\text{Cd}^{2+}$ ,  $\text{Al}^{3+}$ ,  $\text{Cu}^{2+}$ ,  $\text{Na}_2\text{HAsO}_4$ ,  $\text{Pb}^{2+}$ ,  $\text{Hg}^+$ ,  $\text{Hg}^{2+}$ , &  $\text{Ni}^{2+}$  ions and their binding affinity was established.

## **B. Materials and Method**

### ***1. Materials***

Methoxy Polyethylene Glycol Thiol and Gold (III) chloride were purchased from Acros. Curcumin was collected from Sigma Aldrich. Metal salts of:  $\text{Cd}^{2+}$ ,  $\text{Al}^{3+}$ ,  $\text{Cu}^{2+}$ ,  $\text{Na}_2\text{HAsO}_4$ ,  $\text{Pb}^{2+}$ ,  $\text{Hg}^+$ ,  $\text{Hg}^{2+}$ ,  $\text{Ni}^{2+}$  were obtained from local labs in the department. These chemicals were used without any further purification and dissolved in double distilled water. Curcumin was dissolved in methanol.

### ***2. Syntheses of Methoxy PolyethyleneGlycol AuNPs using Curcumin***

In order to achieve mild basic conditions of pH 13, few pellets of NaOH were dissolved in double distilled water and 1 ml was added to the final mixture. Since curcumin is insoluble in water, methanol was used to dissolve it. 30 mM of mPEG thiol were dissolved in 15 ml DDW (double distilled water) and kept at 45 °C for 15 minutes. Then, 1 mM of H<sub>2</sub>AuCl<sub>4</sub> were dissolved in 15 ml of DDW was added. Finally, Curcumin of 10 mM concentration was added to the solution. The solution was kept in the oven at 45 °C for 24 hours. To precipitate the gold nanoparticles, the final solution was centrifuged at 15,000 rpm for 25 min at 20 °C.

### ***3. Sample Preparation for Metal Ion Binding***

For sensing of metal ion, 1 mM of metal ion was dissolved in 15 ml DDW to prepare the stock solution. To prepare different concentrations of metal ions ranging between 0 and 100 μM, first 200 μM of gold nanoparticles was added into labeled vials, then the desired volume of metal ion solution was added to achieve the desired concentration, then the volume was completed to 3 ml. The study was established by fluorescence measurements.

## **C. Results and Discussion**

### ***1. Synthesis and Characterization of Curcumin Mediated mPEG AuNPs.***

#### **a. Visual Identification of AuNPs**

A detailed study of synthesis of gold nanoparticles by mPEG thiol was carried out in this work. Figure 27 shows the Tautomerization reaction between curcumin enol and keto form, which was used as a reducing agent. Curcumin of bright yellow color is a diarylheptanoid. It is considered as a curcuminoid, which are considered natural phenols.

This tautomer is present in its enolic form in organic solvents and in keto form in water [133]. After adding curcumin to the Au salt  $\text{HAuCl}_4$ , a yellow color is first observed, then after achieving mild basic conditions through NaOH, dark pink color appeared in the solution indicating the formation of the gold nanoparticles which was incubated in the oven for 24 hours to achieve an intense color. This color change indicates the formation of the gold nanoparticles. The origin of such coloration is caused by the interaction of the electromagnetic field with the collective oscillation of free conduction electrons; the resonances are named SPR (Surface Plasmon resonance) [134].

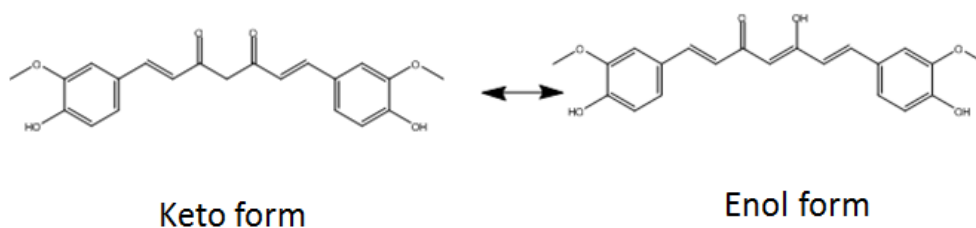


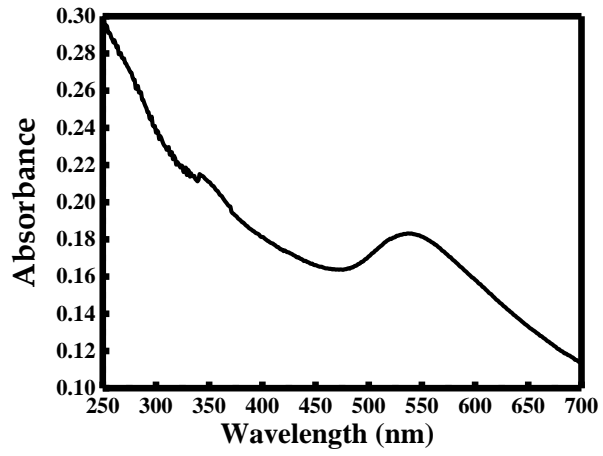
**Fig 27. Shows the Tautomerization reaction between curcumin enol and keto form.**

b. UV–VIS Absorption and SEM Studies

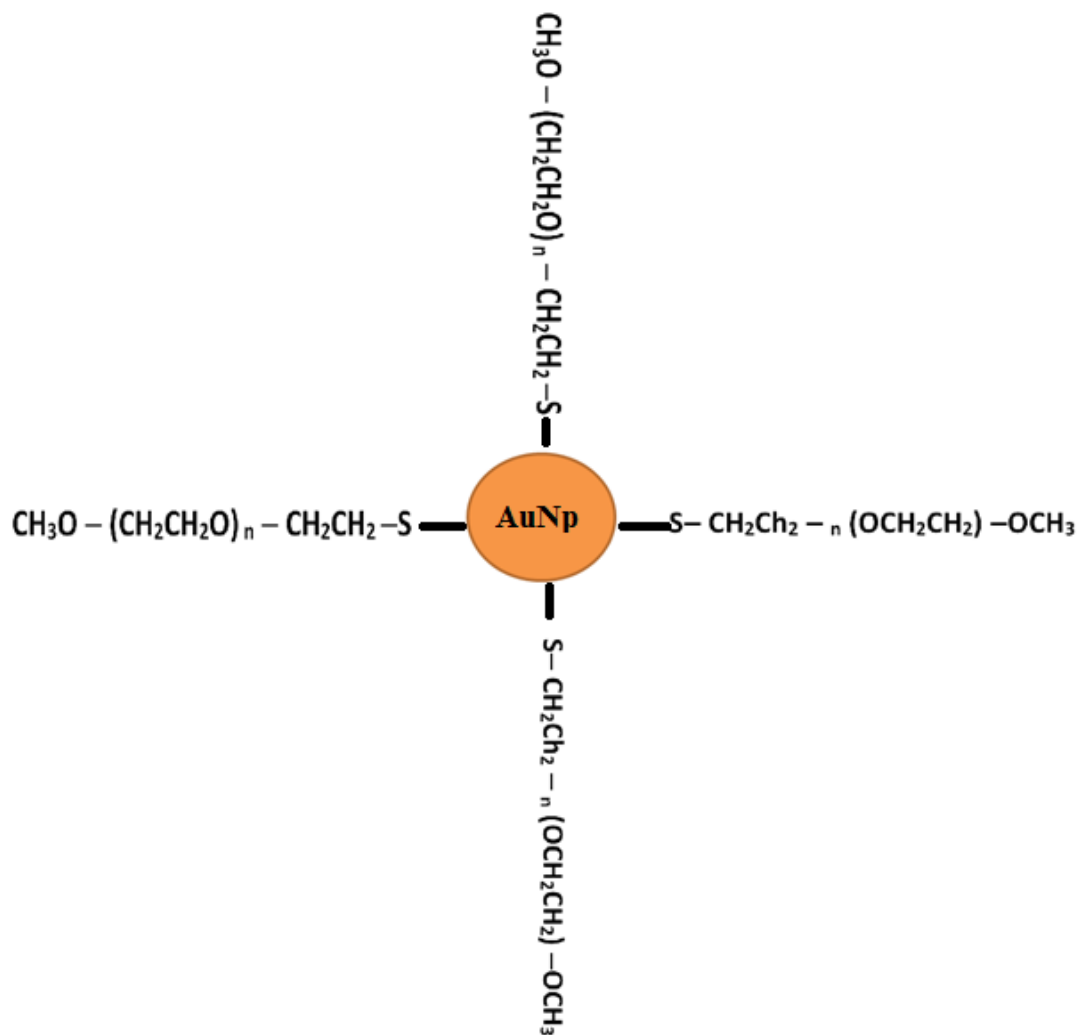
This formed colloidal solution which has a very intense color was inspected by UV-VIS absorption spectroscopy, where the characteristic peak of Au NPs was obtained at wavelength at 539 nm (see Fig 28a). Methoxy polyethylene glycol thiol (mPEG) is chemically linked to the gold surface through Au-Sulfur bond. The other end constituting the methoxy group is pointing toward the colloidal suspension or solution as shown in Fig



28b. From Fig 29A, it can be seen that the morphology consists of spherical like particles with size ranging between 18-40 nm, fig 29 b is the corresponding EDX.



(a)



(b)

**Fig 28: (a) UV-Vis absorption spectrum of PEG thiol AuNPs measured after 24 h; (b) Illustration of ligands containing methoxy PEG-SH used to functionalize the surface of gold nanoparticle.**

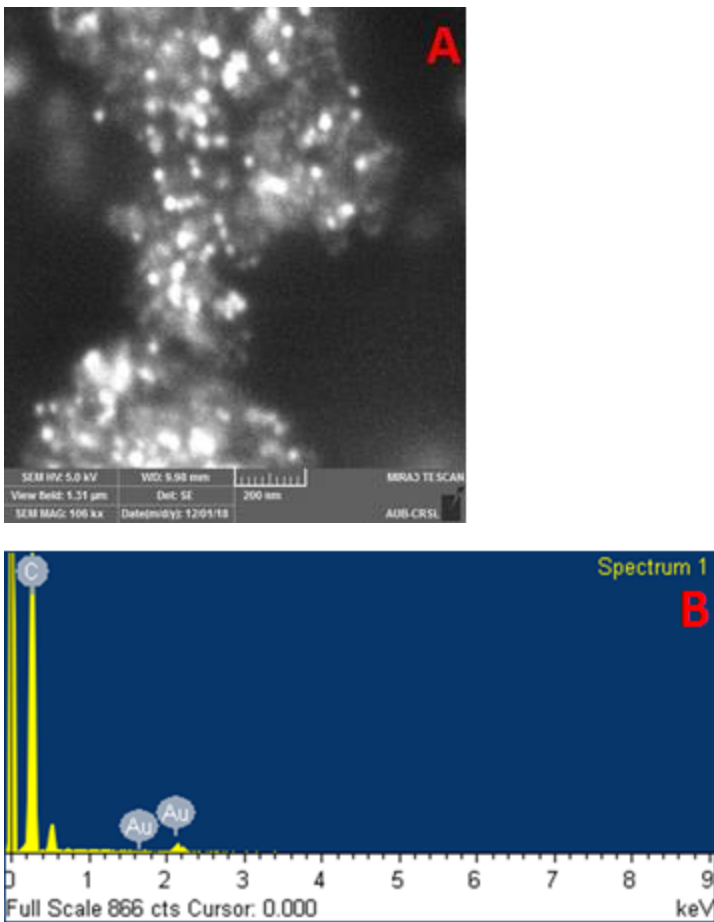


**Fig 29:(a) SEM images reveal that the mPEG Thiol functionalized AuNPs retain their roughly spherical shape, and (b) corresponding EDX image.**

c. XRD, TGA and FTIR Studies

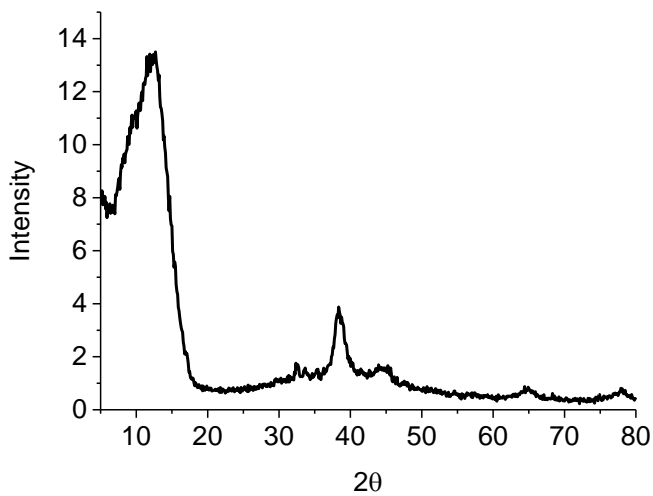


**Fig. 30 XRD patterns observed for Au nanoparticle's colloid.**

A representation of the XRD spectrum is shown in Fig 30. AuNPs shows characteristic peaks at  $38.269^\circ$ ,  $44.600^\circ$ ,  $64.678^\circ$ , and  $77.549^\circ$ . The Bragg reflections attributed to the (111), (200), (220), and (311) sets of lattice planes are seen that may be indexed on the basis of face centered cubic structure of Au[135]. The XRD pattern thus clearly shows that the Au nanoparticles formed by the reduction of  $\text{AuCl}_4^-$  ions by curcumin are crystalline in nature.

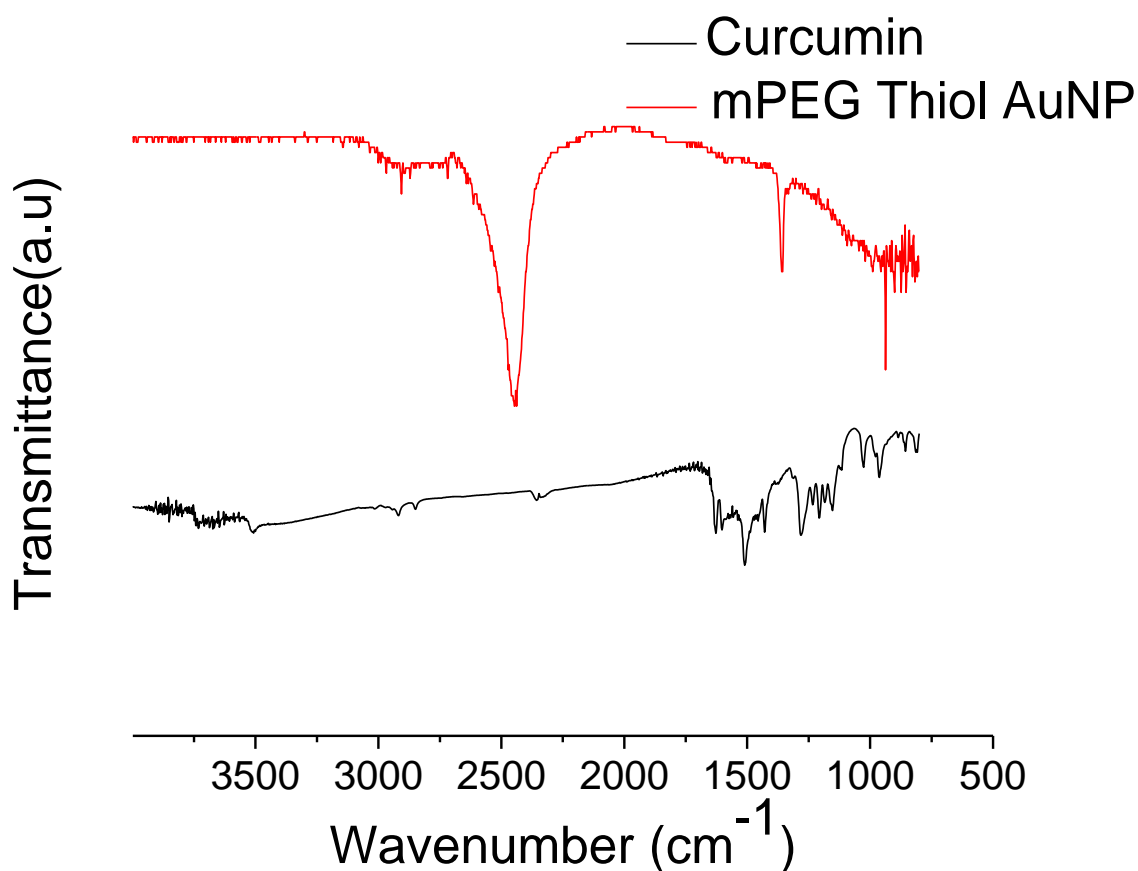


**Fig. 31 FTIR spectrum of curcumin and AuNPs obtained by curcumin extract and mPEG thiol stabilizing agent**

Fig 31 shows FTIR spectrum of curcumin and AuNPs obtained by curcumin extract and mPEG thiol stabilizing agent. Curcumin showed a peak at  $3508\text{ cm}^{-1}$  which correspond to phenolic O-H stretching vibration, another peak is observed at  $1628\text{ cm}^{-1}$  which is associated to the aromatic

moiety C=C stretching , another peak at  $1509\text{ cm}^{-1}$  corresponds to C=O and C=C vibrations),  $1428\text{ cm}^{-1}$  corresponds to olefin C-H bending vibrations[121].For the Au NPs synthesized using mPEG thiol, a peak is observed at  $668.28$  which corresponds to the C-S stretching ,the peaks corresponding to the SH stretching appear in the region  $2600\text{--}2540\text{ cm}^{-1}$  were also observed [136].

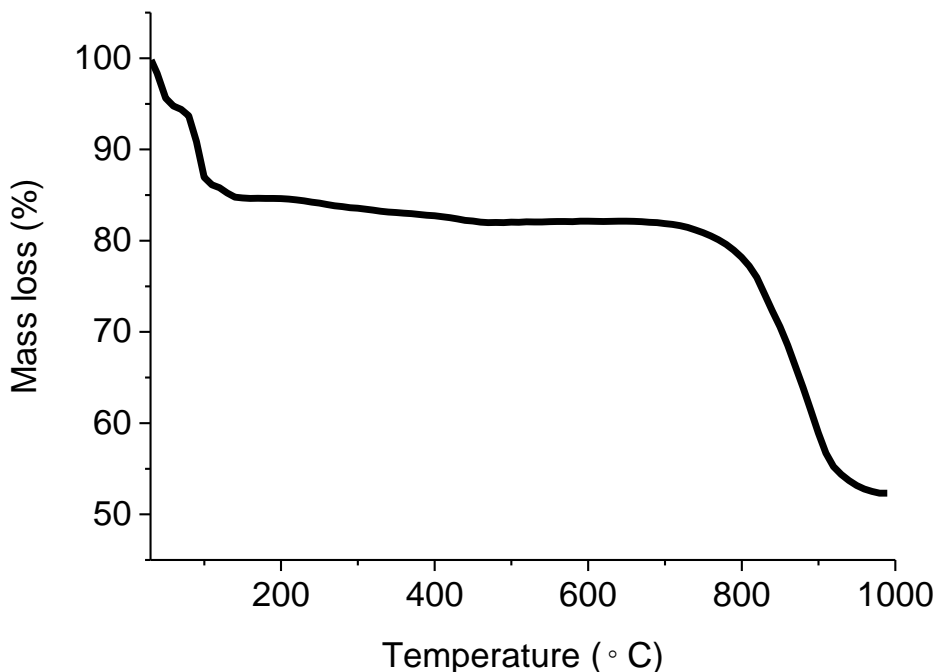


**Figure 32: TGA of mPEG thiol functionalized gold nanoparticles**

The nanoparticles solution was converted to powder before performing characterization. Under inert  $\text{N}_2$ , TGA was performed heating the gold nanoparticle powder from 30 to  $1000\text{ }^\circ\text{C}$  which is presented in Fig 32. 15% weight loss was observed between  $30\text{--}130\text{ }^\circ\text{C}$ . This weight loss corresponds to water loss of our sample. Between  $170\text{--}420\text{ }^\circ\text{C}$ , organics is expected to degrade, so around 5 % of curcumin and mPEG thiol weight loss is monitored. Around 30 % of mPEG thiol is degraded at  $700\text{ }^\circ\text{C}$  this is because of the strong attachment of thiol bond of mPEG thiol to the gold surface [137].

## ***2. Binding of AuNPs with Metal Ions Fluorescence Quenching Study***

The fluorescence spectrum of mPEGT conjugated AuNPs was measured at 425 excitation wavelength and scanned in the emission wavelength range between 440 and 700 nm as shown in Figure 26 A and B (the top black colored spectrum at 0  $\mu\text{M}$  of metal ion). Two peaks were observed, one minor humps at  $\sim 496$  nm due to Raman scattering (normally observed in aqueous media when fluorescence intensity is relatively weak [138]) and the other at  $\sim 540$  nm due to fluorescence emission. This fluorescence spectrum is similar to the fluorescence of curcumin in the aqueous environment [138] indicating curcumin is conjugated along with mPEGT at the surface of AuNPs.

With the successful functionalization of stable mPEGT AuNPs, a series of di- and trivalent metal ions were titrated into a solution of mPEGT modified AuNPs in double distilled water. Various concentrations of each metal ion between 0 and 100  $\mu\text{M}$  in DDW were pipetted into mPEGT AuNP solution. The solution was incubated at room temperature ( $\sim 21$   $^{\circ}\text{C}$ ) in order to allow for complexation between mPEGT and the divalent and trivalent metal cations. The tested metal ions were respectively  $\text{Cd}^{2+}$ ,  $\text{Al}^{3+}$ ,  $\text{Cu}^{2+}$ ,  $\text{Na}_2\text{HAsO}_4$ ,  $\text{Pb}^{2+}$ ,  $\text{Hg}^+$ ,  $\text{Hg}^{2+}$  and  $\text{Ni}^{2+}$ . Before running fluorescence spectral measurement, the solution was vortexed for 30 seconds to make sure of the homogeneity of the solution. Figure 33 depicts fluorescence spectra of PEGT conjugated AuNPs for various concentrations of representative  $\text{Cd}^{2+}$  and  $\text{Al}^{3+}$  ions. The initial fluorescence intensity of the mPEGT functionalized gold nanoparticles which was monitored at 540 nm decreased regularly as the metal ion concentration was increased from 0 to 100  $\mu\text{M}$ .

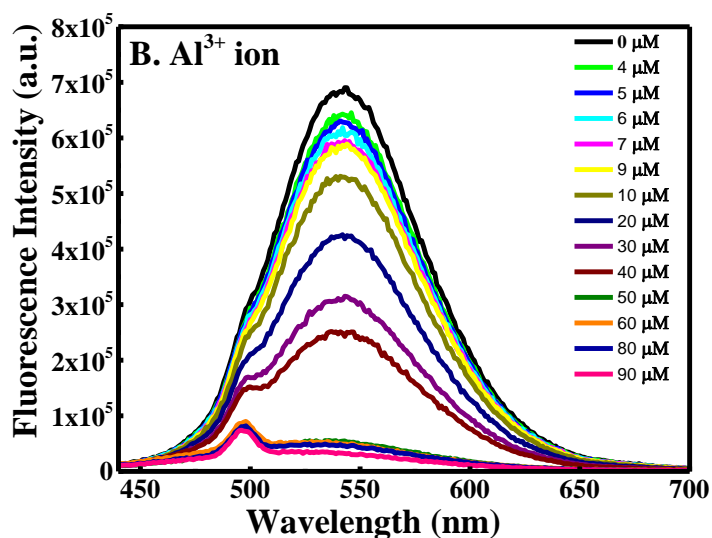
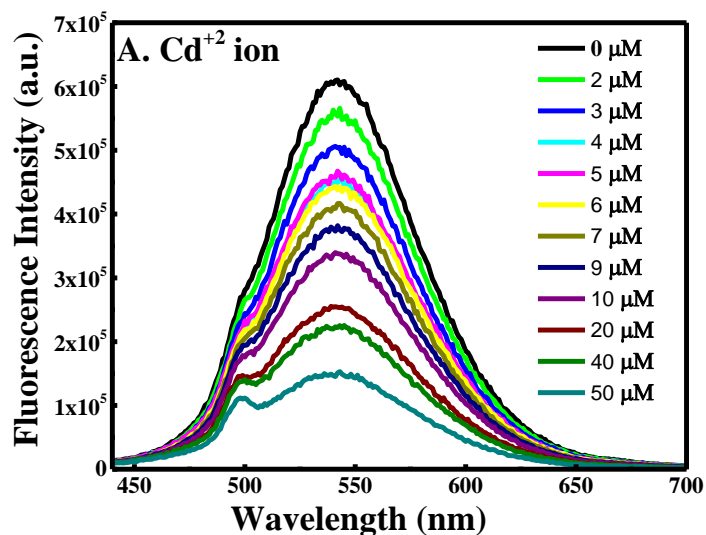


**Figure 33: Fluorescence emission spectra excited at  $\lambda = 425$  nm for mPEGT conjugated AuNPs titrated with varying concentrations of (A)  $\text{Cd}^{2+}$  and  $\text{Al}^{3+}$  ions.**

However, as seen in Figure 33 the emission maximum of AuNPs did not change in the presence of metal ions which suggest that solvent environment around AuNPs remains the same. With further increase in metal ion concentrations, there was also no significant shift of  $\lambda_{\text{em}}^{\text{max}}$ , which suggests there was also no conformational change of the

conjugating ligands around AuNPs under the condition studied here. Nevertheless, the intrinsic fluorescence quenching of mPEGT conjugated AuNPs in the presence of metal ions indicates complex formation between AuNPs and metal ions. Similar results were obtained for other metal ions under investigation.

Although unreacted and free curcumin was removed after centrifugation, curcumin attached with mPEGT conjugated AuNPs during preparation may directly bind with metal ions and influence the fluorescence properties of mPEGT conjugated AuNPs. To test this possibility, interaction of free curcumin in aqueous environment (in DDW as used for mPEG conjugated AuNPs) with various metal ions was investigated. It is reported in literature that fluorescence of curcumin is quenched by  $\text{Hg}^{2+}$  ions [139,140] whereas  $\text{Ni}^{2+}$ ,  $\text{Cu}^{2+}$  and other metal ions have no influence on fluorescence of free curcumin, interestingly in the present case it was found that presence of  $\text{Hg}^{2+}$  ions in solution in the concentration under studied enhanced the fluorescence intensity of free curcumin (see Figure 34). This contrast in the present results could be due to use of organic solvent/host molecule in the literature [139, 140] which facilitate curcumin to come in close contact with  $\text{Hg}^{2+}$  ions. Similar results were found in the presence of  $\text{Ni}^{2+}$  (see Figure 34) and  $\text{Hg}^+$  (not shown) ions. In the present case the enhancement could be due to aggregation/dimerization of hydrophobic curcumin in the presence of metal ions. Therefore, the observed fluorescence quenching of mPEGT conjugated AuNPs in the presence of metal ion is different from the interaction of free curcumin with metal ion. It is reported earlier that metal ions often binds with the methoxy group of the ligands. Therefore, it can be speculated that the metal ions bind with the AuNPs through the methoxy group of the mPEGT associated with AuNPs.



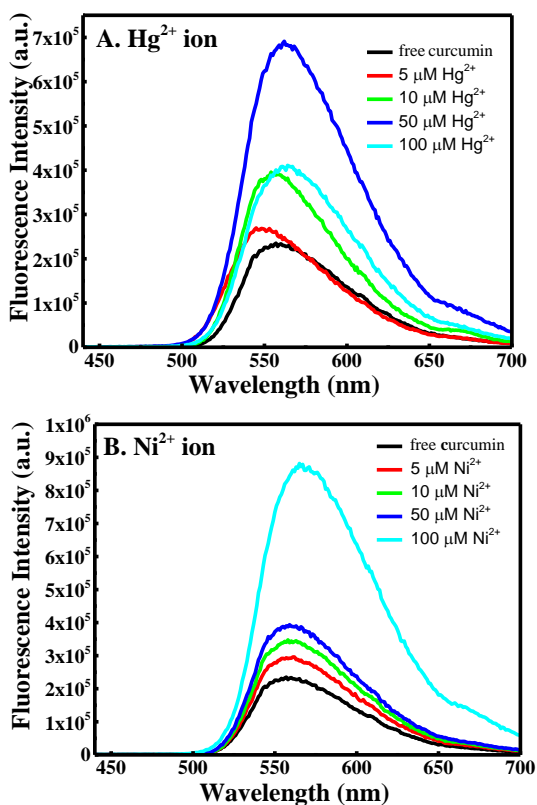


**Figure 34: Fluorescence emission spectra excited at  $\lambda = 425$  nm for free curcumin titrated with varying concentrations of (A)  $\text{Hg}^{2+}$  and  $\text{Ni}^{2+}$  ions.**

Gold nanoparticles functionalized with polymers have been proven an efficient detection system [141]. Quenching of the adsorbed fluorophore is observed, and recovery is monitored after disruption of this adsorption by a target [141]. Because it is considered easy to functionalize gold nanoparticles, different recognition elements & chemical groups can be adsorbed in order to create chemical sensors. In our case methoxy group of mPEGT is pointing toward the solution as depicted in Figure 28(b) and it can be deduced that methoxy ether groups adsorbed to the gold nanoparticles can bind both divalent and trivalent metal ions. An interaction between two molecules usually causes changes in the fluorescence parameters such as quantum yield, intensity or lifetime. There are several

types of mechanisms of quenching called collisional, static, electron transfer or energy transfer at a distance known also as Förster energy transfer. The difference between collisional and static is that in collisional, two molecules diffuse inside the solution and collide because of internal motion or local flexibility. This dynamic quenching occurs during the lifetime of the excited state. However, in static quenching, the quencher molecule binds to the target forming a complex. In this case, quenching takes place by forming a non-fluorescent complex at the ground state. When the complex absorbs light, it directly returns to the fundamental state without emitting any photons [142]. In the case of collisional quenching, the quenching fluorescence intensity can be described by the Stern–Volmer equation:

$$\frac{I_0}{I} = 1 + K_{SV}[\text{metal ion}] = 1 + k_Q\tau_0[\text{metal ion}]$$

Where  $I_0$  and  $I$  are the fluorescence intensities in the absence and presence of metal ion respectively,  $K_{SV}$  is the Stern–Volmer constant.  $k_Q$  is the bimolecular quenching constant expressed in  $M^{-1}s^{-1}$ ,  $\tau_0$  is the excited state lifetime of the AuNPs in the absence of metal ion and  $[\text{metal ion}]$  is the metal ion concentration. This equation describes that the higher the  $K_{SV}$ , the lower concentration of metal ion needed to decrease fluorescence intensity. Plotting  $I_0/I$  as a function of  $[\text{metal ion}]$  yields a linear plot (representative graphs shown in Figure 35) with a slope equal to  $K_{SV}$ . Our results show that Hg (II) and Pb (II) are the two most ions that have the higher  $K_{SV}$  (see Table 2).

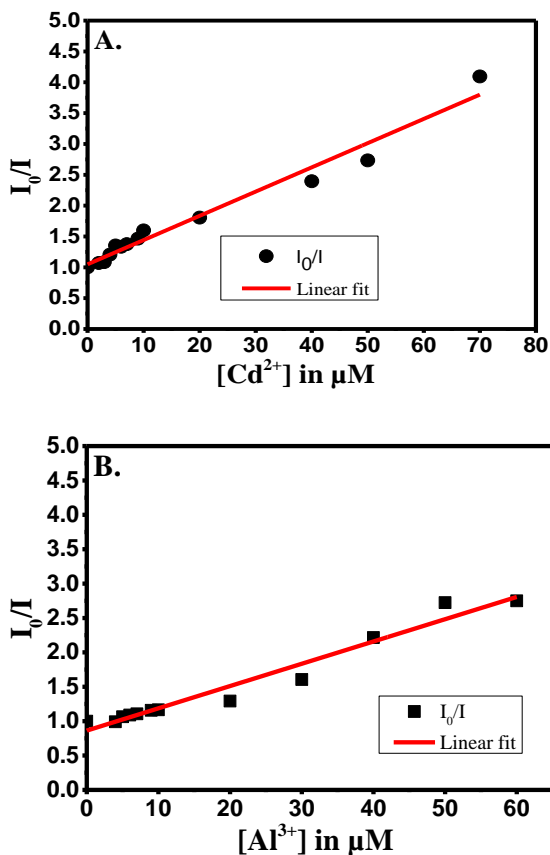


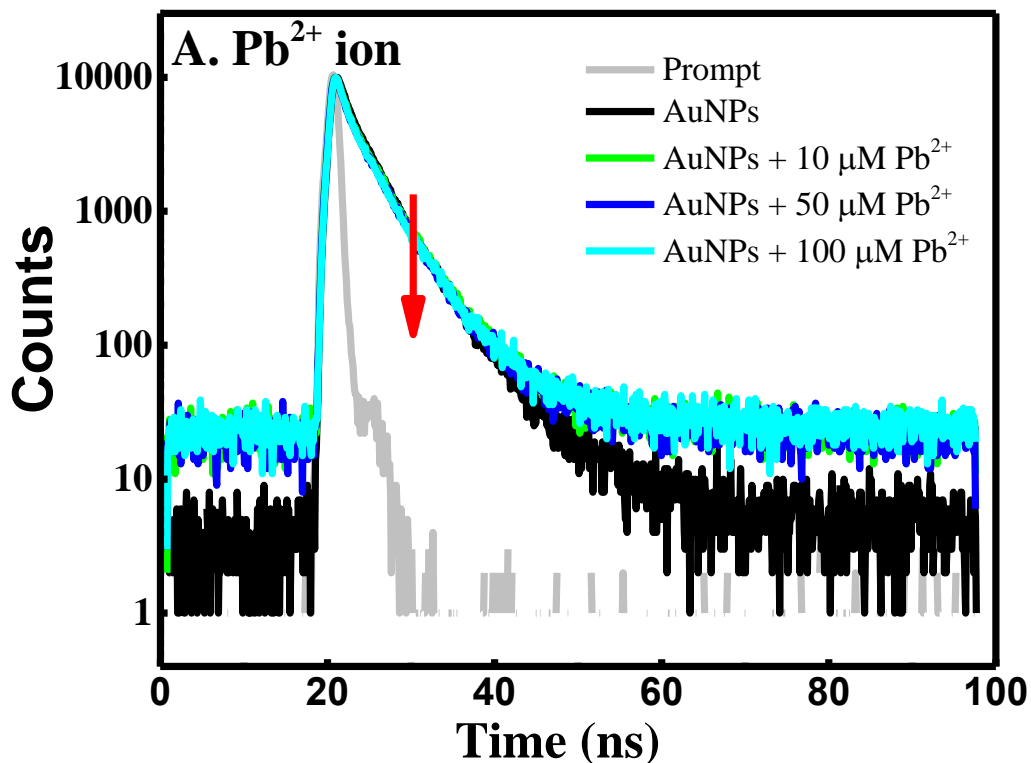
Figure 35: Stern–Volmer plot for fluorescence quenching of mPEGT conjugated AuNPs by (A) Cd<sup>2+</sup> ion and (B) Al<sup>3+</sup> ion.

Table 2: Stern-Volmer constant ( $K_{sv}$ ) and bimolecular quenching rate constant ( $k_Q$ ) for the fluorescence quenching of mPEGT conjugated AuNPs by various metal ions.

Metal ion	$K_{sv}(M^{-1})$	$k_Q(M^{-1}s^{-1})$
Cd <sup>2+</sup>	$3.93 \times 10^4$	$9.31 \times 10^{12}$
Al <sup>3+</sup>	$3.23 \times 10^4$	$7.65 \times 10^{12}$
Cu <sup>2+</sup>	$2.86 \times 10^4$	$6.78 \times 10^{12}$
Na <sub>2</sub> HAsO <sub>4</sub>	$1.77 \times 10^4$	$4.19 \times 10^{12}$
Pb <sup>2+</sup>	$3.46 \times 10^5$	$8.20 \times 10^{13}$
Hg <sup>+</sup>	$9.00 \times 10^4$	$2.13 \times 10^{12}$
Hg <sup>2+</sup>	$1.01 \times 10^5$	$2.39 \times 10^{13}$
Ni <sup>2+</sup>	$2.47 \times 10^4$	$5.85 \times 10^{12}$

For the determination of  $k_Q$ , the excited state lifetime of mPEGT conjugated AuNPs was measured in the absence of metal ion using a 405 nm excitation laser and emission was collected at 540 nm. The fluorescence decay profile as shown in Figure 36 could be best fitted with a biexponential decay. The excited state lifetimes were found to be 1.17 ns (~20 %) and 4.84 ns (~80 %) with an average lifetime of 4.22 ns. The minor first component of excited state lifetime value of mPEGT conjugated AuNPs is about 2-fold higher than that of the free curcumin reported in aqueous environment, however, the second component of excited state lifetime value of mPEGT conjugated AuNPs is within the error margin of free curcumin. This implies that conjugation of curcumin at the surface of AuNPs does influence the excited state properties though it does not change the energy gap between HOMO and LUMO of free curcumin. The  $k_Q$  values for mPEGT conjugated AuNPs in the presence of different metal ions were estimated using average excited state lifetime of 4.22 ns and given Table 3. For dynamic quenching, the maximum value of  $k_Q$  is in the range of  $1 \times 10^{10}$  [143]. However, in this study, the obtained values are in the order of  $10^{12}$  and  $10^{13}$ . This quenching rate constant value suggest the quench reaction between mPEGT conjugated AuNPs and metal ions is diffusion-controlled reaction. This very large value of  $K_{SV}$  suggests that a static quenching sphere quenching mechanism is operative envisaging the presence of AuNPs and metal ions in close proximity within the quenching sphere of action [144]. This quenching sphere of action model assumes the existence of a sphere around the fluorescent molecule within which the probability of immediate quenching is unity. Such quenching process is extremely fast, in picosecond time scale, and effectively de-excites all the fluorescent molecules (AuNPs) without the involvement of the molecular

diffusion. The only observable fluorescent molecules (AuNPs) are those for which there are no quencher in this sphere. This quenching mechanism was further established by measuring excited state lifetime in the presence of various concentration of metal ions such as  $\text{Pb}^{2+}$  and  $\text{Ni}^{2+}$  ions. It is found the average excited state lifetime of mPEGT conjugated AuNPs in the presence of  $\text{Pb}^{2+}$  ion did not change remarkably, which was similar to most of the metal ions except of  $\text{Ni}^{2+}$  ions where a slight decrease (within 15 % even at the highest concentration of  $\text{Ni}^{2+}$  ions) in the excited state lifetime was observed as summarized in Table 4.



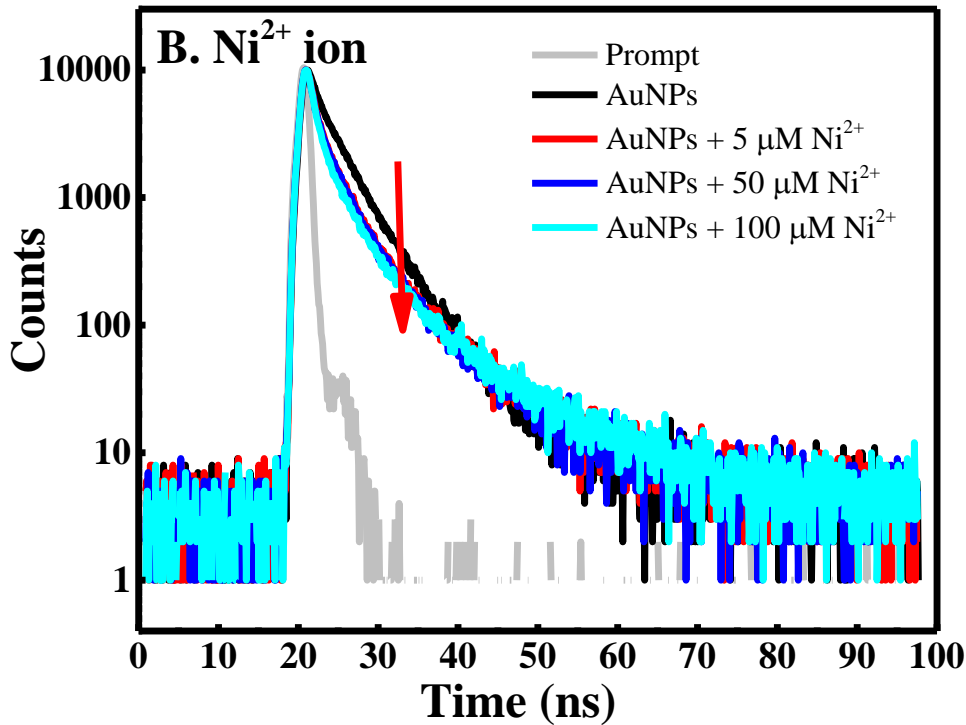


Figure 36: Time-resolved fluorescence decays of mPEGT conjugated AuNPs in the presence of varying concentrations of (A)  $\text{Pb}^{2+}$  and  $\text{Ni}^{2+}$  ions.

Table 3: Excited state lifetimes of mPEGT conjugated AuNPs in the presence of varying concentrations of  $\text{Pb}^{2+}$  and  $\text{Ni}^{2+}$  ions. The excited state lifetime was measured at  $\lambda_{\text{exc}} = 405 \text{ nm}$  and  $\lambda_{\text{em}} = 540 \text{ nm}$ .

Metal ion	[Metal ion] in $\mu\text{M}$	$\tau_1$ (ns)	Relative Amplitude (%)	$\tau_2$ (ns)	Relative Amplitude (%)	$\tau_{\text{average}}$ (ns)	$\chi^2$
$\text{Pb}^{2+}$	0	1.17	20.12	4.84	79.88	4.22	1.46842
	3.33	1.82	14.23	4.73	85.77	4.25	1.34674
	16.66	1.23	13.57	4.68	86.43	4.21	1.50051
	33.33	1.46	20.32	4.82	79.68	4.14	1.60473
$\text{Ni}^{2+}$	0	1.17	20.12	4.84	79.88	4.22	1.46842
	1.66	1.42	42.93	5.52	57.07	3.77	2.39604
	16.66	1.33	40.07	5.20	59.93	3.66	2.28959
	33.33	1.3	48.19	5.69	51.81	3.58	2.18988

### 3. Binding Constant and Binding Sites

In static quenching, there exist a relationship between intensity and the concentration of quencher which is represented below [145]. Binding of small molecules

like metal ions with independently set of equivalent sites in a macromolecule like methoxy poly ethylene glycol layer around the gold nanoparticle can be expressed through the equilibrium between free and bound molecules as [146]

$$\log \frac{I_0 - I}{I} = \log K + n \log [\text{metal ion}]$$

Where K and n are the binding constant and the number of binding sites, respectively. This can be estimated by plotting  $\log [(I_0/I)/I]$  versus  $\log [\text{metal ion}]$  (see Figure 37 for representative graph of  $\text{Hg}^+$  ion)). The best fits obtained provided n values that ranged from 0.42 for arsenic to 1.88 for  $\text{Al}^{3+}$  ion (see Table 4). The K values ranged from  $3.43 \times 10^8 \text{ M}^{-1}\text{s}^{-1}$  for  $\text{Al}^{3+}$  ion to  $3.18 \times 10^1 \text{ M}^{-1}\text{s}^{-1}$  for As. The number of the binding sites can provide insight about the number of sites in the gold nanoparticle that is associated with the metal ion. For instance,  $\text{Cd}^{2+}$ ,  $\text{Cu}^{2+}$ , and  $\text{Hg}^{2+}$  almost bind the mPEGT mediated AuNPs at 1 site. On the other hand, two molecules of these ions (Arsenic,  $\text{Hg}^+$  and  $\text{Pb}^{2+}$  ions) bind to one AuNPs. However,  $\text{Al}^{3+}$  almost bind two gold nanoparticles.

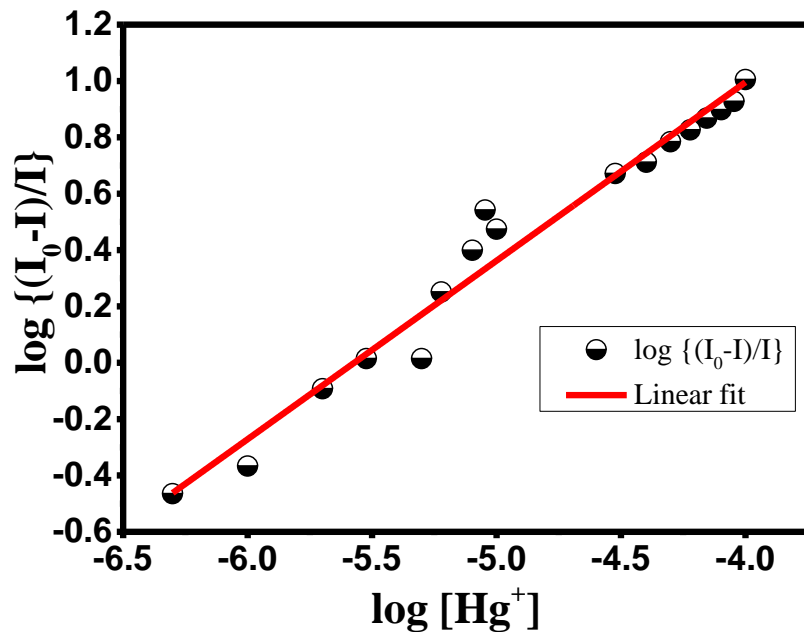


Figure 37: Plot of  $\log\{(I_0-I)/I\}$  vs.  $\log [Hg^+]$  for the estimation of binding constant ( $K$ ) and number of binding sites ( $n$ ).

Table 4: Binding constant ( $K$ ) and number of binding sites ( $n$ ) of various metal ions while associating with mPEGT conjugated AuNPs.

Metal ion	N	K ( $M^{-1}s^{-1}$ )
$Cd^{2+}$	0.96	$2.96 \times 10^4$
$Al^{3+}$	1.88	$3.43 \times 10^8$
$Cu^{2+}$	1.33	$2.61 \times 10^6$
NaHAsO <sub>4</sub>	0.42	$3.18 \times 10^1$
$Pb^{2+}$	0.45	$5.58 \times 10^2$
$Hg^+$	0.63	$3.38 \times 10^3$
$Hg^{2+}$	0.73	$6.65 \times 10^3$
$Ni^{2+}$	0.67	$1.44 \times 10^3$

#### D. Conclusion

Evidently, methoxy polyethylene glycol thiol was used to functionalize greenly synthesized gold nanoparticles, reduced by curcumin which is a nontoxic plant extract. The size of the gold nanoparticles was between 18 to 40 nm. The green synthesized gold



nanoparticles were used to afford an analytical fluorescence method for the determination of metal binding of a number of metal ions in aqueous solution. This is the first work that reports metal binding through fluorescence spectroscopy. The mPEG thiol curcumin mediated gold nanoparticles showed highest respective binding for Pb(II) , Hg(II) , Hg(I) and Cd(II), Al(III) , Ni(II), Cu(II) and As. Life time measurements also proved our hypothesis for Pb(II) and Ni(II) , as life time decreased with increasing metal ion concentration. This fluorometric method provides a prototype for a new method to analyze metal cations in solution.

## CHAPTER IV

### CONCLUSION AND FUTURE PROSPECTS

In this work, three different polyethylene glycols were used (mPEG Amine, mPEG Thiol and PEG Thiol Acid) as a surfactant or stabilizing agents. The functional group that was pointing toward the solution was proved to interact with the analyte for determination of various analytes. Curcumin was proved as a potential reducing agent for the synthesis of gold nanoparticles. It was manifested that the stabilizing agent can serve as a probe for sensing of analytes. The gold nanoparticles had spherical shape but different sizes depending on the temperature, pH, and stabilizing agent.

The Au NPs prepared at pH 13 and at 45 °C are small in size with a diameter equal to 20 nm, which was reflected in a high intensity in RRS peak and UV-vis absorption peak. The formed Au NPs have shown high thermal stability and crystallinity as evidenced by TGA and XRD. The produced AuNPs were successfully used to detect melamine by UV-VIS AND Fluorescence spectroscopy. The concentration range was between 0 and 10mM. The detection limit for melamine was equal to 33nM. The use of curcumin and thiol acid functionalized gold nanoparticles was found to be a high selective probe in measuring melamine, where no interference was occurred when adding Au NPs to dopamine and ascorbic acid. Thereby, the use of curcumin functionalized gold nanoparticles in direct analysis of melamine can be used to develop simple, fast and sensitive novel bio-sensing techniques. Hydrogen bonding between melamine and the acid group of PEG thiol acid is considered the reason for this interaction.

methoxy polyethylene glycol thiol was used as well as a probe to detect metal ions. Interestingly, the greenly synthesized gold nanoparticles, reduced by curcumin interacted with various metal ions which was reflected by fluorescence spectroscopy. The size of the gold nanoparticles was between 18 to 40 nm. The green synthesized gold nanoparticles were used to afford an analytical fluorescence method for the determination of metal binding of a number of metal ions in aqueous solution. This is the first work that reports metal binding through fluorescence spectroscopy. The mPEG thiol curcumin mediated gold nanoparticles showed highest respective binding for Pb(II), Hg(II), Hg(I) and Cd(II), Al(III), Ni(II), Cu(II) and As. Life time measurements also proved our hypothesis for Pb(II) and Ni(II), as life time decreased with increasing metal ion concentration. This fluorometric method provides a prototype for a new method to analyze metal cations in solution. We studied the mechanism of quenching, and it was found that the mechanism of quenching is static in nature as evidenced by high  $k_q$  values and constant lifetime measurements.

Tremendous applications can be employed using the greenly synthesized gold nanoparticles. With using different polymer or stabilizing agent (aptamer for instance), a new system of sensing can be discovered. The interaction is occurring between the analyte and an anchor point of the gold nanoparticle stabilizing agent. Limit of detection and quantification can be established as well, and selectivity studies can be investigated

Another future prospect is cooperation with specialized entities to turn the chemosensor for metal ions into a real platform that can be used by agencies interested

in metal ions determination in water and soil sources. Other metal ions of interest can be studied and a chemo-sensor device can be established.

#### References

- [1] D. Gross, R. Petrucci, General chemistry principles & modern applications, ninth edition, Pearson/Prentice Hall, Upper Saddle River, 2007.
- [2] 11.5 Colloids, Opentextbc.ca. (2020). <https://opentextbc.ca/chemistry/chapter/11-5-colloids/> (accessed 11 March 2020).
- [3] X. The Bakerian Lecture. —Experimental relations of gold (and other metals) to light, Philosophical Transactions Of The Royal Society Of London. 147 (1857) 145-181. doi:10.1098/rstl.1857.0011.
- [4] V. Sharma, K. Park, M. Srinivasarao, Colloidal dispersion of gold nanorods: Historical background, optical properties, seed-mediated synthesis, shape separation and self-assembly, Materials Science And Engineering: R: Reports. 65 (2009) 1-38. doi:10.1016/j.mser.2009.02.002.
- [5] T. Svedberg, R. Fåhræus, A NEW METHOD FOR THE DETERMINATION OF THE MOLECULAR WEIGHT OF THE PROTEINS, Journal Of The American Chemical Society. 48 (1926) 430-438. doi:10.1021/ja01413a019.
- [6] G. Gray, The Ultracentrifuge, Scientific American. 184 (1951) 42-51. doi:10.1038/scientificamerican0651-42.

- [7] S. Eustis, M. El-Sayed, Why Gold Nanoparticles Are More Precious than Pretty Gold: Noble Metal Surface Plasmon Resonance and Its Enhancement of the Radiative and Nonradiative Properties of Nanocrystals of Different Shapes, *Cheminform.* 37 (2006). doi:10.1002/chin.200625211.
- [8] M. Pileni, Nanosized Particles Made in Colloidal Assemblies, *Langmuir.* 13 (1997) 3266-3276. doi:10.1021/la960319q.
- [9] S. Sun, P. Mendes, K. Critchley, S. Diegoli, M. Hanwell, S. Evans et al., Fabrication of Gold Micro- and Nanostructures by Photolithographic Exposure of Thiol-Stabilized Gold Nanoparticles, *Nano Letters.* 6 (2006) 345-350. doi:10.1021/nl052130h.
- [10] P. Schaal, A. Besmehn, E. Maynicke, M. Noyong, B. Beschoten, U. Simon, Electrically Conducting Nanopatterns Formed by Chemical e-Beam Lithography via Gold Nanoparticle Seeds, *Langmuir.* 28 (2012) 2448-2454. doi:10.1021/la204393h.
- [11] J. Turkevich, P. Stevenson, J. Hillier, A study of the nucleation and growth processes in the synthesis of colloidal gold, *Discussions Of The Faraday Society.* 11 (1951) 55. doi:10.1039/df9511100055.
- [12] M. Chow, C. Zukoski, Gold Sol Formation Mechanisms: Role of Colloidal Stability, *Journal Of Colloid And Interface Science.* 165 (1994) 97-109. doi:10.1006/jcis.1994.1210.
- [13] X. Ji, X. Song, J. Li, Y. Bai, W. Yang, X. Peng, Size Control of Gold Nanocrystals in Citrate Reduction: The Third Role of Citrate, *Journal Of The American Chemical Society.* 129 (2007) 13939-13948. doi:10.1021/ja074447k.
- [14] M. Brust, M. Walker, D. Bethell, D. Schiffrin, R. Whyman, Synthesis of thiol-derivatised gold nanoparticles in a two-phase Liquid-Liquid system, *J. Chem. Soc., Chem. Commun.* 0 (1994) 801-802.
- [15] Z. Xu, C. Shen, C. Xiao, T. Yang, H. Zhang, J. Li et al., Wet chemical synthesis of gold nanoparticles using silver seeds: a shape control from nanorods to hollow spherical nanoparticles, *Nanotechnology.* 18 (2007) 115608. doi:10.1088/0957-4484/18/11/115608.
- [16] Das, Minakshi, Kyu Hwan Shim, Seong Soo A. An, and Dong Kee Yi. 2011. "Review On Gold Nanoparticles And Their Applications". *Toxicology And Environmental Health Sciences* 3 (4): 193-205. doi:10.1007/s13530-011-0109-y.
- [17] Y. Chen, Y. Hung, I. Liau, G. Huang, Assessment of the In Vivo Toxicity of Gold Nanoparticles, *Nanoscale Research Letters.* 4 (2009) 858-864. doi:10.1007/s11671-009-9334-6.
- [18] S. Parveen, R. Misra, S. Sahoo, Nanoparticles: a boon to drug delivery, therapeutics, diagnostics and imaging, *Nanomedicine: Nanotechnology, Biology And Medicine.* 8 (2012) 147-166. doi:10.1016/j.nano.2011.05.016.

- [19] M. Brust, M. Walker, D. Bethell, D. Schiffrin, R. Whyman, Synthesis of thiol-derivatised gold nanoparticles in a two-phase Liquid–Liquid system, *J. Chem. Soc., Chem. Commun.* 0 (1994) 801-802. doi:10.1039/c39940000801.
- [20] Anshup, J. Venkataraman, C. Subramaniam, R. Kumar, S. Priya, T. Kumar et al., Growth of Gold Nanoparticles in Human Cells, *Langmuir*. 21 (2005) 11562-11567. doi:10.1021/la0519249.
- [21] S. Skrabalak, J. Chen, Y. Sun, X. Lu, L. Au, C. Cobley et al., ChemInform Abstract: Gold Nanocages: Synthesis, Properties, and Applications, *Cheminform*. 40 (2009). doi:10.1002/chin.200914224.
- [22] J. Chen, Noble Metal Nanoparticle Platform, *Cancer Theranostics*. (2014) 327-346. doi:10.1016/b978-0-12-407722-5.00018-9.
- [23] Sudhakar, S., and P.B. Santhosh. 2017. "Gold Nanomaterials". *Advances In Biomembranes And Lipid Self-Assembly*, 161-180. doi:10.1016/bs.abl.2017.01.003.
- [24] K. Parveen, V. Banse, L. Ledwani, Green synthesis of nanoparticles: Their advantages and disadvantages, (2016). doi:10.1063/1.4945168.
- [25] L. Leopold, I. Tódor, Z. Diaconeasa, D. Rugină, A. Ștefancu, N. Leopold et al. Assessment of PEG and BSA-PEG gold nanoparticles cellular interaction, *Colloids And Surfaces A: Physicochemical And Engineering Aspects*. 532 (2017) 70-76. doi:10.1016/j.colsurfa.2017.06.061.
- [26] A. Kanaras, F. Kamounah, K. Schaumburg, C. Kiely, M. Brust, Thioalkylated tetraethylene glycol: a new ligand for water soluble monolayer protected gold clusters, *Chemical Communications*. 20 (2002) 2294-2295. doi:10.1039/b207838b.
- [27] M. Chebl, M. Abiad, Z. Moussa, D. Patra, Two Modes of Associations of Curcumin with Pre- and Nanoaggregated Chitosan Oligosaccharide Lactate: Ionic Strength and Hydrophobic Bile Salt Modulate Partition of Drug and Self-Assembly Process, *The Journal Of Physical Chemistry C*. 120 (2016) 11210-11224. doi:10.1021/acs.jpcc.6b01486.
- [28] T. Ak, İ. Gülçin, Antioxidant and radical scavenging properties of curcumin, *Chemico-Biological Interactions*. 174 (2008) 27-37. doi:10.1016/j.cbi.2008.05.003.
- [29] N. Chainani-Wu, Safety and Anti-Inflammatory Activity of Curcumin: A Component of Tumeric (*Curcuma longa*), *The Journal of Alternative and Complementary Medicine*. 9 (2003) 161-168. Doi: 10.1089/107555303321223035.
- [30] D. Zhang, M. Fu, S. Gao, J. Liu, Curcumin and Diabetes: A Systematic Review, *Evidence-Based Complementary And Alternative Medicine*. 2013 (2013) 1-16. doi:10.1155/2013/636053.

- [31] Y. Rivera-Espinoza, P. Muriel, Pharmacological actions of curcumin in liver diseases or damage, *Liver International*. 29 (2009) 1457-1466. doi:10.1111/j.1478-3231.2009.02086.x.
- [32] S. Govindaraju, A. Rengaraj, R. Arivazhagan, Y. Huh, K. Yun, Curcumin-Conjugated Gold Clusters for Bioimaging and Anticancer Applications, *Bioconjugate Chemistry*. 29 (2018) 363-370. doi:10.1021/acs.bioconjchem.7b00683.
- [33] K. McNamara, S. Tofail, Nanoparticles in biomedical applications, *Advances In Physics: X*. 2 (2016) 54-88. doi:10.1080/23746149.2016.1254570.
- [34] G. Doria, J. Conde, B. Veigas, L. Giestas, C. Almeida, M. Assunção et al., Noble Metal Nanoparticles for Biosensing Applications, *Sensors*. 12 (2012) 1657-1687. Doi: 10.3390/s120201657.
- [35] R. El Kurdi, D. Patra, Amplification of resonance Rayleigh scattering of gold nanoparticles by tweaking into nanowires: Bio-sensing of  $\alpha$ -tocopherol by enhanced resonance Rayleigh scattering of curcumin capped gold nanowires through non-covalent interaction, *Talanta*. 168 (2017) 82-90. doi:10.1016/j.talanta.2017.03.021.
- [36] W. Hall, S. Ngatia, R. Van Duyne, LSPR Biosensor Signal Enhancement Using Nanoparticle–Antibody Conjugates, *The Journal Of Physical Chemistry C*. 115 (2011) 1410-1414. doi:10.1021/jp106912p.
- [27] S. Maier, Plasmonics - Towards Subwavelength Optical Devices, *Current Nanoscience*. 1 (2005) 17-22. doi:10.2174/1573413052953165.
- [38] V. Amendola, R. Pilot, M. Frasconi, O. Maragò, M. Iatì, Surface plasmon resonance in gold nanoparticles: a review, *Journal Of Physics: Condensed Matter*. 29 (2017) 203002. doi:10.1088/1361-648x/aa60f3.
- [39] H. Müller, Optical Properties of Metal Clusters, *Zeitschrift Für Physikalische Chemie*. 194 (1996) 278-279. doi:10.1524/zpch.1996.194.part\_2.278.
- [40] P. Biagioni, J. Huang, B. Hecht, Nanoantennas for visible and infrared radiation, *Reports On Progress In Physics*. 75 (2012) 024402. doi:10.1088/0034-4885/75/2/024402.
- [41] J. Zuloaga, P. Nordlander, On the Energy Shift between Near-Field and Far-Field Peak Intensities in Localized Plasmon Systems, *Nano Letters*. 11 (2011) 1280-1283. doi:10.1021/nl1043242.
- [42] M. Kats, N. Yu, P. Genevet, Z. Gaburro, F. Capasso, Effect of radiation damping on the spectral response of plasmonic components, *Optics Express*. 19 (2011) 21748. doi:10.1364/oe.19.021748.
- [43] M. Chebl, M. Abiad, Z. Moussa, D. Patra, Two Modes of Associations of Curcumin with Pre- and Nanoaggregated Chitosan Oligosaccharide Lactate: Ionic Strength and Hydrophobic Bile Salt Modulate Partition of Drug and Self-Assembly Process, *The*

Journal Of Physical Chemistry C. 120 (2016) 11210-11224.  
doi:10.1021/acs.jpcc.6b01486.

[44] J. Lakowicz, B. Masters, Principles of Fluorescence Spectroscopy, Third Edition, Journal Of Biomedical Optics. 13 (2008) 029901. doi:10.1117/1.2904580.

[45] N. Strambeanu, L. Demetrovici, D. Dragos, M. Lungu, Nanoparticles: Definition, Classification and General Physical Properties, Nanoparticles' Promises And Risks. (2014) 3-8. doi:10.1007/978-3-319-11728-7-1.

[46] L. Qin, G. Zeng, C. Lai, D. Huang, P. Xu, C. Zhang et al., "Gold rush" in modern science: Fabrication strategies and typical advanced applications of gold nanoparticles in sensing, Coordination Chemistry Reviews. 359 (2018) 1-31. doi: 10.1016/j.ccr.2018.01.006.

[47] N. Elahi, M. Kamali, M. Baghersad, Recent biomedical applications of gold nanoparticles: A review, Talanta. 184 (2018) 537-556. doi:10.1016/j.talanta.2018.02.088.

[48]. H. Li, L. Rothberg, Colorimetric detection of DNA sequences based on electrostatic interactions with unmodified gold nanoparticles, Proceedings Of The National Academy Of Sciences. 101 (2004) 14036-14039. doi:10.1073/pnas.0406115101.

[49] Gopinath S.C.B., Citartan M., Lakshmi priya T., Tang TH., Chen Y. (2015) Gold Nanoparticles in Biosensing Analyses. In: Lungu M., Neculae A., Bunoiu M., Biris C. (eds) Nanoparticles' Promises and Risks. Springer, Cham

[50] K. Saha, S. Agasti, C. Kim, X. Li, V. Rotello, Gold Nanoparticles in Chemical and Biological Sensing, Chemical Reviews. 112 (2012) 2739-2779. doi:10.1021/cr2001178.

[51] Fluorescent Chemosensors for Ion and Molecule Recognition, Instrumentation Science & Technology. 22 (1994) 405-406. doi:10.1080/10739149408001201.

[52] Fluorescent Chemosensors for Ion and Molecule Recognition, Instrumentation Science & Technology. 22 (1994) 405-406. doi:10.1080/10739149408001201.

[53] V. Krishna, K. Wu, D. Su, M. Cheeran, J. Wang, A. Perez, Nanotechnology: Review of concepts and potential application of sensing platforms in food safety, Food Microbiology. 75 (2018) 47-54. doi:10.1016/j.fm.2018.01.025.

[54] D. BRAGA, F. GREPIONI, ChemInform Abstract: From Molecule to Molecular Aggregation: Clusters and Crystals of Clusters, Cheminform. 25 (2010) 51-56. doi:10.1002/chin.199425268

[55] V. Sharma, K. Park, M. Srinivasarao, Colloidal dispersion of gold nanorods: Historical background, optical properties, seed-mediated synthesis, shape separation and



self-assembly, *Materials Science And Engineering: R: Reports*. 65 (2009) 1-38. doi:10.1016/j.mser.2009.02.002.

[56] T. Svedberg, R. Fåhræus, A NEW METHOD FOR THE DETERMINATION OF THE MOLECULAR WEIGHT OF THE PROTEINS, *Journal Of The American Chemical Society*. 48 (1926) 430-438. doi:10.1021/ja01413a019.

[57] G. Gray, The Ultracentrifuge, *Scientific American*. 184 (1951) 42-51. doi:10.1038/scientificamerican0651-42.

[58] S. Eustis, M. El-Sayed, Why Gold Nanoparticles Are More Precious than Pretty Gold: Noble Metal Surface Plasmon Resonance and Its Enhancement of the Radiative and Nonradiative Properties of Nanocrystals of Different Shapes, *Cheminform*. 37 (2006). doi:10.1002/chin.200625211.

[59] M. Pileni, Nanosized Particles Made in Colloidal Assemblies, *Langmuir*. 13 (1997) 3266-3276. doi:10.1021/la960319q.

[60] S. Sun, P. Mendes, K. Critchley, S. Diegoli, M. Hanwell, S. Evans et al., Fabrication of Gold Micro- and Nanostructures by Photolithographic Exposure of Thiol-Stabilized Gold Nanoparticles, *Nano Letters*. 6 (2006) 345-350. doi:10.1021/nl052130h.

[61] P. Schaal, A. Besmehn, E. Maynicke, M. Noyong, B. Beschoten, U. Simon, Electrically Conducting Nanopatterns Formed by Chemical e-Beam Lithography via Gold Nanoparticle Seeds, *Langmuir*. 28 (2012) 2448-2454. doi:10.1021/la204393h.

[62] J. Turkevich, P. Stevenson, J. Hillier, A study of the nucleation and growth processes in the synthesis of colloidal gold, *Discussions Of The Faraday Society*. 11 (1951) 55. doi:10.1039/df9511100055.

[63] M. Chow, C. Zukoski, Gold Sol Formation Mechanisms: Role of Colloidal Stability, *Journal Of Colloid And Interface Science*. 165 (1994) 97-109. doi:10.1006/jcis.1994.1210.

[64] X. Ji, X. Song, J. Li, Y. Bai, W. Yang, X. Peng, Size Control of Gold Nanocrystals in Citrate Reduction: The Third Role of Citrate, *Journal Of The American Chemical Society*. 129 (2007) 13939-13948. doi:10.1021/ja074447k.

[65] M. Brust, M. Walker, D. Bethell, D. Schiffrin, R. Whyman, Synthesis of thiol-derivatised gold nanoparticles in a two-phase Liquid-Liquid system, *J. Chem. Soc., Chem. Commun*. 0 (1994) 801-802.

[66] Z. Xu, C. Shen, C. Xiao, T. Yang, H. Zhang, J. Li et al., Wet chemical synthesis of gold nanoparticles using silver seeds: a shape control from nanorods to hollow spherical nanoparticles, *Nanotechnology*. 18 (2007) 115608. doi:10.1088/0957-4484/18/11/115608.

[67] Das, Minakshi, Kyu Hwan Shim, Seong Soo A. An, and Dong Kee Yi. 2011. "Review On Gold Nanoparticles And Their Applications". *Toxicology And Environmental Health Sciences* 3 (4): 193-205. doi:10.1007/s13530-011-0109-y.

- [68] Y. Chen, Y. Hung, I. Liau, G. Huang, Assessment of the In Vivo Toxicity of Gold Nanoparticles, *Nanoscale Research Letters*. 4 (2009) 858-864. doi:10.1007/s11671-009-9334-6.
- [69] S. Parveen, R. Misra, S. Sahoo, Nanoparticles: a boon to drug delivery, therapeutics, diagnostics and imaging, *Nanomedicine: Nanotechnology, Biology And Medicine*. 8 (2012) 147-166. doi:10.1016/j.nano.2011.05.016.
- [70] M. Brust, M. Walker, D. Bethell, D. Schiffrin, R. Whyman, Synthesis of thiol-derivatised gold nanoparticles in a two-phase Liquid–Liquid system, *J. Chem. Soc., Chem. Commun.* 0 (1994) 801-802. doi:10.1039/c39940000801.
- [71] Anshup, J. Venkataraman, C. Subramaniam, R. Kumar, S. Priya, T. Kumar et al., Growth of Gold Nanoparticles in Human Cells, *Langmuir*. 21 (2005) 11562-11567. doi:10.1021/la0519249.
- [72] S. Skrabalak, J. Chen, Y. Sun, X. Lu, L. Au, C. Cobley et al., ChemInform Abstract: Gold Nanocages: Synthesis, Properties, and Applications, *Cheminform*. 40 (2009). doi:10.1002/chin.200914224.
- [73] R. Sperling, P. Rivera Gil, F. Zhang, M. Zanella, W. Parak, Biological applications of gold nanoparticles, *Chemical Society Reviews*. 37 (2008) 1896–1908. doi:10.1039/b712170a.
- [74] R. El Kurdi, D. Patra, Gold nanoparticles functionalized with Pluronic are viable optical probes for the determination of uric acid, *Microchimica Acta*. 185 (2018). doi:10.1007/s00604-018-2725-6.
- [75] F. Mafuné, J. Kohno, Y. Takeda, T. Kondow, Full Physical Preparation of Size-Selected Gold Nanoparticles in Solution: Laser Ablation and Laser-Induced Size Control, *The Journal Of Physical Chemistry B*. 106 (2002) 7575-7577. doi:10.1021/jp020577y.
- [76] S. Huang, H. Ma, X. Zhang, F. Yong, X. Feng, W. Pan et al., Electrochemical Synthesis of Gold Nanocrystals and Their 1D and 2D Organization, *The Journal Of Physical Chemistry B*. 109 (2005) 19823-19830. doi:10.1021/jp052863q.
- [77] R. Moussawi, D. Patra, Synthesis of Au Nanorods through Prereduction with Curcumin: Preferential Enhancement of Au Nanorod Formation Prepared from CTAB-Capped over Citrate-Capped Au Seeds, *The Journal Of Physical Chemistry C*. 119 (2015) 19458-19468. doi:10.1021/acs.jpcc.5b04447.
- [78] A. Thirumurugan, S. Ramachandran, N. Tomy, G. Jiflin, G. Rajagomathi, Biological synthesis of gold nanoparticles by *Bacillus subtilis* and evaluation of increased antimicrobial activity against clinical isolates, *Korean Journal Of Chemical Engineering*. 29 (2012) 1761-1765. Doi: 10.1007/s11814-012-0055-

- [79] J. Turkevich, P. Stevenson, J. Hillier, A study of the nucleation and growth processes in the synthesis of colloidal gold, *Discussions Of The Faraday Society*. 11 (1951) 55-75. doi:10.1039/df9511100055.
- [80] T. Kunoh, M. Takeda, S. Matsumoto, I. Suzuki, M. Takano, H. Kunoh et al., Green Synthesis of Gold Nanoparticles Coupled with Nucleic Acid Oxidation, *ACS Sustainable Chemistry & Engineering*. 6 (2017) 364-373. doi:10.1021/acssuschemeng.7b02610.
- [81] X. Huang, M. El-Sayed, Gold nanoparticles: Optical properties and implementations in cancer diagnosis and photothermal therapy, *Journal of Advanced Research*. 1 (2010) 13-28. doi:10.1016/j.jare.2010.02.002.
- [82] M. Stewart, K. Susumu, B. Mei, I. Medintz, J. Delehanty, J. Blanco-Canosa et al., Multidentate Poly(ethylene glycol) Ligands Provide Colloidal Stability to Semiconductor and Metallic Nanocrystals in Extreme Conditions, *Journal Of The American Chemical Society*. 132 (2010) 9804-9813. doi:10.1021/ja102898d.
- [83] L. Sun, Z. Zhang, S. Wang, J. Zhang, H. Li, L. Ren et al., Effect of pH on the Interaction of Gold Nanoparticles with DNA and Application in the Detection of Human p53 Gene Mutation, *Nanoscale Research Letters*. 4 (2008) 216-220. doi:10.1007/s11671-008-9228-z.
- [84] K. Sneha, M. Sathishkumar, S. Kim, Y. Yun, Counter ions and temperature incorporated tailoring of biogenic gold nanoparticles, *Process Biochemistry*. 45 (2010) 1450-1458. doi:10.1016/j.procbio.2010.05.019.
- [85] Abd El-Rahman SN, Al-Jameel SS. Protection of curcumin and curcumin nanoparticles against cisplatin induced nephrotoxicity in male rats. *Sch Acad J Biosci* 2014; 2:214-23.
- [86] M. Nadagouda, N. Iyanna, J. Lalley, C. Han, D. Dionysiou, R. Varma, Synthesis of Silver and Gold Nanoparticles Using Antioxidants from Blackberry, Blueberry, Pomegranate, and Turmeric Extracts, *ACS Sustainable Chemistry & Engineering*. 2 (2014) 1717-1723. doi:10.1021/sc500237k.
- [87] M. Daniel, D. Astruc, Gold Nanoparticles: Assembly, Supramolecular Chemistry, Quantum-Size-Related Properties, and Applications Toward Biology, Catalysis, and Nanotechnology., *Cheminform*. 35 (2004) 293-346. doi:10.1002/chin.200416213.
- [88] K. Rovina, S. Siddiquee, N. Wong, Development of melamine sensor based on ionic liquid/nanoparticles/chitosan with modified gold electrode for determination of melamine

in milk product, *Sensing And Bio-Sensing Research*. 4 (2015) 16-22.  
doi:10.1016/j.sbsr.2015.02.003.

[89] T. Niegocki, B. Sell, A. Posyniak, J. Zmudzki, Determination of Melamine in Feed by High Performance Liquid Chromatography Coupled Mass Spectrometry. *Bulletin-Veterinary Institute in Pulawy*. 54(2010) 543-547.

[90] H. Miao, S. Fan, P. Zhou, L. Zhang, Y. Zhao, Y. Wu, Determination of melamine and its analogues in egg by gas chromatography-tandem mass spectrometry using an isotope dilution technique, *Food Additives & Contaminants: Part A*. 27 (2010) 1497-1506. doi:10.1080/19440049.2010.496795.

[91] P. Lutter, M. Savoy-Perroud, E. Campos-Gimenez, L. Meyer, T. Goldmann, M. Bertholet et al., Screening and confirmatory methods for the determination of melamine in cow's milk and milk-based powdered infant formula: Validation and proficiency-tests of ELISA, HPLC-UV, GC-MS and LC-MS/MS, *Food Control*. 22 (2011) 903-913. doi:10.1016/j.foodcont.2010.11.022.

[92] Mauer, A. Chernyshova, A. Hiatt, A. Deering, R. Davis, Melamine Detection in Infant Formula Powder Using Near- and Mid-Infrared Spectroscopy, *Journal Of Agricultural And Food Chemistry*. 57 (2009) 3974-3980. doi:10.1021/jf900587m.

[93] S. Okazaki, M. Hiramatsu, K. Gonmori, O. Suzuki, A. Tu, Rapid nondestructive screening for melamine in dried milk by Raman spectroscopy, *Forensic Toxicology*. 27 (2009) 94-97. doi:10.1007/s11419-009-0072-3.

[94] H. Wang, H. Bai, A. Mao, T. Gan, Y. Liu, Poly(adenine)-templated fluorescent Au nanoclusters for the rapid and sensitive detection of melamine, *Spectrochimica Acta Part A: Molecular And Biomolecular Spectroscopy*. 219 (2019) 375-381. doi:10.1016/j.saa.2019.04.075.

[95] M. Zhang, X. Cao, H. Li, F. Guan, J. Guo, F. Shen et al., Sensitive fluorescent detection of melamine in raw milk based on the inner filter effect of Au nanoparticles on the fluorescence of CdTe quantum dots, *Food Chemistry*. 135 (2012) 1894-1900. doi:10.1016/j.foodchem.2012.06.070.

[96] N. Vasimalai, S. Abraham John, Picomolar melamine enhanced the fluorescence of gold nanoparticles: Spectrofluorimetric determination of melamine in milk and infant formulas using functionalized triazole capped goldnanoparticles, *Biosensors And Bioelectronics*. 42 (2013) 267-272. doi:10.1016/j.bios.2012.10.023.

[97] Q. Wu, Q. Long, H. Li, Y. Zhang, S. Yao, An upconversion fluorescence resonance energy transfer nanosensor for one step detection of melamine in raw milk, *Talanta*. 136 (2015) 47-53. doi:10.1016/j.talanta.2015.01.005.

- [98] L. Li, B. Li, D. Cheng, L. Mao, Visual detection of melamine in raw milk using gold nanoparticles as colorimetric probe, *Food Chemistry*. 122 (2010) 895-900. doi:10.1016/j.foodchem.2010.03.032.
- [99] H. Chi, B. Liu, G. Guan, Z. Zhang, M. Han, A simple, reliable and sensitive colorimetric visualization of melamine in milk by unmodified gold nanoparticles, *The Analyst*. 135 (2010) 1070. doi:10.1039/c000285b.
- [100] N. Kumar, R. Seth, H. Kumar, Colorimetric detection of melamine in milk by citrate-stabilized gold nanoparticles, *Analytical Biochemistry*. 456 (2014) 43-49. doi:10.1016/j.ab.2014.04.002.
- [101] J. Xin, L. Zhang, D. Chen, K. Lin, H. Fan, Y. Wang et al., Colorimetric detection of melamine based on methanobactin-mediated synthesis of gold nanoparticles, *Food Chemistry*. 174 (2015) 473-479. doi:10.1016/j.foodchem.2014.11.098.
- [102] X. Chen, W. Ha, Y. Shi, Sensitive colorimetric detection of melamine in processed raw milk using asymmetrically PEGylated gold nanoparticles, *Talanta*. 194 (2019) 475-484. doi:10.1016/j.talanta.2018.10.070.
- [103] F. Gao, Q. Ye, P. Cui, L. Zhang, Efficient Fluorescence Energy Transfer System between CdTe-Doped Silica Nanoparticles and Gold Nanoparticles for Turn-On Fluorescence Detection of Melamine, *Journal Of Agricultural And Food Chemistry*. 60 (2012) 4550-4558. doi:10.1021/jf300386y.
- [104] P. Ni, H. Dai, Y. Wang, Y. Sun, Y. Shi, J. Hu et al., Visual detection of melamine based on the peroxidase-like activity enhancement of bare gold nanoparticles, *Biosensors And Bioelectronics*. 60 (2014) 286-291. doi:10.1016/j.bios.2014.04.029.
- [105] J. Du, Z. Wang, X. Peng, J. Fan, In Situ Colorimetric Recognition of Melamine Based on Thymine Derivative-Functionalized Gold Nanoparticle, *Industrial & Engineering Chemistry Research*. 54 (2015) 12011-12016. doi:10.1021/acs.iecr.5b02399.
- [106] X. Hu, J. Shi, Y. Shi, X. Zou, M. Arslan, W. Zhang et al., Use of a smartphone for visual detection of melamine in milk based on Au@Carbon quantum dots nanocomposites, *Food Chemistry*. 272 (2019) 58-65. doi:10.1016/j.foodchem.2018.08.021.
- [107] Q. Ren, X. Shen, Y. Sun, R. Fan, J. Zhang, A highly sensitive competitive immunosensor based on branched polyethyleneimine functionalized reduced graphene oxide and gold nanoparticles modified electrode for detection of melamine, *Food Chemistry*. 304 (2019) 125397. doi:10.1016/j.foodchem.2019.125397.
- [108] X. Hu, J. Shi, Y. Shi, X. Zou, M. Arslan, W. Zhang et al., Use of a smartphone for visual detection of melamine in milk based on Au@Carbon quantum dots nanocomposites, *Food Chemistry*. 272 (2019) 58-65. doi:10.1016/j.foodchem.2018.08.021.

- [109] H. Dai, Y. Shi, Y. Wang, Y. Sun, J. Hu, P. Ni et al., Label-free turn-on fluorescent detection of melamine based on the anti-quenching ability of Hg<sup>2+</sup> to gold nanoclusters, *Biosensors And Bioelectronics*. **53** (2014) 76-81. doi:10.1016/j.bios.2013.09.034
- [110] K. Yoshida, T. Mori, S. Watanabe, H. Kawai, T. Nagamura, Synthesis and metal ion-sensing properties of fluorescent PET chemosensors based on the 2-phenylimidazo[5,4-a]anthraquinone chromophore, *J. Chem. Soc., Perkin Trans. 2*. (1999) 393. doi:10.1039/a900424f.
- [111] J. R. Lakowicz, *Principles of Fluorescence Spectroscopy*, Springer, New York, NY, 2013.
- [112] L. Fan, Y. Zhang, C. Murphy, S. Angell, M. Parker, B. Flynn et al., Fluorescent conjugated polymer molecular wire chemosensors for transition metal ion recognition and signaling, *Coordination Chem. Rev.*, **253** (2009) 410-422.
- [113] J.-F. Peng, Y.-h. Song, P. Yuan, X.-y. Cui, G.-l. Qiu, The Remediation Of Heavy Metals Contaminated Sediment, *J. Hazard. Mater.*, **161** (2-3) (2009) 633-640.
- [114] A. Mandal, M. Suresh, E. Suresh, S. Mishra, S. Mishra, A. Das, A chemosensor for heavy-transition metal ions in mixed aqueous–organic media, *Sens. Actuat. B: Chemical*, **145** (2010) 32-38.
- [115] J. Zhao, D. Nelson, Fluorescence study of the interaction of Suwannee River fulvic acid with metal ions and Al<sup>3+</sup>-metal ion competition, *J. Inorg. Biochem.*, **99** (2005) 383-396.
- [116] A. Mohd, A. Parwaz Khan, S. Bano, K. Siddiqi, Interaction of Clofazimine with Divalent Metal Ions: A Fluorescence Quenching Study, *J. Dispersion Sci. Techno.*, **32** (2011) 1465-1469.
- [117] M. Montalti, L. Prodi, N. Zaccheroni, Fluorescence quenching amplification in silica nanosensors for metal ions, *J. Mater. Chem.*, **15** (2005) 2810.
- [118] Y. Chang, Y. Choi, A. Shin, Significant Fluorescence Quenching of Anthrylaminobenzocrown Ethers by Paramagnetic Metal Cations., *Cheminform.* **33** (2010)
- [119] T. Jennings, M. Singh, G. Strouse, Fluorescent Lifetime Quenching near d= 1.5 nm Gold Nanoparticles: Probing NSET Validity, *J. Amer. Chem. Soc.*, **128** (2006) 5462-5467.
- [120] N. Rupcich, W. Chiuman, R. Nutiu, S. Mei, K. Flora, Y. Li et al., Quenching of Fluorophore-Labeled DNA Oligonucleotides by Divalent Metal Ions: Implications for Selection, Design, and Applications of Signaling Aptamers and Signaling Deoxyribozymes, *J. Amer. Chem. Soc.*, **128** (2006) 780-790.

- [121] Y. Posokhov, A. Kyrychenko, A. Ladokhin, Steady-state and time-resolved fluorescence quenching with transition metal ions as short-distance probes for protein conformation, *Anal. Biochem.*, **407** (2010) 284-286.
- [122] Y. Xiao, A. Rowe, K. Plaxco, Electrochemical Detection of Parts-Per-Billion Lead via an Electrode-Bound DNzyme Assembly, *J. Amer. Chem. Soc.*, **129** (2007) 262-263.
- [123] M. Mohajeri, R. Mehdi Rezaee, A. Sahebkar, Cadmium-Induced Toxicity Is Rescued By Curcumin: A Review, *Biofactors*, **43** (5) (2017) 645-661.
- [124] Z. Fang, J. Růžička, E. H. Hansen, An Efficient Flow-Injection System With On-Line Ion-Exchange Preconcentration For The Determination Of Trace Amounts Of Heavy Metals By Atomic Absorption Spectrometry, *Anal. Chim. Acta*, **164** (1984) 23-39.
- [125] V. L. Dressler, D. Pozebon, A. J. Curtius, Determination Of Heavy Metals By Inductively Coupled Plasma Mass Spectrometry After On-Line Separation And Preconcentration, *Spectrochim. Acta Part B: Atomic Spectroscopy*, **53** (11) (1998) 1527-1539.
- [126] L. Cui, J. Wu, H. Ju, Electrochemical Sensing Of Heavy Metal Ions With Inorganic, Organic And Bio-Materials, *Biosens. Bioelectro.*, **63** (2015) 276-286.
- [127] S. Zeng, K. -T. Yong, I. Roy, X.-Q. Dinh, X. Yu, F. Luan, A Review On Functionalized Gold Nanoparticles For Biosensing Applications, *Plasmonics*, **6** (3) (2011) 491-506.
- [128] R. El Kurdi, D. Patra, Role of OH<sup>-</sup> in the formation of highly selective gold nanowires at extreme pH: Multi-fold enhancement in rate of catalytic reduction reaction by gold nanowires, *Phys. Chem. Chem. Phys.*, **19** (2017) 5077 – 5090.
- [129] S. Al Shehab, R. El Kurdi, D. Patra, Curcumin mediated PEG thiol acid conjugated gold nanoparticles for the determination of melamine, *Microchem. J.* **153** (2020) 104382.
- [130] B. Paul, A. Tiwari. A Brief Review on the Application of Gold Nanoparticles as Sensors in Multi Dimensional Aspects IOSR, *J. Environ. Sci. Toxicology and Food Technology (IOSR-JESTFT)* e-ISSN: 2319-2402,p- ISSN: 2319-2399. Volume. 1 Issue. 4, PP 01-07 [www.iosrjournals.org](http://www.iosrjournals.org)
- [131] A. Sugunan, C. Thanachayanont, J. Dutta, J.G. Hilborn, Heavy-Metal Ion Sensors Using Chitosan-Capped Gold Nanoparticles, *Science And Technology Of Advanced Materials* **6** (3-4), (2005) 335-340.
- [132] Z. Osner, R. Holz, D. Becker, An analytical method for detecting toxic metal cations using cyclotrimeratrylene derivative capped gold nanoparticles, *Tetrahedron Lett.*, **56**(40), (2015) pp.5419-5423.

- [133] Y. Manolova, V. Deneva, L. Antonov, E. Drakalska, D. Momekova, N. Lambov, The effect of the water on the curcumin tautomerism: A quantitative approach, *Spectrochim. Acta Part A: Molecul. Biomolecul. Spectrosc.* **132** (2014) 815-820.
- [134] S. Smitha, D. Philip, K. Gopchandran, Green synthesis of gold nanoparticles using *Cinnamomum zeylanicum* leaf broth, *Spectrochim. Acta Part A: Molecul. Biomolecul. Spectrosc.*, **74** (2009) 735-739.
- [135] K. Sneha, M. Sathishkumar, S. Kim, Y. Yun, Counter ions and temperature incorporated tailoring of biogenic gold nanoparticles, *Process Biochem.*, **45** (2010) 1450-1458.
- [136] X. Chen, L. Zou, J. Niu, W. Liu, S. Peng, C. Liu, The Stability, Sustained Release and Cellular Antioxidant Activity of Curcumin Nanoliposomes. *Molecules*, **20(8)** (2015) 14293-14311.
- [137] B. Korthals, M. Morant-Miñana, M. Schmid, S. Mecking, Functionalization of Polymer Nanoparticles by Thiol–Ene Addition. *Macromolecules*, **43(19)** (2010) 8071-8078.
- [138] J. Manson, D. Kumar, B. Meenan, D. Dixon, Polyethylene glycol functionalized gold nanoparticles: the influence of capping density on stability in various media, *Gold Bull.* **44** (2011) 99-105.
- [139] D. Patra, C. Barakat, Synchronous fluorescence spectroscopic study of solvatochromic curcumin dye, *Spectrochim. Acta Part A: Molecul. Biomolecul. Spectrosc.*, **79** (2011) 1034 – 1041.
- [140] S. Prabu, S. Mohamad, Curcumin/beta-cyclodextrin inclusion complex as a new “turn-off” fluorescent sensor system for sensitive recognition of mercury ion, *J. Molecul. Struct.*, **1204** (2020) 127528.
- [141] S-H. Kim, S-Y. Gwon, S. M. Burkinshaw, Y-A. Son, The photo- and electrophysical properties of curcumin in aqueous solution, *Spectrochim. Acta Part A* **76** (2010) 384-387.
- [142] M. Swierczewska, S. Lee, X. Chen, The design and application of fluorophore–gold nanoparticle activatable probes. *Phys. Chem. Chem. Phys.* **13** (2011) 9929.
- [143] J. Albani, Chapter 2: Fluorescence Quenching, in *Structure and Dynamics Of Macromolecules: Absorption And Fluorescence Studies*, 2004, 141-192. doi:10.1016/b978-044451449-3/50004-6.
- [144] H. Crouse, J. Potoma, F. Nejrabi, D. Snyder, B. Chohan, S. Basu, Quenching of tryptophan fluorescence in various proteins by a series of small nickel complexes, *Dalton Trans.*, **41** (2012) 2720.
- [145] D. Patra, A. K. Mishra, Determination of quenching inhibition factor and selective fluorescence quenching study of perylene, pyrene and fluoranthene in micelle by cetyl



pyridinium chloride as a hydrophobic quencher molecule, *Polycyc. Aromat. Comp.*, **18** (4) (2001) 367 – 380.

[146] D. Patra, C. Barakat, Time-resolved fluorescence study during denaturation and renaturation of curcumin-myoglobin complex, *Internat. J. Biolog. Macromolecu.*, **50** (2012) 885 – 890.

[147] A. Srivastava, R. Yadav, V. Rai, T. Ganguly, S. Deb, Surface plasmon resonance in gold nanoparticles, (2012). doi:10.1063/1.4710001.

[148] T. Rao, NANOMANUFACTURING OF GOLD NANOPARTICLE SUPERSTRUCTURES FROM THE “BOTTOM-UP”, Doctor of Philosophy, Doctor of Philosophy, 2013.

[149] 13.7: The Franck-Condon Principle, Chemistry Libretexts. (2020). [https://chem.libretexts.org/Courses/Pacific\\_Union\\_College/Quantum\\_Chemistry/13%3A\\_A\\_Molecular\\_Spectroscopy/13.07%3A\\_The\\_Franck-Condon\\_Principle](https://chem.libretexts.org/Courses/Pacific_Union_College/Quantum_Chemistry/13%3A_A_Molecular_Spectroscopy/13.07%3A_The_Franck-Condon_Principle) (accessed 6 May 2020).

[150] M. Kasha, Characterization of electronic transitions in complex molecules, *Discussions of the Faraday Society*, 9 (1950) 14-19.